Theoretical and Semiempirical Study of the $A0^+$ State of NaI

by

Won Kim (B. Sc. Hons.)

Thesis Submitted for the Degree of Doctor of Philosophy

Department of Physics and Mathematical Physics

University of Adelaide

September 1999

Contents

Summary

The structure of the first excited electronic state (usually labelled as the $A0^+$ state) of NaI has been the subject of close investigation by numerous molecular physicists for decades. The various experimental studies on phototransition dynamics between the $X^1\Sigma^+$ state (the ground electronic state of NaI) and the $A0^+$ state yielded a very reasonable physical model with which one can describe the structure of the $A0^+$ state and phototransition processes involving it. However, despite these achievements, there is disagreement in the literature about the quantitative description of the $A0^+$ state and its potential curve. The aim of this thesis is to contribute towards an understanding of the $A0^+$ state of NaI.

Our research was carried out in two steps. First, the structure of the $A0^+$ state was theoretically investigated by performing various ab initio calculations to obtain potential curves of several low energy electronic states and by examining qualitatively how these potential curves interact via spin-orbit coupling to yield the $A0^+$ state.

Second, a number of relatively recent experimental studies on the phototransition process between the $X^1\Sigma^+$ and the $A0^+$ states were critically reviewed. Each of these experimental studies had a proposed potential curve of the $A0^+$ state, which was examined closely in this research. Validity criteria of the proposed potential curves were derived from information on the intensity structure of NaI absorption spectra. Some potentials suggested in the literature must be rejected. Those potentials which satisfy the criteria were then further examined to see whether they reproduce the experimentally known rovibrational level structure of the $A0^+$ state. Thus we determined which proposed potentials are consistent with the available experimental data. Finally, these potential curves were compared to a theoretical $A0^+$ potential curve that could be estimated from

our ab initio calculation, and it was found that the agreement between the experimental potential curves and our theoretically estimated potential curve is reasonable.

Statement of Originality

This work contains no material which has been accepted for the award of any other degree or diploma in any university or other tertiary instituition and, to the best of my knowledge and belief, contains no material previously published or written by another person, except where due reference has been made in the text.

I give consent to this copy of my thesis, when deposited in the University Library, being available for loan and photocopying.

Won Kim

Date : 29/2/00

Acknowledgements

This research was carried out under the supervision of Dr. Lee Torop, whose guidance and advice were invaluable from the beginning to the end. His supervision is deeply appreciated.

I wish to thank Dr. Donald McCoy for providing many insights in various stages of my research.

Two quantum chemistry calculation packages GAMESS (Silicon Graphics version 22 NOV 1995) and MOLPRO (version 96.4) were used in this research to perform theoretical calculations. I would like to thank Dr. Francis Vaughan, Director of South Australian Centre for Parallel Computing, and Ms. Judy Jenkinson of ANU Supercomputer Facility for their assistance.

Discussions with Dr. Wenhua Qin and his help with the use of Renormalized Numerov method program were also very valuable.

I also wish to thank Mrs. Dallas Kirby for her help with producing the diagrams.

Last but not the least, I thank my mother, who always gave me full support and encouragement for many years.

Chapter 1

Introduction

After the early spectroscopic studies on phototransitions involving the ground state of NaI reported a dense line structure in the absorption spectra whereas those of other alkali halides show a continuous variation of absorption intensity, NaI has been a subject of particular interest to molecular physicists.

An alkali halide molecule in its ground state is bound by ionic attraction and thus has discrete energy levels. Since a line structure of absorption spectra indicates that the associated excited states are also bound and discrete, a question arises as to why only NaI among other alkali halides exhibits bound excited states.

An answer to this question lay in that, since the two lowest potentials describing the ionic (attractive) and the atomic (repulsive) interactions of an alkali halide molecule cross each other due to the ionization potential of the constituent alkali atom being larger than the electron affinity of the halogen atom, there is a chance that the ground and the excited states may switch their character in the neighborhood where such a crossing takes place. This phenomenon is called a curve-crossing transition. For NaI, one may then deduce that there is a larger probability for this transition to occur when

compared to other alkali halides, from which it follows that an NaI molecule in excited electronic state can be held together by the ionic attraction to form bound states while the other alkali halides are more likely to be merely atomic upon excitation from their ground states and thus simply dissociate.

However, the absorption spectra of NaI did not exhibit any typical feature which could be associated with standard absorption spectra between bound states. In addition to this peculiarity, the immensely complex structure of the absorption spectra and the poor resolution of the early studies made it hard to gain information on the excited states of NaI.

The ground state of NaI, on the other hand, could be investigated quantitatively with microwave spectroscopy which established the energies of most rovibrational levels below the atomic dissociation limit, and the corresponding potential curve which governs the nuclear motion under the Born-Oppenheimer approximation scheme could be obtained.

The Born-Oppenheimer approximation, based on the assumption that the motions of electrons are much faster than those of nuclei so that the non-relativistic Schrödinger's equation can be separated into two equations each of which governs electronic and nuclear motion respectively, provides a starting point for a theoretical investigation of any diatomic molecule. One solves the Schrödinger's equation for the electronic motion to obtain the electronic wavefunctions and their energy eigenvalues for various internuclear distances, then these eigenvalues form a potential curve as a function of internuclear distance which governs the vibrational motion of the nuclei. Naturally, a potential curve is a useful tool with which theoretical and experimental studies can be examined and compared to each other. However, theoretical calculation of potential curves is difficult as even the energy eigenvalues of simple molecules like H_2 can not

be solved exactly for and the complexity of the equation increases enormously with the number of electrons.

These theoretical and experimental difficulties were overcome thanks to the development of high-performance computers and of UV laser spectroscopy. The former allowed efficient theoretical calculations of many-electron molecules and the latter made it possible to observe phototransition spectra with a resolution high enough to measure the transition energies accurately. Consequently, physicists could begin to reveal the excited state structure of NaI and derive its potential curves.

The aim of this thesis is to make a contribution to both theoretical and experimental understanding of NaI quantum molecular dynamics, focusing on the $A0^+$ state (the first excited state of the same symmetry as that of the ground state) and its potential curve, the main emphasis being given to the shape of its repulsive limb. Despite the advances that could be achieved via the use of laser spectroscopy and the analysis of data obtained thereof, no satisfactory explanation yet exists regarding the potential curve of the $A0^+$ electronic state and the structure of its rovibrational levels. Furthermore, as will be discussed in this thesis, a number of experimental studies which provided a breakthrough in the understanding of NaI are found to contradict each other and in some occasions lead to unacceptable conclusions. Thus it is also our intent to clarify what is reliable and what is not from these studies.

Chapter 2 gives basic quantum mechanical issues essential to a description of molecular wavefunctions. In Chapter 3 we explain how one solves for the electronic wavefunctions and their energies. Such a theoretical calculation is in general called an 'ab initio' calculation, implying that no assumptions are made from the experimental results and the calculation is carried out solely from theoretical grounds. Chapter 4 presents the

results of our ab initio calculations which include the potential curves of some electronic states which have not yet been reported.

In Chapter 5, we first explain the theory behind the analysis of $X^1\Sigma^+ \leftrightarrow A0^+$ transitions and examine the works of van Veen et al. and of Schaefer et al., both of which provided crucial keys to an understanding of the $A0^+$ state but have not yet been critically evaluated. We will carefully review these studies and explore their credibility. Then in Chapter 6 we discuss more recent experimental studies as well as the $A0^+$ potentials proposed by various researchers, and argue whose results are most reliable and how they fit with theoretical studies. Finally, we summarize what was learned in this research and suggest future work in Chapter 7.

Chapter 2

Basic Quantum Mechanical Formulation of Molecular Dynamics

2.1 Schrödinger's Equation for a Molecule and Born-Oppenheimer Approximation

2.1.1 Non-relativistic Schrödinger's equation for a molecule

For any given molecular system, one may write the non-relativistic Schrödinger's equation as

$$\hat{H}\Psi = E\Psi \tag{2.1}$$

where

$$\hat{H} = \hat{T}^n + \hat{V}^{nn} + \hat{T}^e + \hat{V}^{ne} + \hat{V}^{ee}, \tag{2.2}$$

$$\hat{T^n} = -\sum_{A=1}^{N} \frac{1}{2M_A}\nabla_A^2,$$

$$\hat{V}^{nn} = \sum_{A,B=1}^{N} \frac{Z_A Z_B}{R_{AB}}, \ A < B,$$

$$\hat{T}^{e} = -\sum_{i=1}^{n} \frac{1}{2} \nabla_i^2,$$

$$\hat{V}^{ne} = -\sum_{A=1}^{N} \sum_{i=1}^{n} \frac{Z_A}{r_{Ai}},$$

$$\hat{V}^{ee} = \sum_{i,j=1}^{n} \frac{1}{r_{ij}}, \ i < j$$

and Ψ is a function of $\mathbf{X} \equiv \{\mathbf{X_1}, \mathbf{X_2}, \ldots, \mathbf{X_N}\}$ and $\mathbf{x} \equiv \{\mathbf{x_1}, \mathbf{x_2}, \ldots, \mathbf{x_n}\}$. All the quantities are expressed in atomic units.

The Hamiltonian $\hat{H}$ is composed of nuclear kinetic energy, internuclear repulsion, electronic kinetic energy, nucleus-electron attraction, and electronic repulsion terms. N and n are the numbers of the nuclei and the electrons in a given molecule, respectively. Each $\mathbf{X_A}$ and $\mathbf{x_i}$ represent the spatial and spin coordinates of the Ath nucleus and the ith electron, i.e., they may be expressed as $\mathbf{X_A} \equiv (\mathbf{R_A}, \mathbf{\Sigma_A}), \mathbf{x_i} \equiv (\mathbf{r_i}, \sigma_i)$, where $\mathbf{R}$, $\mathbf{r}$ represent the spatial coordinates and $\mathbf{\Sigma}$, $\boldsymbol{\sigma}$ the spin coordinates of the nuclei and electrons, respectively.

2.1.2 Separation of the electronic and nuclear motions : the Born-Oppenheimer approximation

Usually in a molecular system the electrons move much faster than the nuclei, so we may consider the rate of change of the nuclear positions compared to the electronic motion to be very small. This assumption allows us to regard the electronic part of the energy eigenfunction Ψ to be close to the one obtained by solving the Schrödinger's equation while the nuclei are held stationary, thereby making it plausible to attempt

the separation of the eigenfunction of Eq. (2.1) into electronic and nuclear parts;

$$\Psi \approx \Psi^e \Psi^n. \tag{2.3}$$

Then we have

$$\hat{H}\Psi \approx \hat{H}(\Psi^e \Psi^n) \approx E\Psi^e \Psi^n$$

where the nuclear wave function depends only on the nuclear coordinates(i.e., $\Psi^n = \Psi^n(\mathbf{X})$), so that the action of the electronic kinetic energy operator $\hat{T}^e$ on Ψ^n yields a null result.

The electronic wavefunction Ψ^e depends on both the electronic and nuclear coordinates, but in the current approximation scheme its dependence on the nuclear coordinates may be considered to be weak enough to leave Ψ^e unchanged for a small variation in the nuclear positions. Therefore we may expect the term

$$\hat{T}^n(\Psi^e \Psi^n) - \Psi^e \hat{T}^n \Psi^n = \Psi^n \hat{T}^n \Psi^e - \sum_{A=1}^{N} \frac{1}{M_A} \nabla_A \Psi^n \cdot \nabla_A \Psi^e \tag{2.4}$$

to be generally negligible. Then Eq. (2.1) becomes

$$\Psi^n(\hat{T}^e + \hat{V}^{ne} + \hat{V}^{ee})\Psi^e + \Psi^e(\hat{T}^n + \hat{V}^{nn})\Psi^n \approx E\Psi^e \Psi^n. \tag{2.5}$$

Now, if there exists Ψ^e which satisfies the eigenvalue equation

$$\hat{H}^e \Psi^e = E^e \Psi^e \tag{2.6}$$

where the electronic Hamiltonian $\hat{H}^e$ is defined as

$$\hat{H}^e \equiv \hat{T}^e + \hat{V}^{ne} + \hat{V}^{ee} + \hat{V}^{nn},$$

then Eq. (2.5) can be written as

$$\Psi^e(\hat{T}^n + E^e)\Psi^n \approx E\Psi^e\Psi^n.$$

Therefore

$$\hat{H}^n\Psi^n \approx E\Psi^n \tag{2.7}$$

with $\hat{H}^n \equiv \hat{T}^n + E^e$ the nuclear Hamiltonian.

The above procedure of separating Eq. (2.1) into Eqs. (2.6) and (2.7) was first introduced by Born and Oppenheimer [Born 1927] and thus is usually called the 'Born-Oppenheimer' approximation. We will call it the 'BO' approximation for brevity. Accordingly we will call Eq. (2.6) the BO electronic equation and the following the BO nuclear equation;

$$(\hat{T}^n + E^e)\Psi^n = E^n\Psi^n, \tag{2.8}$$

with E^n the BO estimate of E.

We note that by assuming the faster movement of electrons, compared to the nuclear motion, we achieve a justification of introducing the BO electronic Schrödinger's equation (2.6) and solving it for a fixed position of the nuclei. We must keep in mind that even though we assumed the change in Ψ^e with respect to small variation of the nuclear positions to be negligible so that the term (2.4) can be ignored, still Ψ^e and the corresponding electronic energy E^e would generally be changing as different positions

of the nuclei are used in the term $\hat{V}^{ne}$ in Eq. (2.6). Therefore Ψ^e is normally written as $\Psi^e(\mathbf{x};\mathbf{X})$, indicating that Eq. (2.6) is to be solved for certain nuclear positons. In the same manner E^e may also be written as $E^e(\mathbf{X})$. Then the set of values $E^e(\mathbf{X})$ thus obtained from solving Eq. (2.6) can be used in Eq. (2.8) to solve for the nuclear wavefunction $\Psi^n(\mathbf{X})$ and the total energy E^n.

We see that E^e serves the role of the potential energy function in Eq. (2.8). So this term can be labelled as the 'potential (energy) function' or 'potential (energy) surface'; in the case of diatomic molecules we can simply call it 'potential curve' as, after removing the rotational and translational motions from the equation, E^e becomes a function of the internuclear distance only. Also the spin variables of the nuclear and electronic wavefunctions can be left out because the Hamiltonian we introduced does not depend on spin.

Summarizing, we try to achieve the goal of obtaining an approximate solution to Eq. (2.1) in two steps by introducing the BO approximation;

1. Solve Eq. (2.6) in various nuclear geometries to obtain the electronic energy eigenfunctions and the corresponding potential functions, and

2. Use these results to find the nuclear energy eigenfunctions and the total energy by solving Eq. (2.8).

However, even after incorporating the BO approximation, it is still impossible to solve Eqs. (2.6) and (2.8) exactly. We need to apply further restrictions and approximation methods in various stages of the calculation to make our problem mathematically manageable. We will continue our discussion by looking at the validity of BO approximation.

2.2 The Validity of the BO Approximation and the Adiabatic Approximation Method

In the previous section, we argued that the much faster movement of electrons than that of the nucei in a molecule may enable us to attempt to solve Eq. (2.1) approximately by using the BO approximation. The key point in the procedure was to drop the term (2.4) from the Schrödinger's equation. We now want to formulate this discussion mathematically in order to see the validity of the BO approximation more clearly.

2.2.1 The effect of the kinetic energy operator on the electronic wavefunction

Let us first assume we have found the normalized electronic wavefunction Ψ^e which satisfies Eq. (2.6). Then, without imposing any approximation other than Eq. (2.3), we may write Eq. (2.1) as

$$\Psi^e(\hat{T}^n + E^e)\Psi^n + \Psi^n\hat{T}^n\Psi^e - \sum_{A=1}^{N}\frac{1}{M_A}\nabla_A\Psi^n\cdot\nabla_A\Psi^e \approx E\Psi^e\Psi^n \tag{2.9}$$

By multiplying both sides by Ψ^e and integrating over electronic coordinates we obtain, taking Ψ^e to be normalized at each nuclear geometry,

$$(\hat{T}^n + E^e)\Psi^n + \Psi^n\int\Psi^e\hat{T}^n\Psi^e d\tau_e - \sum_{A=1}^{N}\frac{1}{M_A}\nabla_A\Psi^n\cdot\int\Psi^e\nabla_A\Psi^e d\tau_e \approx E\Psi^e\Psi^n \tag{2.10}$$

where $\int d\tau_e = \int d\mathbf{r} = \int\int\cdots\int dr_1 dr_2\cdots dr_n$ as there is no explicit spin dependence in the Hamiltonian. Furthermore, we assumed the electronic wavefunction Ψ^e to be real,

which is acceptable as Ψ^e will always be bound around the nuclei.

We note that

$$\int \Psi^e \hat{T}^n \Psi^e d\tau_e = \int \Psi^e (\sum_{A=1}^{N} \frac{-1}{2M_A} \nabla_A^2) \Psi^e d\tau_e = -\sum_{A=1}^{N} \frac{1}{2M_A} \int \Psi^e \nabla_A^2 \Psi^e d\tau_e$$

and

$$\int \Psi^e \nabla_A^2 \Psi^e d\tau_e = \frac{1}{2} \int \nabla_A^2 (\Psi^e)^2 d\tau_e - \int (\nabla_A \Psi^e)^2 d\tau_e = -\int (\nabla_A \Psi^e)^2 d\tau_e,$$

because

$$\int \nabla_A^2 (\Psi^e)^2 d\tau_e = \nabla_A^2 \int (\Psi^e)^2 d\tau_e = \nabla_A^2 \cdot 1 = 0$$

for Ψ^e is a normalized wavefunction and ∇_A^2 acts on the nuclear coordinates while the integration is over the electronic coordinates. Similarly the last term in the left side of Eq. (2.10) is also zero.

Hence Eq. (2.10) becomes

$$(\hat{T}^n + E^e + W)\Psi^n \approx E\Psi^n \tag{2.11}$$

where

$$\begin{aligned} W &= \int \Psi^e \hat{T}^n \Psi^e d\tau_e \\ &= \sum_{A=1}^{N} \frac{1}{2M_A} \int (\nabla_A \Psi^e)^2 d\tau_e, \end{aligned}$$

that is, the term W should be added to the nuclear BO equation when the effect of $\hat{T}^n$ on Ψ^e is not ignored. Thus, as long as W is small, which seems to be the case considering that each summand in W is inversely proportional to the mass of the cor-

responding nucleus, the BO scheme would appear to remain valid. Furthermore, the form of Eq. (2.11) suggests that even if the magnitude of W is such that it can not be neglected, all we have to do is simply to add it to the BO nuclear equation (2.8) as a correction.

However, the above discussion does not yet provide a satisfactory answer to the question regarding the accuracy of the BO approximation method. The measure of improvement, which we expect to obtain by the inclusion of the term W, is also unclear.

2.2.2 Matrix elements of the total Hamiltonian in the basis of BO wavefunctions

Another aspect we have neglected so far is the possible presence of the coupling between the different BO solutions, which may be labelled by sets of electronic and nuclear quantum numbers ϵ and ν that we will specify later. Eqs. (2.6) and (2.7) are then rewritten as

$$\hat{H}^e \Psi^e_\epsilon = E^e_\epsilon \Psi^e_\epsilon \tag{2.12}$$

and

$$\hat{H}^n \Psi^n_{\epsilon\nu} = E^n_{\epsilon\nu} \Psi^n_{\epsilon\nu}. \tag{2.13}$$

It should be pointed out that the use of ϵ and ν in labelling the exact solutions of the Eq. (2.1) can only be accepted in an approximate way, because the separation of the wavefunction into the electronic and the nuclear parts was done by introducing the BO approximation which disregards the effect of $\hat{T}^n$ on Ψ^e. For this reason we refer to $\Psi_{(\epsilon\nu)}$ as the exact solution of Eq. (2.1) that can be expanded using a set of BO wavefnctions as a basis, $\Psi_{\epsilon\nu} = \Psi^e_\epsilon \Psi^n_{\epsilon\nu}$ being the leading term in the expansion.

The matrix elements of the Hamiltonian generated by BO wavefunctions are

$$\begin{aligned} H_{\epsilon'\nu',\epsilon\nu} &= \int \Psi^*_{\epsilon'\nu'} \hat{H} \Psi_{\epsilon\nu} d\tau \\ &= E^n_{\epsilon\nu} \int \Psi^*_{\epsilon'\nu'} \Psi_{\epsilon\nu} d\tau + \int \Psi^{n^*}_{\epsilon'\nu'} \Psi^n_{\epsilon\nu} \Psi^e_{\epsilon'} \hat{T}^n \Psi^e_{\epsilon} d\tau \\ &\quad - \sum_A \frac{1}{M_A} \int \Psi^{n^*}_{\epsilon'\nu'} \nabla_A \Psi^n_{\epsilon\nu} \cdot \Psi^e_{\epsilon'} \nabla_A \Psi^e_{\epsilon} d\tau, \end{aligned} \tag{2.14}$$

and in analogy to W used in Eq. (2.11), we will write

$$W_{\epsilon'\epsilon} = \int \Psi^e_{\epsilon'} \hat{T}^n \Psi^e_{\epsilon} d\tau_e. \tag{2.15}$$

The diagonal elements are

$$\begin{aligned} H_{\epsilon\nu,\epsilon\nu} &= E^n_{\epsilon\nu} + \int \Psi^{n^*}_{\epsilon\nu} \Psi^n_{\epsilon\nu} \Psi^e_{\epsilon} \hat{T}^n \Psi^e_{\epsilon} d\tau - \sum_A \frac{1}{M_A} \int \Psi^{n^*}_{\epsilon\nu} \nabla_A \Psi^n_{\epsilon\nu} \cdot \Psi^e_{\epsilon} \nabla_A \Psi^e_{\epsilon} d\tau \\ &= E^n_{\epsilon\nu} + \int \Psi^{n^*}_{\epsilon\nu} \Psi^n_{\epsilon\nu} \sum_{A=1}^{N} \frac{1}{2M_A} \int (\nabla_A \Psi^e_{\epsilon})^2 d\tau_e + 0 \\ &= E^n_{\epsilon\nu} + \int \Psi^{n^*}_{\epsilon\nu} \Psi^n_{\epsilon\nu} W_{\epsilon\epsilon} d\tau_n \end{aligned} \tag{2.16}$$

and if $\nu' \neq \nu$ while $\epsilon' = \epsilon$;

$$H_{\epsilon\nu',\epsilon\nu} = \int \Psi^{n^*}_{\epsilon\nu'} \Psi^n_{\epsilon\nu} W_{\epsilon\epsilon} d\tau_n. \tag{2.17}$$

Finally, when $\epsilon' \neq \epsilon$, the term $\int \Psi^e_{\epsilon'} \nabla_A \Psi^e_{\epsilon} d\tau_e$ no longer vanishes.

$$\begin{aligned} H_{\epsilon'\nu',\epsilon\nu} &= \int \Psi^{n^*}_{\epsilon'\nu'} \Psi^n_{\epsilon\nu} W_{\epsilon'\epsilon} d\tau_n \\ &\quad - \sum_A \frac{1}{M_A} \int \Psi^{n^*}_{\epsilon'\nu'} \nabla_A \Psi^n_{\epsilon\nu} \cdot \Psi^e_{\epsilon'} \nabla_A \Psi^e_{\epsilon} d\tau. \end{aligned} \tag{2.18}$$

2.2.3 Adiabatic approximation method and the assesment of its validity based on the perturbation approach

At this point, it is worthwhile to observe that the diagonal matrix elements $H_{\epsilon\nu,\epsilon\nu}$, expressed as the terms (2.16), are not the eigenvalues of the BO nuclear equations. If we redefine the nuclear Hamiltonian to be

$$\hat{H}^n \equiv \hat{T}^n + E^e_\epsilon + W_{\epsilon\epsilon} \tag{2.19}$$

and use it in Eq.(2.13) to obtain the nuclear wavefunctions and their energies, the diagonal matrix elements become simply the eigenvalues $E^n_{\epsilon\nu}$, that is, the diagonal correction terms $W_{\epsilon\epsilon}$ are absorbed into the energy eigenvalues. Consequently, these energy eigenvalues are closer to the exact energy eigenvalues than the BO energies and, if we use this new set of wavefunctions in the construction of the Hamiltonian matrix the off-diagonal matrix elments with different ν and the same ϵ values vanish, the non-zero off-diagonal matrix elements consisting only of the ones between the wavefunctions with different electronic quantum numbers;

$$\begin{aligned} H_{\epsilon'\nu',\epsilon\nu} &= \int \Psi^{n*}_{\epsilon'\nu'} \Psi^n_{\epsilon\nu} W_{\epsilon'\epsilon} d\tau_n \\ &\quad - \sum_A \frac{1}{M_A} \int \Psi^{n*}_{\epsilon'\nu'} \nabla_A \Psi^n_{\epsilon\nu} \cdot \Psi^e_{\epsilon'} \nabla_A \Psi^e_\epsilon d\tau, \ \epsilon' \neq \epsilon. \end{aligned}$$

This simplified structure of the Hamiltonian matrix which is obtained by introducing the Eq. (2.19) makes the use of perturbation theory much easier.

The modification of $\hat{H}^n$ by Eq. (2.19) was first proposed by Born [Born 1951] and by Born and Huang [Born 1954]. We will call Eq. (2.13) with this new $\hat{H}^n$ an adiabatic

nuclear equation. Without introducing new symbols, we will let $\Psi^n_{\epsilon\nu}$, $E^n_{\epsilon\nu}$ denote the solutions of the adiabatic equations. In case we need to refer to the BO results, we will use $\tilde{\Psi}^n_{\epsilon\nu}$ and $\tilde{E}^n_{\epsilon\nu}$ to represent them.

Being motivated by the discussion supporting the physical justification of the BO approach, we now apply the perturbation theory assuming that the adiabatic wavefunctions and their energies obtained by solving Eqs. (2.12) and (2.13) are close approximations to the exact results, and that there is no degeneracy.

Firstly we set up the reference matrix $\mathbf{H^0}$ and the perturbation matrix $\mathbf{H'}$;

$$\begin{aligned} H^0_{\epsilon'\nu',\epsilon\nu} &= \delta_{\epsilon'\epsilon}\delta_{\nu'\nu}H_{\epsilon'\nu',\epsilon\nu} \\ &= \delta_{\epsilon'\epsilon}\delta_{\nu'\nu}E^n_{\epsilon\nu}, \\ \mathbf{H'} &= \mathbf{H} - \mathbf{H^0}, \text{ i.e.,} \\ H'_{\epsilon'\nu',\epsilon\nu} &= 0 \text{ if } \epsilon' = \epsilon, \\ &= H_{\epsilon'\nu',\epsilon\nu} \text{ otherwise.} \end{aligned}$$

The zeroth order wavefunctions are $\Psi_{\epsilon\nu}$ which are trivial eigenfunctions of the diagonal matrix $\mathbf{H^0}$, with the zeroth order energies $E^{(0)}_{\epsilon\nu}$ being $E^n_{\epsilon\nu}$. Then the higher order correction terms can be obtained by applying usual perturbation methods.

The first-order correction $E^{(1)}_{\epsilon\nu}$ to the energy is

$$E^{(1)}_{\epsilon\nu} = H'_{\epsilon\nu,\epsilon\nu} = 0, \tag{2.20}$$

which is a consequence of using the adiabatic wavefunctions as the zeroth order functions. Had we used the BO wavefunctions as the zeroth order wavefunctions instead, the first

order enrgy terms would not have vanished, but instead would have been

$$\tilde{E}^{(1)}_{\epsilon\nu} = \int \tilde{\Psi}^{n^*}_{\epsilon\nu} \tilde{\Psi}^{n}_{\epsilon\nu} W_{\epsilon\epsilon} d\tau_n.$$

The second order energy corrections and the first order corrections to the wavefunctions, the latter of which is expressed as linear combinations of the zeroth order wavefunctions, are

$$E^{(2)}_{\epsilon\nu} = \sum_{\epsilon'\nu'} \frac{H'_{\epsilon'\nu',\epsilon\nu} H'_{\epsilon\nu,\epsilon'\nu'}}{E^n_{\epsilon\nu} - E^n_{\epsilon'\nu'}}, \quad \epsilon' \neq \epsilon, \tag{2.21}$$

and

$$\Psi^{(1)}_{\epsilon\nu} = \sum_{\epsilon'\nu'} \Psi_{\epsilon'\nu'} \frac{H'_{\epsilon'\nu',\epsilon\nu}}{E^n_{\epsilon\nu} - E^n_{\epsilon'\nu'}}, \quad \epsilon' \neq \epsilon. \tag{2.22}$$

Hence one can state that in order for the adiabatic solutions to be valid the inequality

$$H'_{\epsilon'\nu',\epsilon\nu} \ll E^n_{\epsilon'\nu'} - E^n_{\epsilon\nu} \tag{2.23}$$

must hold, that is, the difference between the adiabatic energy eigenvalues has to be much greater than the magnitude of the corresponding off-diagonal Hamiltonian matrix element.

If two nuclear wavefunctions with similar energy have broad overlap, there is a likelihood that the off-diagonal matrix element becomes large enough compared to the energy difference so that the strong interaction occurs between those two states, causing a breakdown of the adiabatic approximation.

Before we continue our discussion on the validity of the adiabatic approximation method, we will confine our attention to diatomic molecules and firstly look at the symmetry properties of their electronic wavefunctions.

2.3 Symmetry Properties of Electronic Wavefunctions of a Diatomic Molecule

2.3.1 Spatial symmetry of diatomic molecules

It is always advantageous to recognize and exploit symmetry present in a physical system subject to investigation. The presence of symmetry indicates there is a conserved quantity associated with it, which can be identified as an eigenvalue of an associated symmetry operator. A function generated by applying a symmetry operator to an energy eigenfunction of a Hamiltonian is also an energy eigenfunction with the same energy eigenvalue. By looking at the symmetries possessed by a given system, we can understand more easily the dynamics of it, and gain useful information about the structure of the energy eigenfunctions, which in turn can be labelled and distinguished from one another by their behaviour under each symmetry operation. Especially in a situation where it is impossible to obtain the exact eigenfunctions so that we have to resort to approximate methods, the symmetry of the system often provides a shortcut to finding the wavefunction of a correct form, even before paying attention to the Schrödinger's equation of the system.

There is generally more than one type of operation under which a system is symmetric. Any molecule is symmetric under a rotation and a translation of the molecule as a whole unless it is subject to an external field. Translational motion can be separated off by introducing an inertial coordinate system whose origin is not fixed in space but moves along with a molecule, whereas removal of rotational motion from the system is not a straightforward procedure. However this difficulty is partially avoided, as in the first stage of the BO-adiabatic method the nuclei are held stationary, automatically

removing the translational and rotational motions of a molecule. Exact treatment of the translational and rotational motions can be found elsewhere[Kovács 1969].

Furthermore, such a set of operators under which a molecule is symmetric forms a group. Therefore group theory is a useful tool in the study of molecular physics. One particular symmetry group which is of interest is the 'point symmetry group', a set of geometric operations which leave the nuclear framework of a molecule unchanged. Consequently, the electronic Hamiltonian $\hat{H}^e$ in Eq. (2.6) is invariant under the point symmetry group of a given molecule. To which point symmetry group a molecule belongs depends on the relative positions of the nuclei in its equilibrium geometry.

Diatomic molecules possess what is called 'axial symmetry', that is, they are symmetric under any rotation along the internuclear axis joining the two nuclei and under reflection through any plane containing the internuclear axis. An additional symmetry property appears if the molecule is composed of two identical nuclei, being the inversion through the midpoint between the two nuclei. The former point symmetry group is called $C_{\infty v}$ and the latter $D_{\infty h}$.

Classification of the different energy eigenstates according to their symmetry properties involves group representation theory (see [Hammermesh 1962], [Hochstrasser 1966] and [Kaplan 1975] for example), detailed discussion of which will not be presented here. Yet, it is worthwhile to note that application of group representation theory in a qualitative analysis of the electronic energy levels of a given molecule does not require knowledge of the exact energy eigenfunctions or the molecular Hamiltonian (or of the approximate equations derived from it). All we need is to find out under which symmetry groups our equations of interest are invariant, then we become able to answer basic questions regarding degeneracy and selection rules, etc., thereby also reducing the computational

effort when we are at the stage of actual ab initio calculation as we will know which matrix elements are non-zero beforehand. Most modern ab initio calculation packages are designed to make full use of the group representation theory whenever possible.

What is presented below is a concise discussion on how the group representation theory provides a qualitative understanding of the energy level structure.

2.3.2 Group representation theory

Suppose $\hat{o}$ is a coordinate transformation operator acting on a set of coordinates $\mathbf{s} = \{s_1, s_2, ..., s_n\}$. Then, for an arbitrary function f dependent on $\mathbf{s}$, one may define an operator $\hat{O}$ acting on f such that

$$\tilde{f}(\mathbf{s}) \equiv \hat{O}f(\mathbf{s}) = f(\hat{o}^{-1}\mathbf{s}) \tag{2.24}$$

or

$$\hat{O}f(\hat{o}\mathbf{s}) = f(\mathbf{s}). \tag{2.25}$$

In other words, the value of $\tilde{f}$ at $\mathbf{s}$ is given to be the same as the value of the original function f at $\hat{o}^{-1}\mathbf{s}$. If $\hat{o}$ is an element of a group G, $\hat{O}$ also belongs to G(p.81 of [Hammermesh 1962]).

The set of functions $\{f_1 \equiv f, f_2, f_3 ... f_g\}$ generated by the successive application of $\hat{O}$ to an original function f are then said to form a basis for a representation of $\hat{O}$, for it can be assigned to a matrix whose elements satisfy the relation

$$\hat{O}f_j = \sum_{i=1}^{g} O_{ij} f_i. \tag{2.26}$$

The matrices generated from the same basis for each group operators of G obey the same multiplication law as the operators. (The representation thus generated is called a faithful representation if the correspondence between the representing matrices and the symmetry operators is isomorphic.) Furthermore, one can show that any representation can be made into unitary form if the matrices of the representation are nonsingular (p.87 of [Hochstrasser 1966]). We will assume that all the representations in our discussion are unitary.

For a group G of the symmetry operators under which the electronic Hamiltonian $\hat{H}^e$ of a given molecule is invariant, we may use its energy eigenfunctions Ψ^e_ϵ as a basis to form a representation of G. Let $\hat{G}_t$ be one of the operators belonging to G. Then it follows that the transformed function $\hat{G}_t\Psi^e_\epsilon$ is also the energy eigenfunction of $\hat{H}^e$ with the same energy eigenvalue as that of Ψ^e_ϵ,

$$\hat{H}^e(\hat{G}_t\Psi^e_\epsilon) = E^e_\epsilon(\hat{G}_t\Psi^e_\epsilon). \tag{2.27}$$

Therefore, for a non-degenerate case $\hat{G}_t\Psi^e_\epsilon$ can only differ from Ψ^e_ϵ by a constant factor;

$$\hat{G}_t\Psi^e_\epsilon = c\Psi^e_\epsilon, \;\; |c|^2 = 1 \tag{2.28}$$

and if there is a degeneracy,

$$\hat{G}_t\Psi^e_\epsilon = \sum_{\epsilon'} G_{\epsilon'\epsilon}\Psi^e_{\epsilon'} \tag{2.29}$$

where the summation covers the eigenfunctions with the same E^e_ϵ.

In other words, by using the energy eigenfunctions Ψ^e_ϵ as a basis, the representations are made in such a way that the set of degenerate eigenfunctions generating one representation does not serve as a basis for generating other representations, and we can label

the eigenfunctions according to the representations they generate. In the language of group representation theory such representations are called 'irreducible' representations (IRs). Matrices belonging to the same IR can not be simultaneously made to assume the same block-diagonal structure by a single similarity transformation, as that would then mean that the representation is reducible.

For a nondegenerate energy level there exists only a single eigenfunction and it generates a representation by itself, as is shown in Eq. (2.28). Each symmetry operator is then represented by a scalar. Such a representation is said to be one-dimensional. In degenerate cases, Eq. (2.29) applies and the representing matrices are of the dimension equal to the degree of degeneracy of the energy level.

The main usefulness of the group representation theory lies in the fact that every IR for a given group is unique in the sense that no other IR can be generated except by a similarity transformation. Therefore we do not need to have the energy eigenfunctions to find which IR's are possible for a given symmetry group. We will use a point symmetry group $C_{\infty v}$ to illustrate this point. More general discussions can be found, for example, in [Hammermesh 1962].

2.3.3 Spatial symmetry of heterogeneous diatomic molecules : irreducible representations of $C_{\infty v}$

The operators of $C_{\infty v}$ include a rotation by an angle ϕ about a fixed axis (which we will call the z-axis) $\hat{C}(\phi)$, a reflection in a plane (conventionally the xz-plane is chosen) containing the z-axis $\hat{\sigma}_v$, and the identity operation $\hat{I}$. The order of $C_{\infty v}$ is infinite as ϕ can be any angle between 0 and 2π. Consequently there are an inifinite number of planes in which a reflection can be performed.

If we let $\hat{\sigma}_v(\phi)$ denote a reflection in a plane at an angle ϕ from the xz-plane, one finds

$$\hat{\sigma}_v(\phi) = \hat{\sigma}_v \hat{C}(2\phi)$$

so that the only one reflection operator, which we chose to be σ_v, is recognized as an independent element of $C_{\infty v}$. $C_{\infty v}$ is also called a continuous group for its operators are labeled by a continuous parameter ϕ.

The subgroup C_∞ of $C_{\infty v}$ consists of the operators $\hat{C}(\phi)$ and $\hat{I}$ and is Abelian, hence all of its IR's are one-dimensional (p. 322 of [Landau 1977]).

We note that the successive application of two rotations by angles ϕ_1 and ϕ_2 are equivalent to a single rotation by $\phi_1 + \phi_2$;

$$\hat{C}(\phi_1)\hat{C}(\phi_2) = \hat{C}(\phi_1 + \phi_2)$$

so that the representing matrices (which are just scalars for one-dimensional representations) of the rotations, being denoted by $\chi(\phi)$, must also satisfy

$$\chi(\phi_1)\chi(\phi_2) = \chi(\phi_1 + \phi_2),$$

that is, $\chi(\phi)$ must be of a form

$$\chi(\phi) = e^{im\phi}$$

where m must be an integer in order for the representation to be single-valued.

Thus, for C_∞ we have an infinite number of one-dimensional IR's each of which are labeled by m. The function $e^{-im\phi}$ can serve as a basis for generating the IR labeled by m, which we denote as $D^{(m)}$.

To verify this, we make use of Eq. (2.24) and observe that

$$C(\phi')e^{-im\phi} = e^{-im(\phi-\phi')} = e^{im\phi'}e^{-im\phi}.$$

When $e^{-im\phi}$ with non-zero m is reflected in the xz-plane, ϕ changes its sign;

$$\hat{\sigma}_v e^{\pm im\phi} = e^{\mp im\phi},$$

which can be written in matix form

$$\sigma_v = \begin{pmatrix} 0 & 1 \\ 1 & 0 \end{pmatrix}.$$

Unlike C_∞, $C_{\infty v}$ thus has two-dimensional IR's, each of which is generated by the two basis functions $e^{\pm im\phi}$.

From the above consideration it then follows that the electronic energy levels under an axially symmetric attractive electric field generated by two clamped nuclei in a diatomic molecule are doubly degenerate if the value of m, being the projection of the electronic orbital quantum number onto the z-axis (i.e., the internuclear axis), is not zero.

Each electronic level is conventionally labelled by the positive integer $\Lambda = |m|$, the physical interpretation of which is the projection of the magnitude of the total orbital angular momentum of the electronic wavefunction onto the z-axis(which is the internuclear axis). If it is zero we have two one dimensional IR's, one(Σ^+) being symmetric under reflection in a plane containing the z-axis and the other(Σ^-) antisymmetric. For nonzero value of Λ, symmetric and antisymmetric wavefunctions combine to form a two

dimensional IR.

2.3.4 Electron spin

Another basic symmetry property present in any electronic system is that of spin, an intrinsic angular momentum whose value is 1/2 for an electron. The non-relativistic Schrödinger's equation Eq. (2.12) and its energy eigenfunctions do not explicitly depend on spin. However, coupled with the antisymmetry principle stating that the electronic wavefunctions must be antisymmetric under the exchange of any two electrons, electron spin does have indirect influence over the structure of the electronic wavefunction.

Symmetry with respect to the electron spin can be dealt with in a similar way as we treat the rotational symmetry in space. For a system of n-electrons one can generate the spin eigenfunctions in various ways[Pauncz 1979], which become a basis for IRs of the group $SU(2)$, a group of two dimensional unitary matrices with determinant 1. It is necessary to consider $SU(2)$ instead of the pure three dimensional rotation group because, unlike the orbital angular momentum which is always an integer, the total spin can be a half-integer. We refer to [Wigner 1959] for details. The IRs of $SU(2)$ are labelled by their total spin values S and the degeneracy of each IR is determined by their spin multiplicity ($= 2S + 1$) which is normally attached to the upper left side of a Λ symbol to indicate the symmetry property of a given state (for example $^1\Sigma^+$). Finally, the spatial and the spin parts of the wavefunction have to be combined in such a way that the total wavefunction is antisymmetric under the exchange of any two electrons, that is, the total wavefunctions generate the antisymmetric IRs of the permutation group S_n (n = number of electrons). Apart from affecting the form of the spatial wavefunction, the spin wavefunction has no further effect on calculations and

can be ignored thereafter.

So far we have seen that, in the understanding of the electronic wavefunction Ψ_ϵ^e of a heterogeneous diatomic molecular system, three different kinds of symmetry groups are involved; the point symmetry group $C_{\infty v}$ for a description of the spatial symmetry, the group $SU(2)$ for electron spin, and the permutation group S_n for the exchange symmetry. Any trial electronic wavefunction to be used in the ab initio method, therefore, should possess these symmetry properties.

2.3.5 Non-crossing rule

Electronic states with different symmetry properties (i.e., states belonging to different IR's of any of the symmetry groups) in general are expected to have different energies, although at a certain nuclear geometry (or at a certain internuclear distance in the diatomic case) the energy levels may coincide. This is called an accidental degeneracy and is understood to have no relation to molecular symmetry.

On the other hand, there can be states belonging to the same IR but having different energies. Let Ψ_i^e be an eigenfunction of such a state with the energy eigenvalue E_i^e;

$$\hat{H}^e(R)\Psi_i^e(\mathrm{x};R) = E_i^e(R)\Psi_i^e(\mathrm{x};R)$$

where R denotes the internuclear distance between the two nuclei of a diatomic molecule. Differentiating the above equation with respect to R then leads to

$$\frac{\partial \hat{H}^e}{\partial R}\Psi_i^e + \hat{H}^e\frac{\partial \Psi_i^e}{\partial R} = \frac{dE_i^e}{dR}\Psi_i^e + E_i^e\frac{\partial \Psi_i^e}{\partial R}.$$

Next, we multiply by Ψ_j^e, another real eigenfunction with the same symmetry as that

of Ψ_i^e but with the different energy E_j^e, and integrate over the electronic coordinates to obtain

$$\int \Psi_j^e \frac{\partial \hat{H}^e}{\partial R} \Psi_i^e d\tau_e + \int \Psi_j^e \hat{H}^e \frac{\partial \Psi_i^e}{\partial R} d\tau_e = \frac{dE_i^e}{dR} \int \Psi_j^e \Psi_i^e d\tau_e + E_i^e \int \Psi_j^e \frac{\partial \Psi_i^e}{\partial R} d\tau_e$$

whence

$$\int \Psi_j^e \frac{\partial \hat{H}^e}{\partial R} \Psi_i^e d\tau_e = (E_i^e - E_j^e) \int \Psi_j^e \frac{\partial \Psi_i^e}{\partial R} d\tau_e \tag{2.30}$$

for Ψ_i^e and Ψ_j^e are orthogonal to each other and $\hat{H}^e$ is a hermitian operator.

The operator $\partial \hat{H}^e / \partial R$, possessing the same symmetry invariance as that of $\hat{H}^e$, does not cause transitions between states of different symmetry. However for states of the same symmetry, mixing may occur as they are not eigenstates of $\partial \hat{H}^e / \partial R$. Consequently the corresponding matrix element will in general be non-zero. Then it follows that the energy difference between the two states $E_i^e - E_j^e$ can not be zero either. Hence we arrive at what is known as the 'avoided crossing' or 'non-crossing' rule [Landau 1977];

> "In a diatomic molecule potential curves of states with the same symmetry in general do not cross."

As we will discuss in Chapter 5, there is a possibility that strong interaction occurs between states whose potential curves undergo an avoided crossing so that the BO approximation method becomes no longer valid. Then one has to find solutions to Eq. (2.1) by different means, for example, by treating the two potential curves together to set up a system of coupled equations for the nuclear wavefunctions. One may also look for electronic wavefunctions other than the adiabatic ones if the off-diagonal total Hamiltonian matrix element between them, also called non-adiabatic coupling term, is large or hard to calculate, in the hope that the non-adiabatic wavefunctions are easier

to work with. Further details are given in Sections 5.2 and 5.3.

2.4 Nuclear Wavefunctions of a Diatomic Molecule

2.4.1 Rotational symmetry of a nuclear wavefunction : separation of the angular variables

Under the BO-adiabatic approximation scheme, nuclear motion of a molecule is subject to a potential function which is constructed from the electronic energy eigenvalues obtained at various fixed nuclear positions. In the diatomic case a potential function depends on internuclear distance only, hence the nuclear Hamiltonian and Eq. (2.13), unlike their electronic counterparts, become spherically symmetric and therefore their eigenfunctions generate IRs of three dimensional rotation group $R(3)$.

The conventional way to describe the motion of nuclei in a central field is to separate off angular variables to write the nuclear wavefunction as a product of radial and angular wavefunctions

$$\Psi^n_{\epsilon\nu} = \frac{1}{R}\chi_{\epsilon\upsilon}(R)\Theta_{JM}(\theta,\varphi) \tag{2.31}$$

where $\Theta_{JM}(\theta,\varphi)$ is a spherical harmonic;

$$\Theta_{JM}(\theta,\varphi) = N_r P_J^{|M|}(\cos\theta)e^{iM\varphi}.$$

$P_J^{|M|}(\cos\theta)$ is an associated Legendre polynomial and N_r a normalization constant. Here, J is a rotational quantum number while M is the quantum number of the projection of J onto the internuclear axis and can take values from $-J$ to J. Both J and M are integers. The effect of applying an operator $\hat{R}_{\alpha\beta\gamma}$ which rotates a system by Euler angles

(α, β, γ) to a spherical harmonic Θ_{JM} is to generate a linear combination of spherical harmonics with the same J but different M values;

$$\hat{R}_{\alpha\beta\gamma}\Theta_{JM} = \sum_{M'} D^{(J)}_{M'M}(\alpha\beta\gamma)\Theta_{JM'},$$

and it can be further proven that the representation $D^{(J)}$ thus generated by a set of functions $\{\Theta_{JM}; M = -J, -J+1, -J+2, \ldots, J-2, J-1, J\}$ is irreducible. Detailed discussions can be found, for example, in section 9-3 of [Hammermesh 1962]. As rotation operators do not affect the radial function, the nuclear wavefunctions as expressed in Eq. (2.31) also generate IRs of $R(3)$.

Correspondingly, angular variables can be separated off from Eq. (2.13) to yield an equation depending only in R;

$$\left[-\frac{1}{2\mu}\frac{d^2}{dR^2} + E^e_\epsilon(R) + \frac{J(J+1)}{2\mu R^2}\right]\chi_{\epsilon v J}(R) = E^n_{\epsilon v J}\chi_{\epsilon v J}(R) \tag{2.32}$$

where μ is the reduced mass of the two nuclei with masses M_a and M_b;

$$\mu = \frac{M_a M_b}{M_a + M_b}.$$

ϵ is a set of quantum numbers specifying symmetry properties of an electronic wavefuntion, as is described in the previous section. A set of nuclear quantum numbers ν is composed of v and J, the vibrational and the rotational quantum number respectively. $J(J+1)/2\mu R^2$ is a centrifigual potential.

2.4.2 Vibrational wavefunction and the WKB approximation method

For a smoothly varying potential one can use the semiclassical WKB method (chapter VII of [Landau 1977], chapter 2 of [Child 1991]) to approximately solve the equation for the nuclear vibrational wavefunction. If the motion is subject to a single potential (say $V_{\epsilon J}(R) = E^e_\epsilon(R) + J(J+1)/(2\mu R^2)$), the corresponding WKB wavefunction with an energy value $E_{\epsilon vJ}$ is given by

$$\begin{aligned}
\chi_{\epsilon vJ}(R) &= \frac{A^+}{\sqrt{k_{\epsilon vJ}(R)}} \exp\left[+i\int^R k_{\epsilon vJ}(R')dR'\right] \\
&\quad + \frac{A^-}{\sqrt{k_{\epsilon vJ}(R)}} \exp\left[-i\int^R k_{\epsilon vJ}(R')dR'\right], \\
k_{\epsilon vJ}(R) &= \sqrt{2\mu[E_{\epsilon vJ} - V_{\epsilon J}(R)]}
\end{aligned}$$

or equivalently

$$\chi_{\epsilon vJ}(R) = \frac{A}{\sqrt{k_{\epsilon vJ}(R)}} \cos\left[\int^R k_{\epsilon vJ}(R')dR' + \alpha\right],$$

the validity condition for which is(p. 11 of [Child 1991])

$$\left|\frac{dk}{dR}\right| \ll |k^2(R)|$$

or, since the local de Broglie wavelength $\lambda(R) = 1/2\pi k(R)$

$$\left|\frac{d\lambda}{dR}\right| \ll 2\pi.$$

It is apparent that the smooth variation of V ensures the magnitude of dk/dR to be small.

The WKB wavefunction is singular when $k(R) = 0$ (classical turning points) because of the $[k(R)]^{-1/2}$ factor, and the above validity criteria are violated around these turning points. The first inequality also indicates that the WKB method becomes more reliable for higher k values. For this reason the WKB wavefunction is also sometimes called a 'semiclassical' or 'quasi-classical' wavefunction.

For real k, the WKB wavefunction is a generalized form of a free wavefuntion $\exp(\pm ikR)$, kR being replaced by the integral $\int^R k(R')dR'$. In classically forbidden regions where $k(R)$ is imaginary (i.e., $E < V$) $\chi(R)$ becomes

$$\begin{aligned}\chi_{\epsilon vJ}(R) &= \frac{B^+}{\sqrt{|k_{\epsilon vJ}(R)|}} \exp\left[+\int^R |k_{\epsilon vJ}(R')|dR'\right] \\ &\quad + \frac{B^-}{\sqrt{|k_{\epsilon vJ}(R)|}} \exp\left[-\int^R |k_{\epsilon vJ}(R')|dR'\right].\end{aligned}$$

In order for this to be a physically acceptable solution, the amplitude of the wavefunction must decrease exponentially to zero as one moves away from a turning point. So we may write

$$\chi_{\epsilon vJ}(R) = \frac{B}{\sqrt{|k_{\epsilon vJ}(R)|}} \exp\left[-\left|\int^R k_{\epsilon vJ}(R')dR'\right|\right].$$

The remaining job is then to find a way to connect the wavefunctions separated by the turning points, which in turn will help to determine a relationship between the yet unspecified coefficients A_+, A_- and B.

One method is to regard the potential curve in the neighbourhood of a turning point

as a linear function of R and exactly solve a nuclear equation for $\chi(R)$ in that region. Alternatively, as was discussed by Child (section A.2 of [Child 1991]) and by Landau (§47 of [Landau 1977]), the above coefficients can also be obtained by examining their behaviour in the complex plane. Taking a turning point a to be the starting point of integration, all these methods lead to the relation

$$\begin{pmatrix} A^+ \\ A^- \end{pmatrix} = B \begin{pmatrix} \exp -i\pi/4 \\ \exp i\pi/4 \end{pmatrix}. \tag{2.33}$$

Therefore for real k $(E > V(R))$

$$\chi_{evJ} = \frac{2B}{\sqrt{k_{evJ}(R)}} \cos(|\int_a^R k_{evJ}(R')dR'| - \frac{\pi}{4}) \tag{2.34}$$

and for imaginary k $(E < V(R))$

$$\chi_{evJ} = \frac{B}{\sqrt{|k_{evJ}(R)|}} \exp\left[-\left|\int_a^R k_{evJ}(R')dR'\right|\right].$$

These wavefunctions are written in a form invariant to the side of the turning point on which classically allowed and forbidden regions are located (p. 169 of [Landau 1977]).

When a classically allowed region is bound by two turning points a and $b(> a)$, E_{evJ} are quantized and we have discrete energy levels. Taking b as the starting point we get another expression for the WKB wavefunction in the classically allowed region;

$$\chi_{evJ} = 2C \cos\left[\left|\int_b^R k_{evJ}(R')dR'\right| - \frac{\pi}{4}\right]. \tag{2.35}$$

As Eqs. (2.34) and (2.35) should represent the same wavefunction the sum of their

phases must be an integral multiple of π:

$$\left[\left|\int_a^R k_{\epsilon vJ}(R')dR'\right| - \frac{\pi}{4}\right] + \left[\left|\int_b^R k_{\epsilon vJ}(R')dR'\right| - \frac{\pi}{4}\right] = n\pi$$

which can be rewritten as

$$\begin{aligned} \int_a^R k_{\epsilon vJ}(R')dR' - \int_b^R k_{\epsilon vJ}(R')dR' &= \\ \int_a^b k_{\epsilon vJ}(R')dR' &= (n+\frac{1}{2})\pi \end{aligned} \tag{2.36}$$

with $B = (-1)^n C$. Eq. (2.36) is in accordance with the well-known Bohr-Sommerfield quantization rule (§48 of [Landau 1977]). The energy $E_{\epsilon vJ}$ of the nuclear wavefunction is then obtained as a function of $J(J+1)$ and n by evaluating the left side of Eq. (2.36).

Chapter 3

Ab Initio Study of Electronic States of a Diatomic Molecule

3.1 The Variation Method

3.1.1 The variation principle

As was previously mentioned, it is impossible to solve the BO electronic equation (2.12) exactly, except for the molecular hydrogen ion H_2^+ or other single electron diatomic molecular ions. Most ab initio methods to find an approximate solution of Eq. (2.12) are based on a theorem called the 'variation principle' which states that

> "The expectation value of an energy operator $\hat{O}$ with a given normalized wavefunction Ψ which satisfies appropriate boundary conditions always represents an upper bound to the exact lowest eigenvalue $\mathcal{E}_1$ of $\hat{O}$."

That is,

$$\int \Psi^* \hat{O} \Psi d\tau \geq \mathcal{E}_1. \tag{3.1}$$

Once a trial wavefunction containing a set of adjustable parameters is given, one can vary these parameters to find an optimal wavefunction which minimizes the expectation value of a given hermitian operator $\hat{O}$. This procedure is called the variation method. Let $\{c_J | J = 1, \ldots, n\}$ be n such parmeters a wavefunction Ψ depends upon. Then the problem is to solve the following n equations for the c_Js;

$$\frac{\partial}{\partial c_J} \int \Psi^* \hat{O} \Psi d\tau = 0, \quad J = 1, \ldots, n \tag{3.2}$$

with the condition that Ψ is kept normalized. The resultant wavefunction gives the minimum expectation value of $\hat{O}$ that can be obtained with a given trial wavefunction. How close the expectation value and the optimized wavefunction are to the lowest eigenvalue $\mathcal{E}_1$ and the exact ground state wavefunction depends upon the form and the flexibility of the trial wavefunction. As the variation principle indicates that the minimized expectation value thus obtained is an upper bound to $\mathcal{E}_1$ the expectation value will never be minimized below $\mathcal{E}_1$, thus a measure of improvement obtained by using a more suitable and flexible trial wavefunction will in general correspond to the amount by which the expectation value is lowered, that is, the wavefunction with lower energy is generally closer to the exact ground state wavefunction.

3.1.2 Application of the variation method to solve for excited states

When one applies the variation method to solve for an excited state, the situation is somewhat different. The minimized expectation value (say E') is not necessarily higher than the exact eigenvalue (say $\mathcal{E}'$) of that excited state, unless the trial wavefunction

giving E' upon optimization is orthogonal to the exact ground state wavefunction, which is not known in most cases. To prove this (and also the above variation principle) we first expand a trial wavefunction using the complete set of the exact orthonormal eigenfunctions Φ_J as a basis assuming all the levels are discrete;

$$\Psi = \sum_J c_J \Phi_J$$

where Φ_1 is the ground state wavefunction with an eigenvalue $\mathcal{E}_1$, Φ_2 the first excited state with an eigenvalue $\mathcal{E}_2 > \mathcal{E}_1$ and so forth, provided there is no degeneracy. Then

$$\begin{aligned}
\int \Psi^* \hat{O} \Psi d\tau &= \sum_{J=1} c_J \int \Psi^* \hat{O} \Phi_J d\tau \\
&= \sum_{J=1} \mathcal{E}_J c_J \int \Psi^* \Phi_J d\tau \\
&= \sum_{I,J=1} \mathcal{E}_J c_I^* c_J \int \Phi_I^* \Phi_J d\tau \\
&= \sum_{J=1} \mathcal{E}_J |c_J|^2 \\
&\geq \mathcal{E}_1
\end{aligned}$$

for $\sum_J |c_J|^2 = 1$ by the normalization condition. This proves the variation principle. Next, if Ψ is orthogonal to Φ_1, c_1 is zero. The summation will then start from $J = 2$, and by proceeding similarly one finds

$$\int \Psi^* \hat{O} \Psi d\tau \geq \mathcal{E}_2.$$

Therefore, if a trial wavefunction is chosen to be orthogonal to the K eigenfunctions $\Phi_1, \Phi_2, \ldots, \Phi_{K-1}$ and Φ_K the corresponding expectation value will be an upper bound to $\mathcal{E}_{K+1}$.

3.2 Linear Variation Method and Construction of Electronic Wavefunction

3.2.1 Derivation of secular equation using the linear variation method

Based on the discussions presented in the previous section we now apply the variation method to calculate wavefunctions of the electronic Hamiltonian $\hat{H}^e$. As noted previously, $\hat{H}^e$ is a hermitian operator and the electronic wavefunction Ψ_ϵ^e can be assumed to be real. Our aim is to find approximate solutions for various states of a diatomic molecule.

An electronic state of a heteronuclear diatomic molecule is labelled by a symbol ${}^{2S+1}\Lambda^{\pm}$, the + or − sign appearing only for Σ states($\Lambda = 0$). States with different labels (e.g., different S or different Λ) belong to different IRs of a symmetry group and are orthogonal to each other. Hence the minimized eigenvalue of a trial wavefunction belonging to one IR will be an upper bound to the eigenvalue of the lowest eigenstate of the same IR provided that variation of the trial wavefunction does not change its symmetry.

In the previous section, in order to prove the variation principle we expressed a trial wavefunction as a linear combination of the exact eigenfunctions. Any set of mutually orthonormal functions can be used in a like manner to construct a trial wavefunction, its coefficients then becoming variable parameters

$$\Psi_\epsilon^e = \sum_{J=1}^{n} c_J \Phi_J$$

so that

$$\begin{aligned} \int \Psi_\epsilon^e \hat{H}^e \Psi_\epsilon^e d\tau &= \sum_{I,J=1}^{n} c_I c_J \int \Phi_I \hat{H}^e \Phi_J d\tau \\ &\equiv \sum_{I,J=1}^{n} c_I c_J H_{IJ}^e. \end{aligned} \tag{3.3}$$

The normalization condition is expressed as

$$\sum_{J=1}^{n} |c_J|^2 = 1 \tag{3.4}$$

where n is the number of functions used to expand Ψ_ϵ^e and is also the number of parameters to be optimized. Our job is then to find values of linear coefficients c_J which minimize the above expectation value under the constraint (3.4). This is called the linear variation method. We will assume that the expansion functions are generated to possess the correct symmetry properties of a given molecular system ('symmetry adapted'). Such an expansion function is conventionally called a CSF (configuration state function).

The normalization condition (3.4), which places a restriction on variation of the coefficients, is taken into account by using the Lagrange undetermined multiplier method to minimize a modified function L instead of the expectation value of $\hat{H}^e$;

$$\frac{\partial L}{\partial c_K} = 0, \quad K = 1, 2, \ldots, n-1 \tag{3.5}$$

where

$$L(c_1, c_2, \ldots, c_n, E^e) = \sum_{I,J=1}^{n} c_I c_J H_{ij}^e - E^e \sum_{J=1}^{n} (|c_J|^2 - 1) \tag{3.6}$$

and E^e is an undetermined Lagrange multiplier. Substituting Eq. (3.6) into Eq. (3.5) results in a set of following equations for the c_Js (p. 37 of [Szabo 1989]);

$$\sum_{J=1}^{n} H_{IJ}^{e} c_J = E c_I, \;\; I = 1, 2, \ldots, n-1, n \tag{3.7}$$

which can be rewritten in matrix form as

$$\mathbf{H}^e \mathbf{c} = E^e \mathbf{c}, \tag{3.8}$$

an eigenvalue problem for the matrix $\mathbf{H}^e$. Thus the Lagrange multiplier E^e is an electronic energy eigenvalue. The eigenvalues are found by solving the secular equation

$$|\mathbf{H}^e - E^e \mathbf{I}| = 0 \tag{3.9}$$

and the eigenvectors are obtained by solving Eq. (3.8) with each value of E^e calculated from Eq. (3.9). They are orthogonal to each other. The number of E^es one finds is the same as the number of CSFs used.

3.2.2 Relationships between the eigenvalues of the secular equation

In addition to the variation principle stated above, the eigenvalues obtained with the linear varitaion method follow another useful relation. Let

$$E_1, E_2, \ldots, E_{n-1}, E_n; \;\; E_I < E_J \text{ if } I < J$$

be n eigenvalues we found by solving Eq. (3.9), the corresponding eigenfunctions being $\Psi_1^e, \Psi_2^e, \ldots, \Psi_{n-1}^e, \Psi_n^e$ which are linear combinations of CSFs $\Phi_1, \Phi_2, \ldots, \Phi_{n-1}, \Phi_n$. In order to obtain better solutions one may increase the number of CSFs. We let Φ_{n+1} be a function such that

$$\int \Psi_I^e \Phi_{n+1} d\tau = 0 \text{ for all } I = 1, 2, \ldots, n-1, n$$

and use the linear variation method with a new set of CSFs $\Psi_1^e, \Psi_2^e, \ldots, \Psi_{n-1}^e, \Psi_n^e$ and Φ_{n+1}. $\mathbf{H}^e$ will then be diagonal up to the n-th row and column

$$H_{IJ}^e = \delta_{IJ} E_I, \quad I, J = 1, 2, \ldots, n-1, n$$

and the last $((n+1)$-th) row and column being

$$H_I^e \equiv H_{n+1I}^e = H_{In+1}^e = \int \Psi_I \hat{H}^e \Phi_{n+1} d\tau.$$

Hence the left side of Eq. (3.9) becomes [MacDonald 1933]

$$\begin{aligned} |\mathbf{H}^e - E\mathbf{I}| &= (H_{n+1}^e - E) \prod_{I=1}^{n} (E_I - E) - \sum_{K=1}^{n+1} |H_K^e|^2 \prod_{I(\neq K)=1}^{n} (E_I - E) \\ &\equiv f(E) \end{aligned}$$

which can be looked at as a function of E, an n-th degree polynomial of E.

We note that

$$\lim_{E \to -\infty} f(E) = \infty, \quad \lim_{E \to \infty} f(E) = (-1)^n \infty$$

and

$$\begin{aligned} f(E_I) &\geq 0 \text{ if } I \text{ is even,} \\ &\leq 0 \text{ if } I \text{ is odd.} \end{aligned}$$

Thus if $f(E)$ is plotted against E, roots of $f(E)$ (say E'_I) must lie in such a way that

$$E'_1 \leq E_1 \leq E'_2 \leq E_2 \leq \ldots E'_{n-1} \leq E_{n-1} \leq E'_n \leq E_n \leq E'_{n+1}. \tag{3.10}$$

As the dimension of the matrix $\mathbf{H}^e$ increases, one may assume that its eigenfunctions and eigenvalues will converge to the exact answers. Hence one can conclude that the following inequalities will hold for any value of n;

$$\mathcal{E}_I \leq E_I, \;\; I = 1, 2, \ldots, n-1, n, \tag{3.11}$$

that is, the eigenvalue E_I calculated using the linear variation method is not only an upper bound to the exact ground state energy $\mathcal{E}_1$ but also to $\mathcal{E}_I$ of the exact I-th state. The corresponding wavefunction Φ_I does not need to satisfy the orthogonality condition of the previous section in order for the inequality (3.11) to be true. This upper boundedness of the energy values enables us to assess the accuracy of not only the ground state solutions but also the excited states with relative ease, making the linear variation scheme one of the most favoured ab initio calculation methods especially when one is interested in the excited states.

3.2.3 Construction of a trial electronic wavefunction : a configuration state function

The fact that the linear differential equations (3.5) are converted into the matrix eigenvalue equation (3.8) is also a great advantage in performing the calculation as, once trial wavefunctions are chosen, the rest of the procedure consists merely of solving the associated eigenvalue equation. Therefore the quality of solutions calculated using the linear variation method is determined by how adequately the trial wavefunctions are chosen to reproduce the behavior of actual solutions and how many such functions are employed in the calculation.

The most commonly used trial wavefunction in the ab initio calculation of an N-electron system is an antisymmetrized product of N one-electron functions ϕ_ps called a 'Slater determinant'

$$\Phi = (N!)^{-1/2} \begin{vmatrix} \phi_p(\mathbf{x}_1) & \phi_q(\mathbf{x}_1) & \dots & \phi_r(\mathbf{x}_1) \\ \phi_p(\mathbf{x}_2) & \phi_q(\mathbf{x}_2) & \dots & \phi_r(\mathbf{x}_2) \\ \vdots & \vdots & & \vdots \\ \phi_p(\mathbf{x}_{N-1}) & \phi_q(\mathbf{x}_{N-1}) & \dots & \phi_r(\mathbf{x}_{N-1}) \\ \phi_p(\mathbf{x}_N) & \phi_q(\mathbf{x}_N) & \dots & \phi_r(\mathbf{x}_N) \end{vmatrix}$$

or equivalently in alternative form

$$\Phi = \hat{\mathcal{A}} \prod_{m=1}^{N} \phi_{p_m}(\mathbf{x}_m) \tag{3.12}$$

where $\hat{\mathcal{A}}$ is an antisymmetrizer

$$\hat{\mathcal{A}} = (N!)^{-1/2} \sum_P \epsilon(P)\hat{P}.$$

$\hat{P}$ is a permutation operator which permutes coordinate indices m. $\epsilon(P)$, called a parity of $\hat{P}$, is 1 for even permutations and -1 for odd permutations. $\hat{P}$ is even if it takes an even number of successive interchanges of two indices to obtain the same ordering of the whole N indices as the one produced by $\hat{P}$, and odd otherwise. Any Φ's of the above form and their linear combinations satisfy the antisymmetry principle.

In the non-relativistic picture a one-electron function ϕ_p is written as a product of a spatial function ψ_p and a spin function ω;

$$\phi_p(\mathbf{x}) = \psi_p(\mathbf{r})\omega(\sigma)$$

so that $\Phi(\mathbf{x})$ becomes

$$\Phi(\mathbf{x}) = \hat{\mathcal{A}} \prod_{m=1}^{N} \psi_{p_m}(\mathbf{r}_m)\omega(\sigma_m),$$

σ_m taking values $1/2$ or $-1/2$ corresponding to up or down spin of the m-th electron. Following chemical terminology one may call ϕ_p an orbital, or more precisely a spin orbital to remind one of the presence of a spin function ω in ϕ_p. One simple way to express a one-electron spin function is to let α denote a spin up and β a spin down function.

When the spatial function ψ_p belongs to an IR of $C_{\infty v}$, so do the product of ψ_p's and linear combinations thereof. ψ_p is called a 'restricted' orbital if the same spatial function is used to represent electrons of both spin. Spatial symmetry of an orbital,

determined by the magnitude of the projection of its orbital angular momentum λ, is specified by a lower case greek letter (for example, σ, π, δ and so forth).

Restricted spatial orbitals of $C_{\infty v}$ symmetry generate a shell structure similar to that of atomic cases. The antisymmetry principle enforced on molecular wavefunction by the operator $\hat{\mathcal{A}}$ ensures that only one electron can be assigned to each spin orbital. Alternatively, one may say that (in spin free formalism) each non-degenerate spatial orbital (an orbital of σ symmetry) may hold up to two electrons and others (for example π, δ orbitals which are all doubly degenerate) up to four. A wavefunction Φ whose spatial orbitals are fully occupied is called a 'closed shell' wavefunction which is totally symmetric ($^1\Sigma^+$ state for the electronic ground state of most diatomic molecules), and in this case a single Slater determinant becomes a spin eigenfunction.

However, spin symmetry may or may not in general be fulfilled by a single Slater determinant; if not, several determinants need to be combined together to generate a spin eigenfunction. Thorough discussions regarding spin symmetry and use of direct product representation to generate antisymmetric many-electron wavefunction of correct spin and spatial symmetry can be found elsewhere (e.g., see [Pauncz 1979, Kaplan 1975]).

3.2.4 Generation of the Hamiltonian matrix element using trial electronic wavefunctions

Once we have constructed a molecular wavefunction antisymmetric with respect to the exchange of any two electronic coordinate indices, the spin part of the wavefunction plays no further part in the calculation and can be omitted. Provided that spatial orbitals ψ_p are orthogonal to each other and the trial wavefunctions Φ_i are spin eigenfunctions, the

Hamiltonian matrix element H^e_{IJ} in Eq. (3.3) can be written as [Werner 1985]

$$H^e_{IJ} = \sum_{p,q} \gamma^{IJ}_{pq} h_{pq} + \frac{1}{2} \sum_{p,q,r,s} \Gamma^{IJ}_{pqrs} g_{pqrs} \tag{3.13}$$

where

$$\begin{aligned} \hat{h}_i &= -\frac{1}{2}\nabla_i^2 + \sum_{A=1}^{2} -\frac{Z_A}{r_{Ai}}, \\ \hat{g}_{ij} &= \frac{1}{r_{ij}}, \\ h_{pq} &= \int \psi_p(\mathbf{r}_1)\hat{h}_1\psi_q(\mathbf{r}_1)d\mathbf{r}_1 \end{aligned}$$

and

$$g_{pqrs} = \int \psi_p(\mathbf{r}_1)\psi_r(\mathbf{r}_2)\hat{g}_{12}\psi_q(\mathbf{r}_1)\psi_s(\mathbf{r}_2)d\mathbf{r}_1 d\mathbf{r}_2.$$

The terms γ^{IJ}_{pq} and Γ^{IJ}_{pqrs}, called the coupling coefficients, are determined by the structure of the expansion functions and are independent of the form of ψ. From the elements γ and Γ one can construct the following matrices $\boldsymbol{\gamma}$ and $\boldsymbol{\Gamma}$;

$$\gamma_{pq} = \sum_{IJ} c_I c_J \gamma^{ij}_{pq} \tag{3.14}$$

$$\Gamma_{pqrs} = \sum_{ij} c_I c_J \Gamma^{IJ}_{pqrs} \tag{3.15}$$

which are called the first order and the second order density matrices respectively. The Eq. (3.3) can then be expressed as

$$\bar{E}^e_\epsilon \equiv \int \Psi^e_\epsilon \hat{H}^e \Psi^e_\epsilon d\tau \tag{3.16}$$

$$= \sum_{pq} \gamma_{pq} h_{pq} + \frac{1}{2} \sum_{pqrs} \Gamma_{pqrs} g_{pqrs}. \tag{3.17}$$

One can write Eq. (3.17) in a simpler form if the terms Γ_{pqrs} and g_{pqrs} are treated as the elements of matrices $(\mathbf{\Gamma}^{rs})$ and $(\mathbf{g}^{rs})$ in the p-th row and the q-th column. Since γ and $\mathbf{h}$ are already symmetric matrices due to the orbitals being real, Eq. (3.17) then turns into

$$\bar{E}^e_\epsilon = \mathrm{tr}(\mathbf{h}\gamma) + \frac{1}{2}\sum_{rs}\mathrm{tr}[(\mathbf{g}^{rs})(\mathbf{P}^{sr})] \tag{3.18}$$

where $(\mathbf{P}^{sr})$ is a symmetrized density matrix whose elements are

$$(\mathbf{P}^{sr}) = \frac{1}{2}((\mathbf{\Gamma}^{sr}) + (\mathbf{\Gamma}^{sr})^t),$$

a superscript t denoting the transpose of a matrix. Parentheses are used to remind that the matrices are built from the quadruply indexed elements.

We will further define two other matrices $\mathbf{Q}_{sr}$ and $\mathbf{K}_{rs}$ for later use;

$$(\mathbf{Q}^{sr})_{pq} = \frac{1}{2}(\Gamma_{psqr} + \Gamma_{spqr}) \tag{3.19}$$

$$(\mathbf{K}^{rs})_{pq} = g_{prsq}. \tag{3.20}$$

3.3 LCAO-MO : Basis Set

3.3.1 Generation of molecular orbitals : linear combination of atomic orbitals

Spatial orbitals needed to build electronic trial wavefunctions are usually constructed from one electron functions called atomic orbitals ξ centered at each constituent atom

(two atoms in diatomic case);

$$\psi_p = \sum_\mu d_{\mu p} \xi_\mu. \tag{3.21}$$

This method of construction is called the LCAO(Linear Combination of Atomic Orbitals)-MO(Molecular Orbital) method, ψ's being called molecular orbitals(MOs hereafter) in analogy to atomic orbitals(AOs). If one wants to distinguish AOs centered at different atoms, one may rewrite Eq. (3.21) as

$$\psi_p = \sum_\alpha d_{\alpha p} \xi_\alpha^A + \sum_\beta d_{\beta p} \xi_\beta^B$$

where the index α is for AOs centered at the atom A and β for those centered at the atom B.

3.3.2 Gaussian-type atomic orbitals

Basis set is a term used to denote a collection of atomic orbitals chosen to generate molecular orbitals. Most commonly employed AOs are cartesian functions of the form

$$\xi = N^c_{pqr\kappa} x^p y^q z^r e^{-\kappa r^2}$$

or spherical functions

$$\xi = N^s_{n\kappa} r^{n-1} e^{-\kappa r^2} \Theta_{lm}(\theta, \varphi),$$

which are called Gaussian Type Orbitals(GTOs). N^c and N^s are normalization constants. The origin of the coordinates x, y, z and r is at the corresponding nucleus. GTOs carry designations s, p, d and so forth, according to which irreducible representation of the three-dimensional rotation group they belong to. For spherical GTOs

the value of orbital angular momentum quantum number l determines the designation, while cartesian GTOs are labelled according to the following;

$$\begin{aligned}
\xi[s] &= N^c_{000\kappa} e^{-\kappa r^2}, \\
\xi[p_x] &= N^c_{100\kappa} x e^{-\kappa r^2}, \\
\xi[p_y] &= N^c_{010\kappa} y e^{-\kappa r^2}, \\
\xi[p_z] &= N^c_{001\kappa} z e^{-\kappa r^2}, \\
\xi[d_{xx}] &= N^c_{200\kappa} x^2 e^{-\kappa r^2}, \\
\xi[d_{xy}] &= N^c_{110\kappa} xy e^{-\kappa r^2}, \\
\xi[d_{xz}] &= N^c_{101\kappa} xz e^{-\kappa r^2}, \\
\xi[d_{yy}] &= N^c_{020\kappa} y^2 e^{-\kappa r^2}, \\
\xi[d_{yz}] &= N^c_{011\kappa} yz e^{-\kappa r^2}, \text{ and} \\
\xi[d_{zz}] &= N^c_{002\kappa} e^{-\kappa r^2}.
\end{aligned}$$

Thus, we have two different kinds of coefficients to optimize in an ab initio calculation. One is a set of coefficients c (which we shall call 'configuration coefficients') in Eq. (3.8), the other being a set of d (orbital coefficients).

GTOs have the problem of displaying an incorrect behaviour near the nucleus, known as the 'cusp' problem[Wilson 1987] due to the term $e^{-\kappa r^2}$, whereas the appropriate atomic orbitals, which are conventionally called Slater Type Orbitals(STOs) should be of the form $e^{-\kappa r}$ and thus have non-zero values of $d\xi/dr$ at $r = 0$. STOs, however, are harder to work with, especially in the evaluation of the two-center integrals g_{pqrs}. A common solution to this problem is to approximate a single STO with several GTOs of

various exponents and of the same symmetry as that of the chosen STO,

$$\xi' = N' \sum_{i=1}^{n} d'_i \xi(\kappa_i). \tag{3.22}$$

A basis set made up of n such functions ξ' is called an STO-nG basis. Fig. 3.1 show a comparison between STO and STO-nG AOs with various n values. Although it takes a larger number of GTOs than of STOs to obtain a result of similar accuracy, it is generally understood that the ease with which Hamiltonian matrix elements are computed more than compensates the disadvantage of having to employ more AOs. The coefficients d'_i in Eq. (3.22) are called 'contraction' coefficients, which are usually kept constant during an ab initio calculation, and ξ' is called a contracted GTO (CGTO). A core electron, an inner electron that is tightly bound around a nucleus, is not thought to contribute appreciably towards the formation of a molecule and thus is considered to be well represented by a single CGTO which is constructed based on atomic calculation results. Outer electrons, also called valence electrons, are seen to be closely related to molecular binding so that the orbital coefficients of MOs of the outer electrons will be dependent upon the internuclear distance and hence can not be contracted. Furthermore, in order to properly describe molecular wavefunction, extra uncontracted GTOs in addition to the ones obtained from atomic results are employed to give more flexibility to valence orbitals.

Reviews and listings of various kinds of basis sets, which we will not go into in detail, can be found in numerous references (see, for example, [Dunning 1977], [Huzinaga 1984] and [Wilson 1987]).

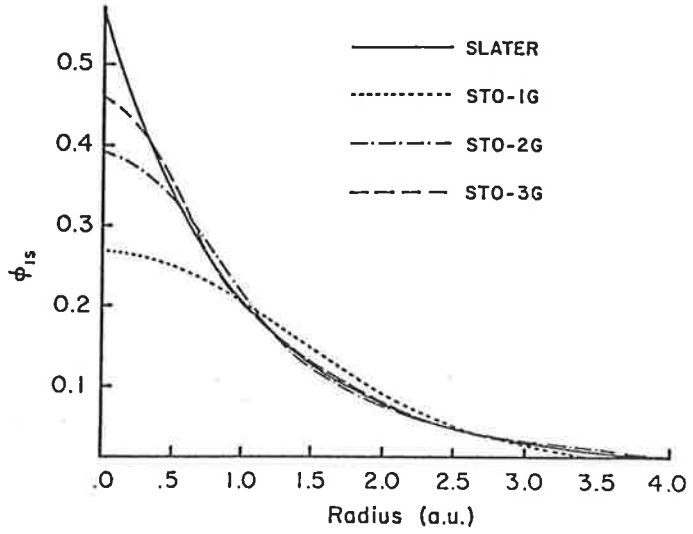

Figure 3.1: Comparison of the $1s$ STO($\kappa = 1.0$) and the STO-1G, STO-2G and STO-3G GTO's, taken from p.158 of [Szabo 1989].

3.4 Optimization of an Electronic Wavefunction : Overview of the HF and post-HF Methods

Having chosen a basis set with which we want to represent molecular orbitals, our job is to build a total electronic wavefunction and find the values of the configuration coefficients and the orbital coefficients which minimize the Hamiltonian expectation value. If one is allowed to vary the configuration coefficients only, the problem is equivalent to solving the eigenvalue equation (3.8). This is called the CI(configuration interaction) method.

In the early days of ab initio calculations, just a single Slater determinant was employed as a trial wavefunction, the orbital coefficients being the only variable parameters during the optimization process. This procedure is called the HF-SCF(Hartree Fock-self consistent field) method, a brief explanation of which will be given in the beginning of

the next section.

Although the HF-SCF method provides a reliable wavefunction for the ground states of closed shell molecules(electronic states of $^1\Sigma^+$ symmetry), a single Slater determinant is not sufficient to properly represent the excited state wavefunctions and the states of nonzero spin values ($S \neq 0$). Two or more Slater determinants are needed to construct an electronic wavefunction which is also a spin eigenfunction in case of nonzero spin. In addition, it was also soon realised that, even for the closed shell ground state, the HF-SCF wavefunction is reasonable only around the equilibrium internuclear distance and is inadequate to describe an electronic wavefunction at a large internuclear distance, where one needs more than one Slater determinant in general to describe the dissociative behaviour of a given molecule correctly.

In order to resolve the above deficiencies of the HF-SCF method, one may proceed to perform a CI calculation using the MOs obtained from the HF-SCF calculation (HF-MOs). If all the CSFs that can be generated from the HFMOs are used in the CI calculation, the resultant wavefunction is the best approximation to the exact eigenfunction of $\hat{H}^e$ that can be obtained with a given basis set. This is called the FCI (Full CI) method. However, even with a basis set of moderate size-say, a basis set of 20 or so AOs-the number of total CSFs becomes very large and it is not only impractical but also almost impossible to perform an FCI calculation in most cases.

Even when a CI calculation with a limited number of MOs and/or CSFs is performed, which is referred to as a truncated CI, one still has to face several problems. First of all, the virtual HFMOs (the unoccupied HFMOs obtained as a byproduct of a HF-SCF calculation) are not localized near the same region where the occupied MOs have nonzero amplitudes and are generally highly oscillatory and diffuse. Hence one

still needs to include a large number of CSFs in the CI calculation to achieve a worthwhile improvement over the HF-SCF result. Instead of HFMOs, Löwdin [Löwdin 1955] suggested the use of natural orbitals (NOs) in a CI calculation which will then involve a smaller number of CSFs than the CSFs constructed from the HFMOs. However, in order to obtain the exact NOs(which are the eigenfunctions of the first order density matrix) it is still required to perform a CI calculation with the original MOs (be they HFMOs or not), which defeats the initial purpose of wanting to avoid a long CI. In the actual calculation, approximate NOs(for example, INOs obtained by the iterative natural orbital method [Bender 1966]) are used instead. Other methods in which the virtual orbitals are modified to perform better in CI have been also suggested (for example, see [Beebe 1979]).

Next, the selection of CSFs also requires some consideration. In a conventional CI calculation, the CSFs are usually chosen by the degree of the electron excitation with respect to the reference wavefunction(s) (that is, the number of electrons that are promoted from the occupied orbitals to the virtual orbitals) which one needs to carry out to construct those CSFs. For example, if one employs only singly and doubly excited CSFs in a CI calculation, it is called an SDCI (singly and doubly excited configuration interaction) calculation. But this method may still result in a huge number of CSFs unless the list of MOs to be used in a CI are also truncated. There are other selection schemes that are based on perturbation theory, cluster expansion approach, and so forth, but they have been used mainly for closed shell ground state wavefunctions. Another drawback of these selection schemes is that since they are not based on the variation method the calculated expectation value is no longer an upper bound to the exact eigenvalue of the electronic Hamiltonian.

It is beyond the scope of this thesis to discuss thoroughly the technical aspects of the difficulties mentioned above. Instead we shall only focus on understanding these difficulties in relation to the calculation of the potential energy surface for the ground and the low excited electronic states. What we want to obtain is a set of potential curves which characterize the several electronic states with a uniform accuracy. Here a 'uniformly accurate' wavefunction in the ideal case means a wavefunction whose energy expectation values differ from the FCI energy values by the same amount at all internuclear distances, thereby producing a potential curve that is parallel to the FCI potential curve of the same electronic state. The HF-SCF method is, as was indicated above, adequate only for a description of the ground state in a region around the equilibrium internuclear distance. Thus the conventional truncated CI methods in which the CSFs are chosen by, for instance, the degree of electron excitation (SDCI for example) from the HF wavefunction may not produce a uniformly accurate potential curve. In addition, we want to obtain uniformly accurate potential curves of not only the ground state but also of several excited states, and we further want these potential curves to be uniformly accurate with respect to each other.

Therefore it is natural to look for a method which incorporates both the efficient orbital optimization scheme of the HF-SCF and the conceptual simplicity of the CI methods and thus is applicable not only to the closed shell ground state but also is capable of handling other states of various molecular symmetry with an equal accuracy. The MR-CI (Multi Reference CI) method in which two or more Slater determinants are chosen as the reference wavefunction compensates for the deficiency of single reference CI methods, but may still suffer from the requirement of having to use a large number of configurations as the MOs that are used in a CI are the ones obtained from the HF-SCF

procedure.

In the MCSCF (Multi Configuration Self Consistent Field) method, a trial wavefunction is made up of several CSFs each of which is constructed to belong to the same appropriate IRs of symmetry groups and both its orbital coefficients and configuration coefficients are optimized to yield the stationary expectation value of the electronic Hamiltonian $\hat{H}^e$. Since not only the configuration coefficients but also the orbital coefficients are optimized at each internuclear distance, one may expect that the MCSCF method is capable of providing the optimized electronic wavefunctions (including the excited state wavefunctions) of any symmetry over a wide range of internuclear distance by using a relatively moderate number of CSFs. Although there still remains a question of how one should choose MOs and CSFs that are to be used in this calculation, for several decades the MCSCF method has been gradually receiving more interest for reasons stated above and is the procedure which is chosen as the primary method of electronic wavefunction calculation in this thesis.

3.5 The MCSCF-CASSCF Method

3.5.1 The Hartree-Fock (HF) method

Use of the variation method to find the optimal orbital coefficients of a single determinant closed shell wavefunction that minimzes the expectation value of the electronic Hamiltonian leads to the matrix equation (p. 142 of [Szabo 1989])

$$\mathbf{FD} = \mathbf{SD}\varepsilon \tag{3.23}$$

where $\mathbf{D}$ is a square matrix whose columns are made up of the orbital coefficients $d_{\mu p}$, and $\mathbf{S}$ is the overlap matrix with elements $S_{\mu\nu} = \int \xi_\mu \xi_\nu d\mathbf{r}$. The elements of ε are the Lagrangean multipliers introduced to ensure that the MO's are orthonormal. $\mathbf{F}$ is the so-called Fock matrix

$$F_{\mu\nu} = h_{\mu\nu} + \sum_{p}^{n/2} \sum_{\sigma\lambda} d_{\sigma p} d_{\lambda p} (2g_{\mu\nu\sigma\lambda} - g_{\mu\lambda\sigma\nu}), \tag{3.24}$$

with n being the number of electrons. The meanings of $h_{\mu\nu}$ and $g_{\mu\nu\sigma\lambda}$ are the same as those in Section 3.2. Because of the dependence of $\mathbf{F}$ on $\mathbf{D}$, Eq. (3.23) is solved iteratively. This optimisation process can be further simplified if the basis functions used to express the MO's are orthogonal by themselves, in which case $\mathbf{S}$ becomes the identity matrix so that Eq. (3.23) reduces to

$$\mathbf{FD} = \mathbf{D}\varepsilon. \tag{3.25}$$

Thus the optimization of the orbital coefficients is carried out in the following order;

1. For a given basis set, find a matrix $\mathbf{Z}$ which diagonalizes $\mathbf{S}$ by the similarity transformation; $\mathbf{Z}^t\mathbf{S}\mathbf{Z} = \mathbf{I}$.

2. Choose an initial guess of a matrix $\mathbf{D}$. The p-th column of $\mathbf{D}$ is an array of the orbital coefficients of the MO ψ_p as in the Eq. (3.21).

3. Construct $\mathbf{F}$ and solve the equation $\tilde{\mathbf{F}}\tilde{\mathbf{D}}' = \tilde{\mathbf{D}}'\varepsilon$ where $\tilde{\mathbf{F}} = \mathbf{Z}^t\mathbf{F}\mathbf{Z}$.

4. Construct a matrix $\mathbf{D}' = \mathbf{Z}\tilde{\mathbf{D}}'$, the elements of which generate a new set of the orbital coefficients.

5. Compare $\mathbf{D}'$ with $\mathbf{D}$. If they are not close enough, replace $\mathbf{D}$ with $\mathbf{D}'$ and repeat steps 3 and 4.

This is the HF method.

3.5.2 Optimization of a multideterminant wavefunction : the unitary transformation approach

Generalization of the HF method to the optimization of multideterminant electronic wavefunction carries a number of complications. As in Eq. (3.3) the energy expectation value of a multideterminant wavefunction depends on both the configuration and the orbital coefficients, thereby making the corresponding Fock matrix more complex and orbital optimization harder to perform. Since any single determinant wavefunction is invariant to a unitary transformation of the orbitals in the wavefunction, it is possible to convert Eq. (3.23) into the simple matrix eigenvalue equation (3.25) by a unitary transformation of the orbitals which does not change the minimized energy expectation value while rendering $\mathbf{S}$ diagonal (see p. 121 of [Szabo 1989]). This is not possible for a multideterminant wavefunction as some orbitals that appear in one determinant are not present in the other. Due to the complex nature of the Fock matrix, in the early attempts of optimizing a multideterminant wavefunction by HF-like iterative methods one needed to impose further constraints on the optimization process which in turn resulted in a poorer convergence and initial guess orbitals had to be chosen very carefully. Early MCSCF methods and their drawbacks are discussed, for example, in [Werner 1980] and [Lengsfield III 1980].

To avoid these problems, more recent MCSCF schemes employ a method in which the variation of the orbital coefficients are represented by an exponentially parametrized

unitary matrix $\mathbf{U} \equiv \exp(\mathbf{R})$ acting on the orbitals(c.f., [Werner 1987], [Shepard 1987] and [Jørgensen 1981]);

$$\Psi_\epsilon^e = \sum_{J=1}^{n} c_J[\exp(\mathbf{R})\Phi_J] \tag{3.26}$$

where $\exp(\mathbf{R})\Phi_J$ is defined to be a CSF whose orbitals are transformed as

$$\phi'_p = \sum_q [\exp(\mathbf{R})]_{qp}\phi_q. \tag{3.27}$$

We note that in order for $\mathbf{U} = \exp(\mathbf{R}) = \mathbf{I}+\mathbf{R}+\mathbf{R}^2/2+\cdots$ to be a unitary matrix(or an orthogonal matrix as the orbitals are assumed real) $\mathbf{R}$ must be antisymmetric ($\mathbf{R}^t = -\mathbf{R}$). The energy expectation value is then written in the form

$$\bar{E} = \sum_{IJ} c_I c_J \int [\exp(\mathbf{R})\Phi_I]\hat{H}^e[\exp(\mathbf{R})\Phi_J]d\tau_e \tag{3.28}$$

where the superscript e and the subscript ϵ are omitted for notational convenience.

There exist several optimization methods which feature slightly different expressions for $\bar{E}$. We will only briefly look at the procedure adopted by Werner [Werner 1987] and Werner and Knowles [Werner 1985], in which one first defines a matrix $\mathbf{T}$ and changes in the orbitals $\Delta\phi_p$ as

$$\Delta\phi_p = \phi'_p - \phi_p = \sum_q T_{qp}\phi_p \tag{3.29}$$

and

$$\mathbf{T} = \mathbf{U} - \mathbf{I} = \mathbf{R} + \frac{1}{2}\mathbf{R}^2 + \cdots, \tag{3.30}$$

after which $\bar{E}$ is expanded up to the second order in $\mathbf{T}$. With the intermediate procedures

omitted, this results in the following expression

$$E^{(2)}(\mathbf{T}) = E^{(0)} + \mathrm{tr}[\mathbf{T}^t(\mathbf{A}+\mathbf{B})] \tag{3.31}$$

with

$$\mathbf{A} = \mathbf{h}\gamma + \sum_{rs}(\mathbf{g}^{rs})(\mathbf{P}^{sr}) \tag{3.32}$$

$$\mathbf{B} = \mathbf{A} + \mathbf{h}\mathbf{T}\gamma + \sum_{rs}[(\mathbf{g}^{rs})\mathbf{T}(\mathbf{P}^{sr}) + 2(\mathbf{K}^{rs})\mathbf{T}(\mathbf{Q}^{sr})]. \tag{3.33}$$

A superscript on E denotes the highest power of $\mathbf{T}$ included in the energy expression.

A small variation of $\mathbf{U}$(and thus $\mathbf{T}$ as well) in $\mathbf{R}$ is then considered up to the second order in $\mathbf{R}$;

$$\begin{aligned}\mathbf{U}(\mathbf{R}+\Delta\mathbf{R}) &= \mathbf{U}(\mathbf{R})\mathbf{U}(\Delta\mathbf{R}) \\ &= \mathbf{U} + \mathbf{U}(\Delta\mathbf{R} + \frac{1}{2}(\Delta\mathbf{R})^2 + \cdots)\end{aligned}$$

which according to Werner and Knowles[Werner 1985] leads to the following stationary condition

$$\mathbf{U}^t\mathbf{B} - \mathbf{B}^t\mathbf{U} = 0 \tag{3.34}$$

that is to be solved for $\mathbf{U}$. In other words $E^{(2)}(\mathbf{T})$ is stationary with respect to the orbital variation if $\mathbf{U} = \mathbf{I} + \mathbf{T}$ satisfies Eq. (3.34).

To find a stationary condition for a column vector of the orthonormal configuration coefficients $\mathbf{c}$, $E^{(2)}(\mathbf{T})$ is written in the alternative form

$$E^{(2)}(\mathbf{T}) = \mathbf{c}^t\mathbf{H}^{(2)}\mathbf{c}$$

where $\mathbf{H}^{(2)}$ is an electronic Hamiltonian matrix that depends on $\mathbf{T}$ up to the second order, elements of which are

$$H_{IJ}^{(2)} = \sum_{pq}(\mathbf{U}^t\mathbf{h}\mathbf{U})_{pq}\gamma_{pq}^{IJ} + \frac{1}{2}\sum_{pqrs} g_{pqrs}^{(2)}\Gamma_{pqrs}^{IJ}.$$

$g_{pqrs}^{(2)}$ is the second order approximation to the two-electron integral between the unitarily transformed orbitals

$$g_{pqrs}^{(2)} = -g_{pqrs} + (\mathbf{U}^t\mathbf{G}^{rs}\mathbf{U})_{pq} + (\mathbf{U}^t\mathbf{G}^{pq}\mathbf{U})_{rs} + (1+\hat{\tau}_{pq})(1+\hat{\tau}_{rs})(\mathbf{T}^t\mathbf{K}^{pr}\mathbf{T})_{qs}.$$

$\hat{\tau}_{pq}$ is a permutation operator that interchanges the orbital indices p and q. Application of the variation method to obtain optimal $\mathbf{c}$ results in the eigenvalue equation similar to Eq. (3.8);

$$\mathbf{H}^{(2)}\mathbf{c} = E^{(2)}\mathbf{c}. \tag{3.35}$$

Since Eqs. (3.34) and (3.35) depend on both the orbital and the configuration variation they can not be solved straightforwardly. With a given set of initial guess orbitals, optimization procedure of Werner et al. begins by solving Eq. (3.35) for $\mathbf{c}$ while $\mathbf{U}$ is initially set to the identity matrix, from which the elements of $\Delta\mathbf{R}$ are found consequently. $\Delta\mathbf{R}$ is then used in Eq. (3.34) to update $\mathbf{U}$ and the new set of orbitals are obtained from $\mathbf{T} = \mathbf{U} - \mathbf{I}$ and Eq (3.27). This cycle is repeated until Eq. (3.34) is satisfied to the desired accuracy. In principle, one may not only calculate for the lowest state of given symmetry but also for any excited states by choosing which root of Eq. (3.35) to solve for. However, since an excited state eigenfunction must meet the further condition that it should be orthogonal to all of the lower eigenfunctions, for a fixed number of MOs the

optimization of the wavefunction belonging to a higher root of Eq. (3.35) has a lesser degree of freedom, producing a result of poorer quality when compared to the wavefunctions of lower roots. This issue is discussed in some detail by Shepard [Shepard 1987]. As we are only interested in the lowest and the first excited states at most, it will be reasonable to assume that the problem with the quality of excited state wavefunctions is not a serious concern for our purpose.

One of the advantages Werner's method has over other second order MCSCF schemes is that the energy expectation value is expanded up to the second order not in $\mathbf{R}$, but in $\mathbf{T}$ which is of infinite order in $\mathbf{R}$ so that $E^{(2)}(\mathbf{T})$ is a closer approximation of the true energy expectation value than $E^{(2)}(\mathbf{R})$ (E that is expanded up to the second order in $\mathbf{R}$) is. In practical terms, this means that an optimization with $E^{(2)}(\mathbf{T})$ has a larger radius of convergence. Consequently the effectiveness of the optimization becomes less sensitive to the choice of initial guess orbitals, which has always been a crucial factor and also a serious concern in obtaining a reliable solution with MCSCF calculation. More detailed reviews and discussions of the various MCSCF procedures and computational adaptation thereof, some of which also includes comparison of different methods, can be found in the references mentioned above.

3.5.3 Choice of molecular orbitals : complete active space (CAS) scheme

Another aspect that has to be considered in MCSCF calculations is a choice of CSFs; what and how many CSFs to choose. This also involves a determination of the number of orbitals to be employed. The main purpose of employing the MCSCF method is to find an optimal electronic wavefunction that does not contain too many CSFs but yields a

uniformly accurate potential curve over a wide range of nuclear geometry. Since an FCI result is independent of orbital variation due to using all the orbitals and CSFs that can be generated from a given basis set, one may deduce that inclusion of a larger number of CSFs and orbitals renders the motivation behind the use of MCSCF less meaningful even though a larger calculation produces a result closer to the FCI limit. Furthermore, the calculation must be able to provide an impartial treatment of all the electronic states of interest, which would in general require a very careful selection of orbitals and CSFs for each electronic state. Therefore, in addition to the time taken to carry out the CI and orbital optimization calculation, these selection procedures themselves that one has to perform for several electronic states may also become extremely time consuming as more orbitals and CSFs are added to the calculation.

An optimization of an electronic wavefunction based on the CAS (Complete Active Space) method [Roos 1987] presents a way to avert some if not all of these difficulties. In the CAS approach every CSF that can be generated from a set of chosen orbitals is included in a MCSCF calculation. Thus a selection process of the CSFs is avoided and within the expansion space spanned by given orbitals the calculation is not biased towards any irreducible representation of a particular molecular symmetry. The idea of the CAS method has been around since as early as late 1960s but its satisfactory computational implementation was not possible until 1980s due to an inability to process a large number of CSFs. However, after the introduction of the UGA(Unitary Group Approach) method [Karwowski 1992, Paldus 1992] and the advancement in computer technology which enabled the use of vector processing machines, effective algorithms that can put the CAS scheme into practice became available.

In a CAS-MCSCF (or CASSCF in short) procedure, with a given set of initial guess

orbitals which are usually obtained from HF calculations, one only has to decide what orbitals should be optimized and how many electrons are included in the calculation. Initial orbitals are divided into three groups; the first group is of core orbitals which are kept occupied and held fixed during the optimization, the second group is made of active orbitals (also called valence orbitals) that should be optimized. The last group consists of external orbitals which do not appear in any of the CSFs. In a similar manner electrons are also grouped and identified as core electrons and active electrons. As one restricted spatial orbital can hold up to two electrons, the number of orbitals in a calculation is the number of all electrons minus twice the number of core orbitals. The minimum number of active electrons are determined by the nature of bonding interaction of a given molecule; for example if a covalent diatomic molecule is single bonded the minimum number of active electron is one, two if double bonded, and so forth. For ionic diatomic molecules all the electrons that are located in the outermost subshells in each nuclei are usually treated as active electrons, which means at least eight electrons are kept active in most ionic cases.

The innermost electrons that are tightly bound close to the constituent nuclei are almost completely chemically inactive and they are considered not to participate in molecular formation. Active orbitals are made up of the occupied orbitals that are not chosen as the core orbitals and some of the virtual orbitals (orbitals that were not occupied in the preceding HF calculation). There is no universal guideline on which and how many virtual orbitals should be chosen as active orbitals, except that it is customary to have at least one virtual active orbital for each occupied active orbital. For example, if the occupied active orbitals consist of 3σ, 4σ and 1π then the selected virtual orbitals should include at least 5σ, 6σ and 2π. An article by Roos [Roos 1987] contains in-

depth discussions of orbital selection using various examples. Another nice source of CAS method discussions is a series of articles by Ruedenberg et al. [Ruedenberg 1982, Ruedenberg 1982a, Ruedenberg 1982b], in which the method is called a FORS (Fully Optimized Reaction Space) method but is equivalent to the CAS scheme.

The main calculational strategy adopted in this research is CASSCF optimization of electronic wavefunctions based on the second order energy minimization method by Werner and Knowles [Werner 1985]. Issues more specific to the NaI molecule are discussed in the next chapter.

Chapter 4

Ab Initio Calculation of NaI

4.1 Effective Core Potential

For a molecule consisting of heavy atoms, the large number of the electrons makes the calculation of electronic wavefunctions and their energies prohibitively expensive of computer time and memory, especially when one wants to use post-HF methods, as the number of CSFs increases drastically in proportion to the number of electrons. Introducing the idea of the core orbitals which are kept doubly occupied helps to avoid this difficulty to a certain degree, which may be still insufficient if a molecule contains an atom belonging to the third or higher row in the chemical table.

A method was thus sought for with which chemically inactive inner electrons (core electrons) can be removed from a calculation without seriously affecting its accuracy. This can be achieved by replacing the core electrons with a potential function that simulates the electrostatic interaction arising from them. Such a potential function is called an effective core potential (ECP), a model potential, or a compact effective potential (CEP) etc., among which we will use the term ECP hereafter.

In order to obtain an ECP for a given atom, one must first solve the corresponding all electron atomic HF equation for the spatial atomic orbitals and their HF energy eigenvalues. Efficient numerical procedures are available and known to yield very accurate HF solutions in atomic cases. Then the AOs are divided into two groups, one being the core group and the other the valence group. An ECP proposed by Stevens, Basch and Krauss[Stevens 1984], which is often referred to as an SBK-ECP, is constructed from the set of 'pseudo' valence orbitals ζ_{li} of a following form

$$\begin{aligned} \zeta_{li}(r) &= \sum_{k=0} c_k r^{N+k} \text{ if } r \leq R_l, \\ \zeta_{li}(r) &= \psi_{li}(r) \text{ if } r \geq R_l. \end{aligned} \tag{4.1}$$

R_l is a match point dependent upon an atomic orbital angular momentum quantum number l, and $\psi_{li}(r)$ is an AO obtained from the all electron calculation. In other words, for radial distances greater than some preset value R_l, $\zeta_{li}(r)$ is defined to be the same as the valence AO $\psi_{li}(r)$, and for smaller distances, a polynomial expansion in r whose value approaches zero smoothly as r approaches zero. The coefficients c_k are found by ensuring that $\zeta_{li}(r)$ is analytic at $r = R_l$. Stevens et al. chose the values of R_l to coincide with the location of the outermost maximum of the radial function $r\psi_{lj}(r)$. The value of N is set to 3 and the summation over k is from 0 to 4.

The valence-only atomic HF equation is written as [Stevens 1984]

$$\left[-\frac{1}{2}\nabla_A^2 - \frac{Z_{\text{eff}}}{r} + \frac{l(l+1)}{2r^2} + \hat{V'}_{\text{val}} + \hat{V}_l^{\text{eff}}\right]\zeta_{li} = \epsilon_{li}\zeta_{li}, \tag{4.2}$$

with Z_{eff} a nuclear charge minus the number of core electrons and $\hat{V'}_{\text{val}}$ the Coulomb and exchange operators summed over the occupied pseudo valence orbitals. $\hat{V}_l^{\text{eff}}$ is an

l-dependent component of an ECP $\hat{V}^{\text{eff}}$ whose effect on $\zeta_{li}(r)$ is defined as

$$\hat{V}^{\text{eff}}(r)\zeta_{li}(r) = \sum_{l=0}^{\infty} \hat{V}_l^{\text{eff}}(r) \sum_{m=-l}^{l} \Theta_{lm} \int \Theta_{lm}^{*} \zeta_{li} d\tau, \tag{4.3}$$

or alternatively

$$\hat{V}^{\text{eff}}(r)\zeta_{li}(r) = \hat{V}_{L+1}^{\text{eff}}(r) + \sum_{l=0}^{L} [\hat{V}_l^{\text{eff}}(r) - \hat{V}_{L+1}^{\text{eff}}(r)] \sum_{m=-l}^{l} \Theta_{lm} \int \Theta_{lm}^{*} \zeta_{li} d\tau \tag{4.4}$$

where L is equal to the maximum value of l and the eigenvalue ϵ_{li} is the same as that of the all electron orbital ψ_{li}. Discussions regarding the l-dependence of ECPs can be found elsewhere [Kahn 1976, Stevens 1984, Stevens 1992]. Stevens et al. [Stevens 1984, Stevens 1992] presents two ways of getting an ECP; one method is to invert Eq. (4.2) to obtain V_l^{eff} directly from ζ_{li} and ϵ_{li}, the other being an iterative method in which a parametrized trial ECP is adjusted until the variationally determined subsequent pseudo-orbitals and their eigenvalues are sufficiently close to ζ_{li}s obtained from Eqs. (4.1) and ϵ_{li}s. The latter method was employed by Stevens et al. with the trial ECP $\tilde{V}_l^{\text{eff}}$ expressed as

$$\tilde{V}_l^{\text{eff}} = r^{-2} \sum_{l} A_{lj} r^{n_{lj}} \exp(-B_{lj} r^2) \tag{4.5}$$

where $n_{lj} = 0, 1,$ or 2 and A_{lj}, B_{lj} are parameters to be optimized.

Relativistic effects can be taken into account by using the Dirac-Fock equation instead of the HF equation when obtaining the all-electron results [Stevens 1984].

The choice of ECP in our calculation was based mainly on the options available within the ab initio packages used in this research, so the details regarding the derivation and comparison of the various ECPs will not be presented here.

4.2 Results of CASSCF calculations

4.2.1 Introductory remarks

The potential curves of the several low energy electronic states of NaI were calculated using the ab initio packages MOLPRO ([MOLPRO], [Werner 1985], [Knowles 1985]) and GAMESS [Schmidt 1993]. Both packages support the use of ECP and CASSCF methods. The two lowest $^1\Sigma^+$ states and the lowest $^1\Pi$ and $^3\Pi$ states were of main interest in this research, which are understood to play a major role in the formation of the transition spectra observed in various UV laser spectroscopic investigations [Berry 1979].

Results obtained with GAMESS will not be shown here as GAMESS had serious problems in handling spatial symmetry, which are briefly explained in this section.

Initial guess orbitals needed in a CASSCF calculation were in most instances taken from the CASSCF orbitals obtained at nearby internuclear distance, except the first CASSCF orbitals that had to be calculated from the HF orbitals. Then the subsequent CASSCF calculations were done with internuclear distance increased (or decreased) by 0.1 or 0.2 Å from the previous location.

There were a number of difficulties encountered during the calculation, especially with the two states of $^1\Sigma^+$ symmetry, whose potential curves exhibit an avoided crossing. The sum of the energies of two neutral atoms Na and I is smaller than the sum of the energies of two ions Na^+ and I^-, thus the lower adiabatic $^1\Sigma^+$ state, being the electronic ground state of NaI molecule, is ionic for small internuclear distances and then becomes atomic at large internuclear distances, dissociating to neutral Na and I atoms. On the other hand, the upper adiabatic $^1\Sigma^+$ state (which we shall refer to as the excited state, dropping the word 'first' for convenience) shows the opposite behaviour; atomic at small

Atom	l	j	A_{lj}	n_{lj}	B_{lj}
Na	$0(s)$	1	10.8390	0	1.3780
	$1(p)$	1	2.3030	0	0.6639
	$2(d)$	1	-1.7770	0	0.9249
I	$0(s)$	1	95.2644	0	3.3151
		2	0.7518	0	1.6575
	$1(p)$	1	53.7980	0	4.0000
		2	24.6479	0	2.0000
	$2(d)$	1	12.7669	0	1.1050
		2	-0.4228	0	0.5525

Table 4.1: Parameters for the ECP potentials (c.f., Eq. (4.5)) employed in this calculation.

internuclear distances and then dissociating to two ions Na^+ and I^-. Such a change of characteristics of the wavefunction can make the use of the adiabatic approximation inadequate in the region where the change takes place. In CASSCF calculations, this may prevent the wavefunctions from converging.

The ECPs and basis sets used in our calculations are those given by Fuentealba et al. [Fuentealba 1982] and Igell-Mann et al. [Igell-Mann 1988]. The basis sets were further augmented by adding two d-type polarization functions, and an s- and p-type diffuse functions that share the same gaussian exponent (which are called L-type functions). They are shown in Tab. 4.1 and Tab. 4.2.

4.2.2 CASSCF calcualtions

Spatial symmetry of the MOs and the total electronic wavefunctions are only partially recognized within the symmetry group C_{2v}, the Abelian subgroup of the axially symmetric group $C_{\infty v}$, by MOLPRO. Thus it is necessary to find the relations between the IRs of C_{2v} and $C_{\infty v}$. This can be achieved by comparing the character (sum of the

Atom	Type	Exponent	Contraction Coefficient
Na	s	2.60443	0.008824
		0.51772	-0.183227
		0.05820	0.652017
	s	0.02314	1.000000
	p	0.49921	0.018547
		0.07922	0.276211
		0.02995	0.587004
	p	0.01261	1.000000
	L	0.00760	1.000000
	d	0.35000	1.000000
	d	0.08750	1.000000
I	s	2.91470	0.193703
		1.36857	-0.716446
		0.40516	0.630846
	s	0.14502	1.000000
	p	1.17651	-0.218693
		0.45937	0.441181
		0.16607	0.617221
	p	0.06128	1.000000
	L	0.03680	1.000000
	d	0.53200	1.000000
	d	0.13300	1.000000

Table 4.2: List of the basis sets employed in this calculation.

diagonal elements of a matrix representing given symmetry operation) tables of these two groups. For example, Σ^+ and Π states (IRs) in which we are interested correspond respectively to A_1 and $B_{1,2}$ states (IRs) of C_{2v}. The one-to-two correspondence for Π states result from the fact that Π and other non-zero Λ states are doubly degenerate and thus belong to two-dimensional IRs, whereas for C_{2v} which is Abelian all four IRs are one-dimensional. The MOs are labelled in a similar manner; σ orbitals are of A_1 symmetry and π orbitals of $B_{1,2}$. The character table for C_{2v} as well as the meanings of A_1 and $B_{1,2}$ can be found, for example, in chapter 4 of [Hammermesh 1962].

An initial HF calculation at the internuclear distance $R = 2.8$ Å, was performed in order to obtain the initial guess orbitals to be used in the CASSCF calculation. Ten and forty six electrons and protons in Na and I respectively, are replaced by ECPs, leaving eight electrons in the active space, which was chosen to be made of six σ and three π orbitals. The number of CSFs generated from this active space for each electronic state is given in Tab. 4.3. This was the largest CASSCF calculation one could perform in a reasonable time with the computing facility we used. Although the spatial symmetry of an electronic wavefunction is identified only in reference to the C_{2v} group, MOLPRO has an option of specifying the value of Λ so that the axial symmetry of the wavefunction can be properly accounted for.

GAMESS can use the C_{4v} group to identify the spatial symmetry of MOs and total electronic wavefunctions, and the CASSCF calculation is carried out under the C_{2v} group. This means that while the construction of the wavefunction and the CI part of the calculation is done under the C_{2v} group, and the MOs are varied and optimized under the constraint that they belong to the IRs of C_{4v}. However for the Π states, it was found that such a constraint was not maintained during the calculation and the symmetry of some of the σ MOs could only be identified under the C_{2v} group or not be identified at all.

The optimization of the two $^1\Sigma^+$ states could be initially performed both in C_{4v} and C_{2v} without the optimized MOs losing their symmetry, although there were convergence problems when R was greater than 6 Å which is to be expected since the adiabatic potential curves approach close to each other there. However, the values of calculated energy depended critically upon the initial guess and type of symmetry used in the optimization.

Since these problems made it difficult to trust the results of our calculation, an alternative way was sought for to obtain more reliable results. The program MOLPRO was thus chosen and we will discuss the results obtained with it.

Except for $^1\Sigma^+$ states, there was little difficulty in achieving convergence within fewer than five iterations. However, the optimization of the ground state or the first excited $^1\Sigma^+$ state wavefunction still carried the problem of the wavefunctions becoming divergent when R was greater than 6.5 Å. For the ground state, although converged results could be obtained for R larger than 6.5 Å, the calculation began to diverge at $R = 7.8$ Å. Therefore we chose to perform another series of optimizations starting from $R = 10$ Å, taking the orbitals optimized an initial guess. Thereby we could obtain a converged result for the ground $^1\Sigma^+$ state at $R = 10$ Å, which was then used as an initial guess for a calculation with $R = 9.5$ Å, and so on. This new series of optimizations was carried out until $R = 6$ Å. The energies obtained in the new series of calculations turned out to be lower than those from the old calculations where 7.0 Å$\leq R \leq$ 7.6 Å, and were accepted as more accurate results in that region.

Problems with the symmetry of the MOs were not enountered. Thus it seems reasonable to assume that the results with MOLPRO are more reliable than the GAMESS results. The potential curves are shown in Fig. 4.1, which includes all the states that can be generated from the ground atomic states of Na and I. All the potentials are vertically shifted by an equal amount in order to make their horizontal asymptotes for large R coincide with the estimate 3.18 eV of the atomic dissociation limit[van Veen 1979]. Although the calculations for the excited $^1\Sigma^+$ state failed to converge near the crossing region, they provide a starting point for obtaining a theoretical estimate of the shape of the inner limb of the corresponding potential curve.

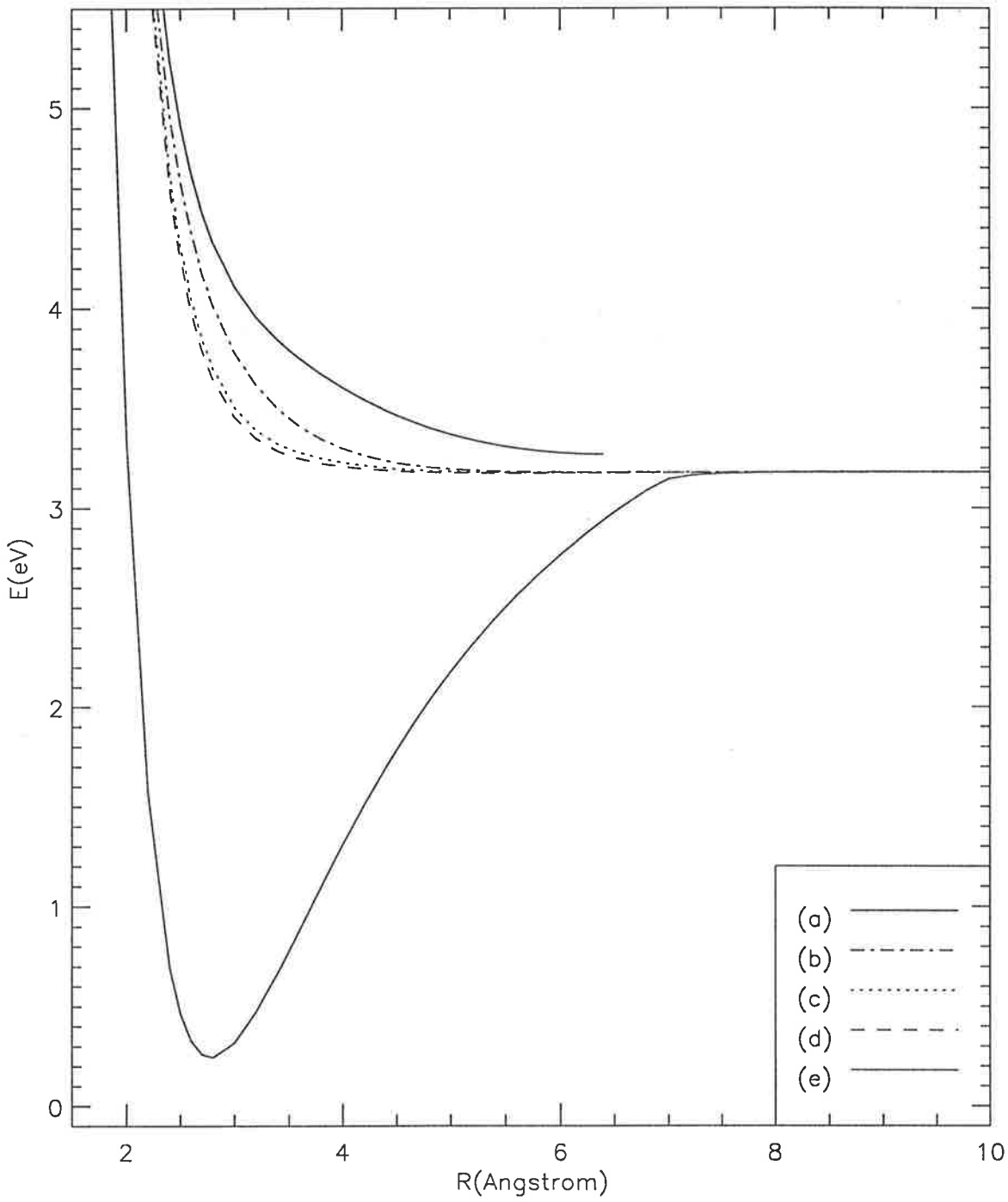

Figure 4.1: CASSCF calculation of the potential curves of NaI; (a) the first excited $^1\Sigma^+$ (top solid line), (b) $^3\Sigma^+$, (c) $^1\Pi$, (d) $^3\Pi$ and (e) the ground state $^1\Sigma^+$ (bottom solid line).

4.2.3 State-averaged CASSCF followed by SDCI

In order to overcome the convergence difficulties and obtain the first excited $^1\Sigma^+$ state potential curve for R greater than 6.5 Å, state-averaged (SA) CASSCF calculations with a smaller number of MOs in the active space were performed, which were then followed by multi-reference (MR) SDCI calculations using the CASSCF wavefunctions as reference functions and allowing the single and double excitations to all of the remaining external MOs (MOs not optimized in CASSCF step). The purpose of using the state-averaging method, in which the wavefunctions of more than one state are weighted as appropriate and then added together to form a single hypothetical wavefunction, is to stabilize the excited state wavefunctions during the orbital optimization process by combining them with the converged ground state wavefunctions. As a result, one obtains a single set of optimized MOs instead of two sets (or three if three states are combined together), from which the electronic wavefunctions and their eigenvalues are found by CI calculations within the chosen active space. Since the results optimized by the state-averaging method are less accurate than those obtained by the pure optimization for each state, MRSDCI calculations were subsequently performed. Furthermore, we had to use a smaller sized active space (that is, smaller number of active orbitals) for state-averaged optimization in order to prevent the number of CSFs for the subsequent SDCI calculations from becoming unmanageably large. Four σ and one π orbitals are chosen as active orbitals in our SA-CASSCF calculations. The number of CSFs generated for each CASSCF and MRSDCI calculation are shown at Tab. 4.3.

In a state-averaged CASSCF calculation, density matrices $\boldsymbol{\gamma}$ and $\boldsymbol{\Gamma}$ are replaced by

method	symmetry	number of CSFs
CASSCF	$^1\Sigma^+$	18153
	$^1\Pi$	17640
	$^3\Pi$	28344
	$^3\Sigma^+$	28248
SA-CASSCF	$^1\Sigma^+$	492
MRSDCI	$^1\Sigma^+$	44172

Table 4.3: Number of CSFs generated by CASSCF and SA-CASSCF-MRSDCI calculations.

[Werner 1987]

$$\gamma_{pq} = \sum_n W_n \sum_{IJ} c_I^n c_J^n \gamma_{pq}^{IJ} \tag{4.6}$$

$$\Gamma_{pqrs} = \sum_n W_n \sum_{IJ} c_I^n c_J^n \Gamma_{pqrs}^{IJ} \tag{4.7}$$

with W_n a weight factor for the n-th state. Thus instead of finding the purely optimized states, the optimization of MOs is done in an averaged fashion. Two states are combined with equal weight, that is, W_1 and W_2 are both set to 0.5.

With the use of the state-averaged optimisation method the previous convergence difficulties were overcome and thus the potential curves in the region of the avoided crossing and beyond were obtained. The results are shown in Fig. 4.2.

4.2.4 Dipole moments of the CASSCF-SDCI wavefunctions

As a check on the reasonableness of the result of the ab initio calculation, we consider the electric dipole moment. Fig. 4.3 shows the plot of the electric dipole moments of NaI versus R for the two $^1\Sigma^+$ states. The dipole moment $\boldsymbol{\mu}_i(R)$ for electronic state $\Psi_i^e(\mathbf{r};R)$ is

$$\boldsymbol{\mu}_i(R) = \int \Psi_i^e(\mathbf{r};R)\mathbf{r}\Psi_i^e(\mathbf{r};R)d\tau_e. \tag{4.8}$$

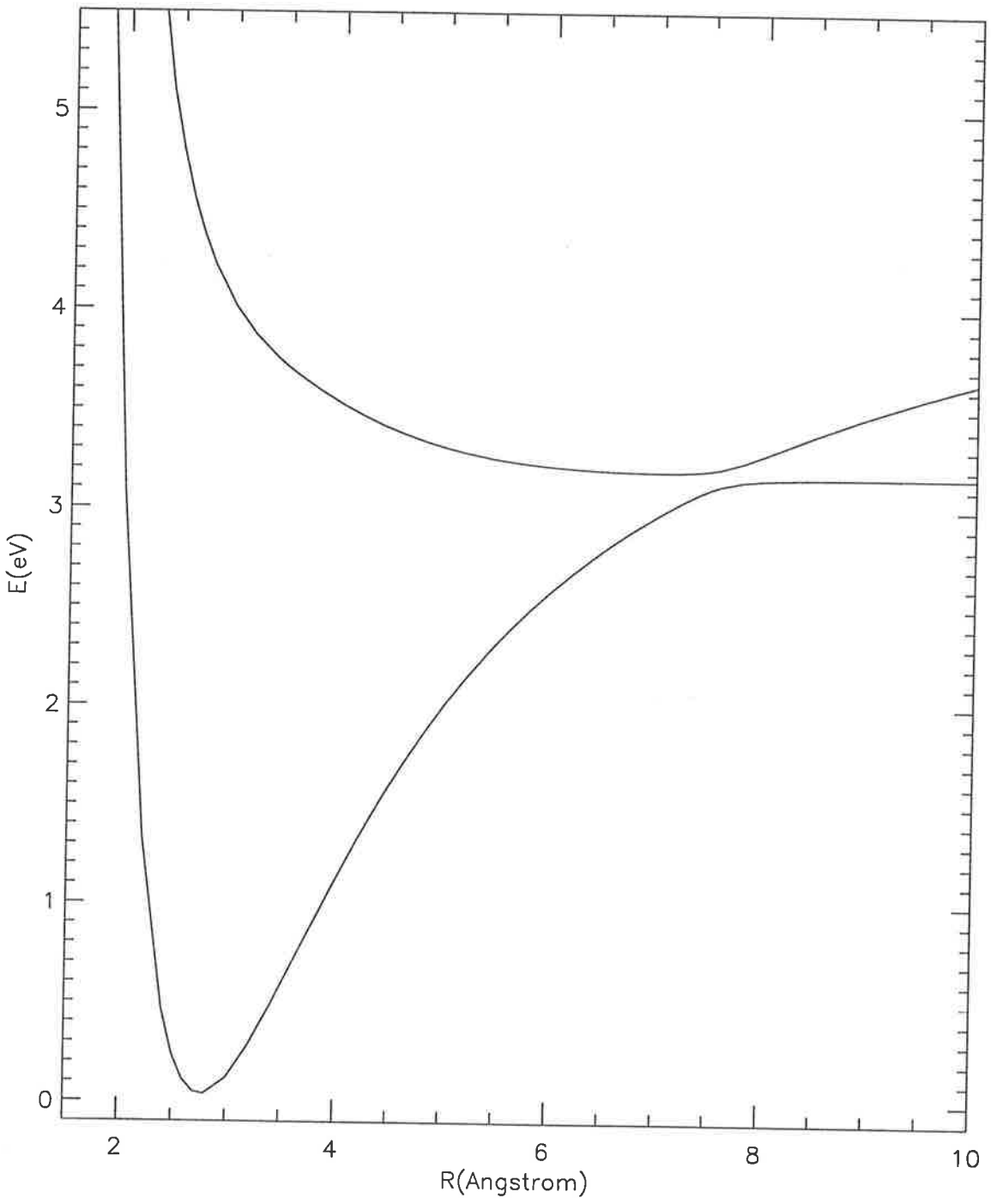

Figure 4.2: SA-CASSCF-MRSDCI calculation of the ground (lower solid line) and the first excited (upper solid line) $^1\Sigma^+$ states.

Due to the axial symmetry of a diatomic molecule, $\boldsymbol{\mu}_i$ is always directed along the internuclear axis.

One usefulness of optimizing for a common set of MOs lies in that it becomes possible to conveniently calculate the transition dipole moment

$$\boldsymbol{\mu}_{ij}(R) = \int \Psi_i^e(\mathbf{r}; R)\mathbf{r}\Psi_j^e(\mathbf{r}; R)d\tau_e$$

between two states, magnitudes of which are also plotted in Fig. 4.3. As the transition dipole moment is usually assumed constant when one considers transitions involving a change in electronic states, it is of interest to examine how the magnitude of the transition dipole moment changes, especially in a region of R where a large overlap between the vibrational wavefunctions of the initial and the final electronic states is expected. It is also called a Franck-Condon region, and is normally located around the minimum of the ground state potential curve. Fig. 4.3 shows that the variation of the transition dipole moment in R behaves smoothly in the Franck-Condon region (2.5 Å$\leq R \leq$ 3.5 Å). Thus our ab initio calculation justifies the approximation method of assuming the transition dipole moment to be constant.

The peaks of μ_{12} coinciding with the closest approach of the two curves is physically well justified as the largest mixing between thr two adiabatic states is expected occur there. The behaviour of individual dipole moments, being almost linear where the corresponding wavefunctions are ionic while being nearly zero when atomic, is also physically correct.

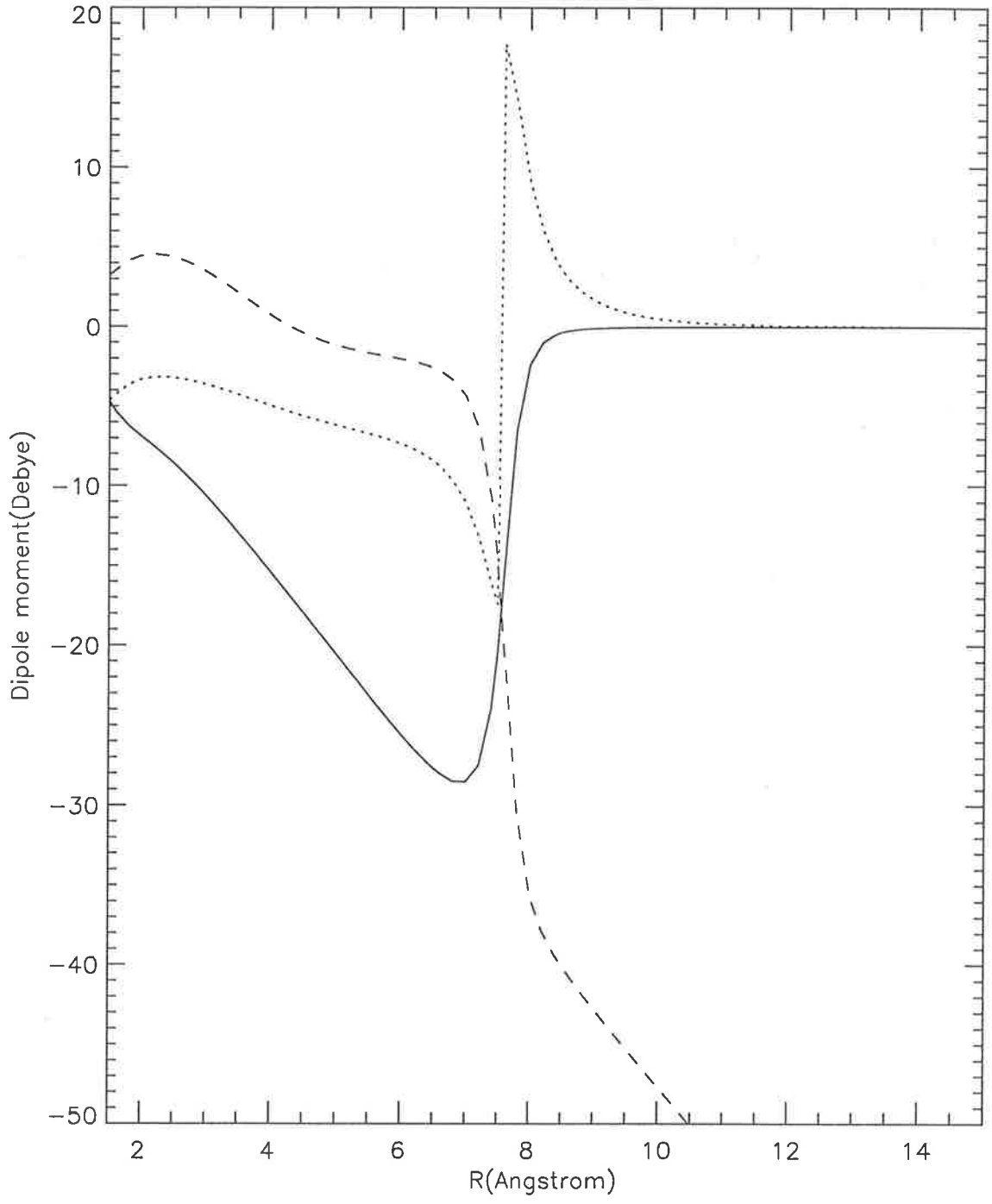

Figure 4.3: Dipole moments of the ground (solid line) and the first excited (broken line) $^1\Sigma^+$ states, and the transition (dotted line) dipole moments between them.

4.3 Discussions on the effects of spin-orbit interaction and other ab initio calculations

Our discussion in this section will be brief, as our ab initio results do not include the calculation of spin-orbit coupling effects.

It is well understood [Condon 1981] that the multiplet splitting (energy difference between the atomic states with the same total spin and orbital angular momentum quantum numbers L and S but with different total angular momentum quantum numbers J) can be explained by the spin-orbit couplings between the individual electronic orbital and spin angular momenta $\mathbf{l}$ and $\mathbf{s}$. The magnitude of this coupling effect increases with increasing atomic number. For an iodine atom whose atomic number is 53 and ground state is ^2P, the energy difference between the states $^2P_{J=3/2}$ and $^2P_{J=1/2}$ is known to be 0.94 eV [Berry 1979] which is not ignorable in understanding the energy level structure of iodine. Thus spin-orbit coupling has appreciable influence on the shape of the NaI potential curves.

4.3.1 Spin-Orbit coupling for atomic cases

For a many electron atom with its atomic number Z, the spin-orbit Hamiltonian $\hat{H}^{SO}$ can be written as [Lefebvre-Brion 1986]

$$\hat{H}^{SO} = \frac{\alpha^2}{2}\sum_i \left(\frac{Z}{r_i^3}\mathbf{l}_i \cdot \mathbf{s}_i\right) - \frac{\alpha^2}{2}\sum_{i\neq j}\frac{1}{r_{ij}^3}(\mathbf{r}_{ij}\times\mathbf{p}_i)\cdot(\mathbf{s}_i + 2\mathbf{s}_j) \tag{4.9}$$

where α is the fine structure constant, r_i the distance from the nucleus to the i-th electron, r_{ij} the distance between the i-th and the j-th electron (while $\mathbf{r}_{ij}$ is a vector

whose magnitude is r_{ij} and is directed from the position of the i-th electron to the position of the j-th electron), and $\mathbf{p}_i$ the momentum of the i-th electron measured in the atom fixed coordinate frame. $\mathbf{l}_i$ and $\mathbf{s}_i$ are the orbital and the spin angular momentum of the i-th electron.

The first term in Eq. (4.9) describes the sum of the spin-orbit coupling of each electron in the nuclear electric field. The first part in the second term (involving $\mathbf{s}_i$) is the sum of the spin-orbit coupling of one electron under the electric field generated by another electron, the second part (with $\mathbf{s}_j$) being the interaction between spin of an electron and the magnetic field generated by the orbital motion of another.

Because of the difficulties in calculating the two-electron interaction of the spin-other orbit coupling, the effect of $\hat{H}^{SO}$ is evaluated approximately by introducing

$$H^{SO} \approx \frac{\alpha^2}{2} \sum_i \frac{Z^{\text{eff}}}{r_i^3} \mathbf{l}_i \cdot \mathbf{s}_i \tag{4.10}$$

with a suitably chosen value of Z^{eff} for a given atom [Koseki 1995]. Further details on the calculation of spin-orbit coupling (including molecular as well as atomic cases) can be found in [Lefebvre-Brion 1986] and references therein.

4.3.2 Spin-Orbit coupling in diatomic molecules

The following account of spin-orbit coupling in diatomic molecules is mainly taken from [Richards 1981] and [Lefebvre-Brion 1986]. We will only make a few elementary remarks without discussing any mathematical details.

Generalization of Eqs. (4.9) and (4.10) to molecular cases is straightforward, as only

a nuclear index needs to be introduced into these operators. Thus we have

$$\hat{H}^{SO} = \frac{\alpha^2}{2} \sum_A \sum_i \left(\frac{Z}{r_{iA}^3} \mathbf{l}_i \cdot \mathbf{s}_i \right) - \frac{\alpha^2}{2} \sum_{i \neq j} \frac{1}{r_{ij}^3} (\mathbf{r}_{ij} \times \mathbf{p}_i) \cdot (\mathbf{s}_i + 2\mathbf{s}_j) \tag{4.11}$$

and

$$H^{SO} \approx \frac{\alpha^2}{2} \sum_A \sum_i \frac{Z_A^{\text{eff}}}{r_{iA}^3} \mathbf{l}_i \cdot \mathbf{s}_i \tag{4.12}$$

where the nuclear index A runs over the nuclei present in a molecule.

The expectation value of $\hat{H}^{SO}$ for a state withquantum numbers Λ and S is called a diagonal effect, the magnitude of which can be expressed as $A\Lambda\Sigma$ where Σ is a projection of S onto the internuclear axis. A is called a spin-orbit coupling constant. Thus the diagonal spin-orbit effect causes multiplet splitting of a given nonzero S and nonzero Λ electronic state in a way similar to the occurrence of atomic multiplet structure. For example, from a $^3\Pi$ state three states of different Ω (the magnitude of the sum of the projections of L and S onto the internuclear axis) arise; $^3\Pi_0$, $^3\Pi_1$, and $^3\Pi_2$. The energy of $^3\Pi_1$ is unaffected by the diagonal effect because its Σ is zero, while $^3\Pi_0$ and $^3\Pi_2$ are separated from $^3\Pi_1$ by an equal amount. The order of these three states depends on the sign of A, which is positive if the reference state contains a less than half-filled MO and negative if more than half-filled (which is the case for the lowest $^3\Pi$ state of NaI). The magnitude of A also depends on R.

Selection rules governing what $^{2S+1}\Lambda$ states can interact via off-diagonal spin-orbit effect are

- $\Delta S = 0, \pm 1, \ \Delta O = 0$
- $\Delta\Lambda = 0, \pm 1$

- $\Delta\Sigma = -\Delta\Lambda$
- $\Delta\Omega = 0$

where O is the quantum number of the total electronic angular momentum.

Now we will apply the above rules to the electronic states of NaI. We are particularly interested in the excited states of the same symmetry as that of the ground state, which is a $^1\Sigma^+$ state. However, since Λ and Σ may not be separately conserved under the strong influence of a spin-orbit coupling, the electronic states may only be labelled by Ω. This is called a Hund's coupling case (c) [Herzberg 1950]. $^1\Sigma^+$ states are 0^+ states, and in addition, a $^3\Pi$ state has as a component a 0^+ state. These two states $^1\Sigma^+_{0+}$ and $^3\Pi_{0+}$ interact via off-diagonal spin-orbit coupling. No other states that produce 0^+ states (e.g., $^5\Pi$, $^5\Delta$) can interact with those two states according to the above selection rules.

Unfortunately, we could not calculate the spin-orbit coupling effects with either the ab initio packages GAMESS or MOLPRO. Thus we will instead look at two ab initio calculations reported during the 1990s.

4.3.3 Calculation of the dissociation energies

Sakai et al. [Sakai 1992] performed MRSDCI calculation on the two lowest $^1\Sigma^+$ states of NaI using effective core model potentials of their own. Three CSFs were chosen as the reference configurations, from which all the other CSFs are generated by a single or a double excitation and included in the CI calculation. Their reference CSFs differ from each other by a number of electrons distributed to two outermost σ MOs, namely $(4a_1^2)$, $(4a_1^1, 5a_1^1)$ and $(5a_1^2)$ according to their notation. We note that a_1 in C_{2v} symmetry corresponds to σ in $C_{\infty v}$. Further details are shown in their article. Since the values of

their potentials are shown for only several points around the equilibrium position and they did not perform spin-orbit calculations, their potential curves will not be examined here.

However, Sakai et al. made a number of additional comments regarding the calculation of dissociation energy and the effects of the spin-orbit coupling, which are worth receiving some attention. They first argued that the mere difference between the minimum value of the ground state potential and the value at large R can not be directly compared to the atomic dissociation energy obtained experimentally, unless the effect of spin-orbit coupling is considered in the ab initio calculation. They instead used the formula which is also suggested and recommended by Bauschlicher et al. [Bauschlicher 1982];

$$D_e = E(\mathrm{Na}^+) + E(\mathrm{I}^-) - E(\mathrm{NaI}, R_e) - \mathrm{IP(Na)} + \mathrm{EA(I)}, \tag{4.13}$$

where each term on the right side respectively represents the energy of the ground state positive sodium ion, of the ground state negative iodine ion, of NaI at its ground state equilibrium internuclear distance, and the last two terms are the ionization potential of Na and the electron affinity of I. The advantage of using Eq. (4.13) is that only the states of atomic character are affected by the spin-orbit coupling, since both Na^+ and I^- in their ground states are closed-shell ions whose spin and orbital angular momenta are both zero. Then one can expect the attractive limb of the excited $^1\Sigma^+$ state potential to be almost unchanged by the spin-orbit coupling, and the ionic dissociation limit as well.

When Eq. (4.13) was applied to calculate the atomic dissociation limit, it was found to be just above 3 eV and lower than Sakai et al.'s estimate of 3.09 eV which is

closer to fairly reliable experimental estimates of 3.15 eV [Bluhm 1993] and 3.18 eV [van Veen 1979]. The main reason why the use of Eq. (4.13) led to a poorer estimate in our calculation than that of Sakai et al. may be that the basis set and ECP used in our calculation was not adequate enough for a calculation of Na^+I^-, although our difference between the ground state minimum and the energy value at large R was larger than that of Sakai et al. (3.08 eV). Thus further studies are required in order to obtain more accurate theoretical estimate of atomic and ionic dissociation limits.

4.3.4 Study of Koseki et al. : ab initio calculation of spin-orbit coupling

Another study we will look at is that of Koseki et al. [Koseki 1995] who, with their proposal of the Z^{eff} values to be used in spin-orbit calculation for various atoms, reported results of spin-orbit calculations on the various electronic states of NaI using GAMESS. We will also explain in this subsection why we believe they could perform spin-orbit calculations while we could not.

The resultant potential curves of Koseki et al. are shown in Fig. 4.4 together with the curves they obtained without performing spin-orbit calculation. Note that their labelling of the excited electronic states is different from that employed in this thesis. The potentials in (b) of Fig. 4.4 were reported to be non-degenerate spin-mixed states, and we regard the solid curves in (b) as 0^+ potential curves as they avoid each other while the lowest potential amongst them is almost the same as the $X^1\Sigma$ (note that Koseki et al. did not use + or − labels) potential in (a).

Although it was stated that the SA-MCSCF wavefunctions were employed in their calculations, no further information was given so that it is not clear what accuracy

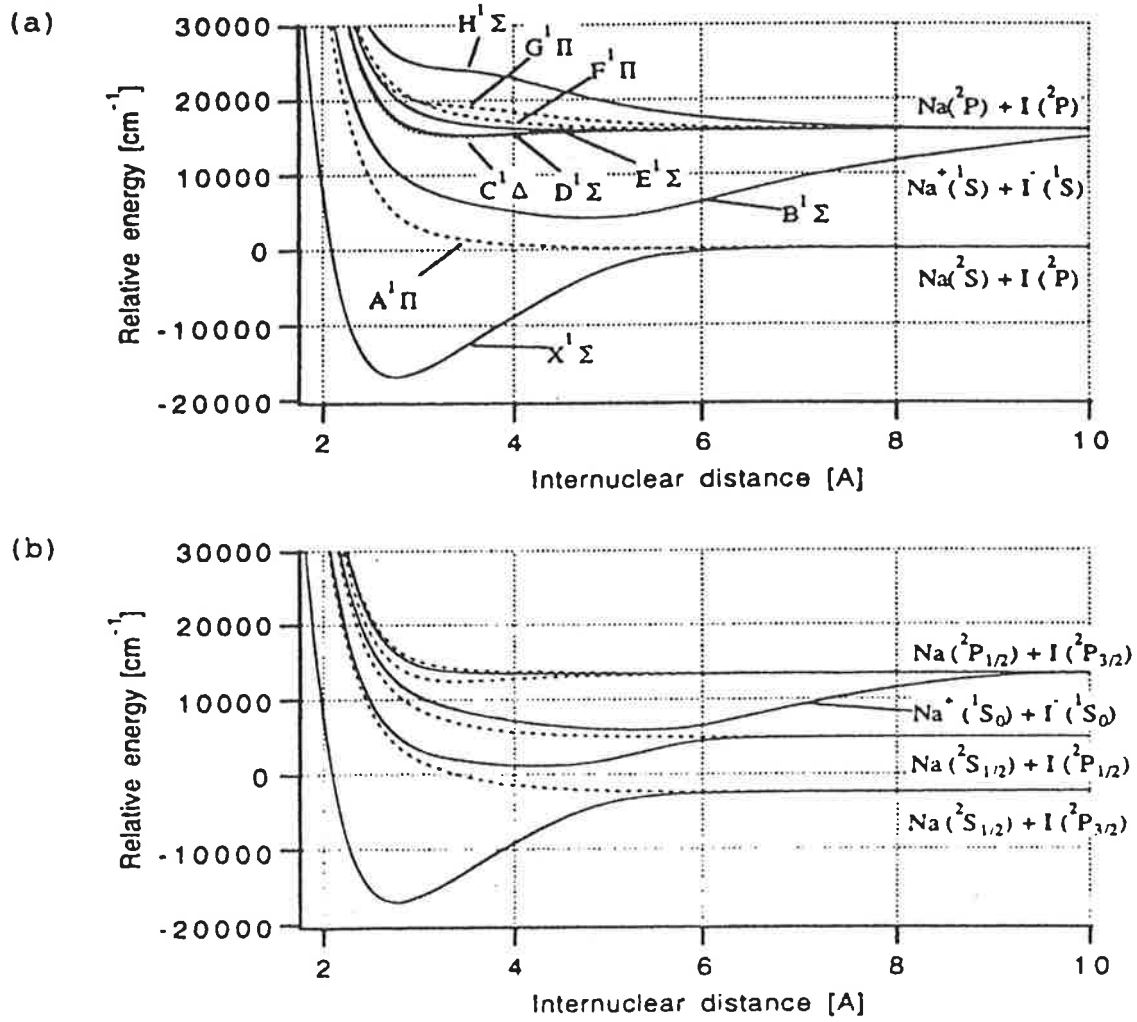

Figure 4.4: Potential curves of Koseki et al.; (a) potentials obtained without spin-orbit calculations, and (b) potentials of non-degenerate states obtained with spin-orbit calculations.

should be expected from their results. Furthermore, their value of D_e, whether spin-orbit correction is included or not, is even less than 2.3 eV while the experimental studies showed D_e to be larger than 3.0 eV. Thus the accuracy of their calculation is questionable. The gap between the two atomic dissociaton limits appears to be around 8000 cm^{-1} (or roughly 1 eV) which is in qualitative accordance with the known estimate of iodine multiplet splitting, however. Overall, it appears that the size of their calculation was smaller than our calculation reported in this thesis. This may have prevented their optimized MOs from losing the symmetry which could then have enabled the spin-orbit calculation using GAMESS. Our attempts to perform the spin-orbit calculation with GAMESS were not successful because of the symmetry problem and it was not possible to reproduce the results of Koseki et al. due to a lack of information on their calculation method. Thus we can only roughly examine from their results what impact the spin-orbit effect has on the shape of the potential curves.

From Fig. 4.4 one observes that the ground state potential near the equilibrium internuclear distance is left almost unchanged, while the lowest atomic dissociation limit decreased by about 2500 cm^{-1} when spin-orbit effects are taken into account (compare two bottom curves in (a) and (b)). This is in agreement with the discussion that the ionic states should not be affected by the spin-orbit coupling, because the attractive limbs of the excited 0^+ potentials are also left without any appreciable changes except for another avoided crossing that occur due to the introduction of the second dissociation limit (due to $I(^2P_{1/2})$) which lies below the ionic dissociation limit.

It could also be confirmed from Koseki et al. that there are two excited 0^+ states, which are expected to arise from the first excited $^1\Sigma^+$ and the lowest $^3\Pi$ states. The lower potential among the two (that is, the second lowest solid curve in (b) of Fig. 4.4)

will be of main interest when we discuss the experimental results. If one compares the spin-orbit corrected 0^+ potential to the excited $^1\Sigma^+$ potential (which is labelled in Fig. 4.4 as $B^1\Sigma$), one notices that there are a couple of important changes. First, the corrected potential lies lower than the $^1\Sigma^+$ potential. Second, which is less obvious but yet significant nonetheless, the minimum of the corrected potential lies at smaller R value to make the bottom of the potential deeper than that of the $^1\Sigma^+$ potential.

Another observation which could be made from the results of Koseki et al. was the similarity between the repulsive limb of the first excited 0^+ potential and that of the uncorrected $^1\Pi$ potential. We will keep this in mind when our ab initio curves are compared to the experimental potentials later in this thesis.

Since GAMESS had a difficulty handling the symmetry of MOs in the CASSCF calculation, which threw doubts on the reliability of the resultant potential curves and in turn made it impossible to carry out the spin-orbit calculation, while MOLPRO was not yet capable of spin-orbit calculations, which is a subject of future implementation, our theoretical study of NaI potential curves could not proceed any further and is left for future work. One aspect that can be said clearly at the present stage, however, is that the $^3\Pi$ state in addition to the $^1\Sigma^+$ states must be included in consideration when one investigates the excited 0^+ states of NaI.

Chapter 5

UV Spectrum of NaI

5.1 Structure of UV Spectrum of NaI : General Discussions

5.1.1 General discussion of diatomic molecular spectra

Visible and UV (ultra violet) spectra of a diatomic molecule are understood to arise from the transitions between the molecular states belonging to different potential curves (which will thus be called electronic transitions). Spectra of electronic transitions between two bound states in general consist of a multitude of transition lines, and are also referred to as 'band' spectra, detailed discussions of which are presented in [Herzberg 1950] (chapters 2 and 5 therein). If the upper state potential curve is repulsive, what one will observe from the transition spectrum instead of the discrete line structure is a continuous variation of the spectrum intensity. Such a spectrum is referred to as a continuous spectrum.

One area of our particular interest is the rotational structure (also called the 'fine'

structure) of a band spectrum, which can be obtained in high resolution with modern laser spectroscopy. The word 'band' usually refers to a group of transition lines, the initial and the final states of which have fixed vibrational quantum numbers. A band may be labelled in the form $v'' - v'$ band, v'' and v' being the vibrational quantum numbers of the states belonging to the lower and higher potential curves respectively. Lower potential curve here implies the curve whose minimum value is lower than the minimum of the other.

Transitions observable in the absorption or emission spectrum of a heterogeneous diatomic molecule obey the following selection rules for two Hund's case (a) or (b) states (p. 240 of [Herzberg 1950]) based on electric dipole radiative interaction;

- $\Lambda' - \Lambda'' = 0$ or ± 1,
- $S' - S'' = 0$,

and for $\Sigma(\Lambda = 0)$ states

- $\Sigma^+ \leftrightarrow \Sigma^+, \Sigma^- \leftrightarrow \Sigma^-$

while $\Sigma^+ \leftrightarrow \Sigma^-$ is forbidden. S is the total electron spin quantum number of a molecule. Finally, transition occurs only between the states whose total angular momentum quantum number J differ from each other by 1 or 0;

- $J' - J'' = 0, \pm 1$, while transition being forbidden if $J' = J'' = 0$.

A transition line of a given band is then given an additional label, determined by the difference between the values of J of the two associated states. A line is said to belong to

- the P branch if $\Delta J \equiv J' - J'' = -1$,

- the R branch if $\Delta J = 1$, and
- the Q branch if $\Delta J = 0$.

The above selection rules for photoemission and photoabsorption process are effective only when the associated quantum numbers are well defined. If there is a situation in which one or more quantum numbers are not well conserved quantities, some part of the selection rules may become meaningless and have to be modified. Here we will only discuss a case relevant to NaI, known as Hund's coupling case (c) (p. 224 of [Herzberg 1950]).

5.1.2 Selection rules for phototransitions for Hund's case (c)

As we have briefly discussed in Section 4.3, electronic states of a diatomic molecules composed of heavy atoms need to be labelled according to Hund's case (c) by Ω as their spin and the orbital angular momenta can not be interpreted as separately conserved quantum numbers. The associated phototransition selection rules are then written as

- $\Omega' - \Omega'' = 0, \pm 1$,

and for $\Omega' = \Omega'' = 0$

- $0^+ \leftrightarrow 0^+, 0^- \leftrightarrow 0^-$

while $0^+ \leftrightarrow 0^-$ is forbidden. The selection rule for J is the same as that stated above, with $\Delta J = 0$ forbidden (no Q branches) if $\Omega' = \Omega'' = 0$.

In the electrostatic approximation, the ground state is $^1\Sigma^+$. As its Λ and S are both zero, the diagonal spin-orbit coupling $A\Lambda\Sigma$ of a $^1\Sigma^+$ state is also zero. Since the electronic ground state of NaI is energetically well separated from the excited states, the

off-diagonal spin-orbit coupling between the ground state and other excited states will be negligible. Consequently, the spin and the orbital angular momentum of the ground electronic state are well conserved and can be safely used to label the ground electronic state as $X^1\Sigma^+$, X being the general notation for the ground state of a molecule. The first excited 0^+ state will be labelled $A0^+$. Dipole allowed transitions which include the ground state are thus $X^1\Sigma^+ \leftrightarrow A0^+$ and $X^1\Sigma^+ \leftrightarrow 1$ transitions.

5.1.3 Formation of a bound excited electronic state due to an avoided crossing of potential curves

The theoretical explanation of the presence of a low excited bound state for the NaI molecule comes from the theory of curve crossing [Berry 1957]. The two lowest 0^+ states dissociate to either the ionic $Na^+ + I^-$ or the neutral Na+I atoms. At large internuclear distances, if one regards the interaction between two atoms as being merely electrostatic, the corresponding potential curve is of form $-1/R$ for the ions. Since the ionic dissociation limit (that is, the sum of the lowest energies of Na^+ and I^-) lies higher than the atomic limit, as R decreases from infinity the ionic potential curve approaches the atomic one which should be almost horizontal, eventually crossing and going below the atomic potential curve. The R value at which those two curves cross is called a nonadiabatic (or diabatic) crossing point, which will be denoted by R_x. Thus a search for the ground state using the ab initio method should result in a wavefunction whose character changes from ionic to atomic, as it does in the calculations reported in chapter 4 and in references therein. Then by the same reasoning the first excited adiabatic 0^+ state is ionic at large internuclear distances and becomes atomic as R gets smaller than R_x. This results in a bound excited state adiabatic potential curve. However,

such a change of characteristics of an electronic wavefunction may make it inadequate to express a molecular wavefunction under the adiabatic approximation scheme. Mathematically, this corresponds to a situation where the off-diagonal Hamiltonian matrix element $H_{\epsilon'\nu',\epsilon\nu}$ is no longer negligible. In semiclassical terms, if motion of the nuclei is not sufficiently slow upon close approach of two potential curves, there is not enough time for the electronic wavefunction to change from ionic to atomic or vice versa.

The discussion regarding the avoided crossing given below is somewhat different from what was given in Chapter 2, in that we will use the notion of potential curves which can cross each other even though the corresponding electronic wavefunctions are of the same symmetry. We will follow this line of approach in more detail, in order to further explore the validity of the adiabatic approximation method.

5.2 Nonadiabatic Molecular Dynamics : Coupled Equations for Nuclear Motion

5.2.1 Description of a curve crossing system using diabatic wavefunctions

The interaction between two adiabatic states at an avoided crossing can perhaps be best illustrated by imagining two states which do not change their nature from being ionic to atomic, or vice versa. Such non-adiabatic states, conventionally referred to as diabatic states, are often described as orthonormal linear combinations of the adiabatic states;

$$\Psi_1^e = \Psi_-^e \cos\theta + \Psi_+^e \sin\theta, \text{ and} \tag{5.1}$$

$$\Psi_2^e = -\Psi_-^e \sin\theta + \Psi_+^e \cos\theta, \tag{5.2}$$

the subscripts 1 and 2 denoting the ionic and the atomic diabatic wavefunction respectively. $-$ and $+$ labels refer to the ground and the excited adiabatic state. It is also assumed that no other states of the same symmetry and similar energy are present at the crossing region.

By letting θ vary from 0 to $\pi/2$ as R changes from 0 to infinity, the diabatic Ψ^es behave as

$$\Psi_1^e = \Psi_-^e \quad \text{if } R \ll R_X \tag{5.3}$$

$$= \Psi_+^e \quad \text{if } R \gg R_X, \tag{5.4}$$

and

$$\Psi_2^e = \Psi_+^e \quad \text{if } R \ll R_X \tag{5.5}$$

$$= -\Psi_-^e \quad \text{if } R \gg R_X, \tag{5.6}$$

and are expected to vary slowly with R around the crossing point since they do not change their nature, unlike the adiabatic wavefunctions. Consequently a significant mixing of two adiabatic wavefunctions will take place, and the diabatic wavefunctions will no longer be the eigenfunctions of the electronic Hamiltonian $\hat{H}^e$.

Using Eqs. (5.1) and (5.2) we then obtain, as the adiabatic wavefunctions are eigenfunctions of $\hat{H}^e$,

$$E_1^e \equiv H_{11}^e$$

$$
\begin{aligned}
&= \int \Psi_1^e \hat{H}^e \Psi_1^e d\tau_e \\
&= E_-^e \cos^2\theta + E_+^e \sin^2\theta \\
E_2^e &\equiv H_{22}^e \\
&= \int \Psi_2^e \hat{H}^e \Psi_2^e d\tau_e \\
&= E_-^e \sin^2\theta + E_+^e \cos^2\theta \\
H_{12}^e &= (E_+^e - E_-^e)\cos\theta \sin\theta \\
&= H_{21}^e.
\end{aligned}
$$

We will call E_1^e and E_2^e the diabatic potential curves. The off-diagonal matrix element H_{12}^e is called the (diabatic) electronic coupling term.

5.2.2 Electronic coupling function

To find more about θ, one starts by expressing the adiabatic wavefunctions Ψ_-^e and Ψ_+^e as linear combinations of Ψ_1^e and Ψ_2^e (i.e., an inverse transformation of Eqs. (5.1) and (5.2));

$$
\begin{aligned}
\Psi_-^e &= \Psi_1^e \cos\theta - \Psi_2^e \sin\theta \\
\Psi_+^e &= \Psi_1^e \sin\theta. + \Psi_2^e \cos\theta
\end{aligned}
\tag{5.7}
$$

Then

$$
\begin{aligned}
H_{-+}^e &= E_1^e \cos\theta \sin\theta + H_{12}^e(\cos^2\theta - \sin^2\theta) - E_2^e \cos\theta \sin\theta \\
&= \frac{1}{2}(E_1^e - E_2^e)\sin 2\theta + H_{12}^e \cos 2\theta \\
&= 0
\end{aligned}
$$

as the adiabatic wavefunctions are the eigenfunctions of $\hat{H}^e$.

Therefore

$$\tan 2\theta = \frac{2H_{12}^e}{E_2^e - E_1^e} \equiv \frac{1}{\rho}, \tag{5.8}$$

from which it follows that

$$\cos\theta = \sqrt{\frac{1}{2}\left(1 + \frac{\rho}{\sqrt{\rho^2+1}}\right)} \tag{5.9}$$

$$\sin\theta = \sqrt{\frac{1}{2}\left(1 - \frac{\rho}{\sqrt{\rho^2+1}}\right)} \tag{5.10}$$

and

$$E_-^e = \frac{1}{2}(E_1^e + E_2^e) - \sqrt{\frac{1}{4}(E_2^e - E_1^e)^2 + (H_{12}^e)^2} \tag{5.11}$$

$$E_+^e = \frac{1}{2}(E_1^e + E_2^e) + \sqrt{\frac{1}{4}(E_2^e - E_1^e)^2 + (H_{12}^e)^2}. \tag{5.12}$$

Eqs. (5.8), (5.9) and (5.10) also allow H_{12}^e to be rewritten as

$$H_{12}^e = \frac{1}{2}\sqrt{(E_+^e - E_-^e)^2 - (E_2^e - E_1^e)^2}, \tag{5.13}$$

from which a few qualitative remarks can be made.

In a region far away from the crossing, H_{12}^e will be nearly zero. This is consistent with the suggested trait of the diabatic electronic wavefunctions (Eqs. (5.3), (5.4), (5.5) and (5.6)). As two adiabatic potential curves draw close to each other they go through an avoided crossing, while the diabatic curves cross. At the crossing point $E_2^e - E_1^e$ is zero, thus

$$H_{12}^e(R = R_x) = \frac{1}{2}[E_+^e(R_x) - E_-^e(R_x)]$$

which is the maximum value of H^e_{12}, and also the smallest difference between the adiabatic potential curves. This value is usually referred to as 'electronic coupling strength'. Therefore it seems reasonable to assume that the change of H^e_{12} over R is similar to that of a gaussian function;

$$H^e_{12}(R) \sim A\exp(B|R - R_x|^n), \;\; n = 1, 2, \ldots$$

where

$$A = H^e_{12}(R_x).$$

5.2.3 Relationship between adiabatic and diabatic nuclear equations

Taking only the above two states (either diabatic or adiabatic ones) into consideration, one can set up the Schrödinger's equations for the nuclear wavefunctions. It suffices to discuss the rotationless vibration only since rotation can be taken into account simply by adding the centrifigual potential term to the equation and multiplying the vibrational wavefunctions by a spherical harmonic.

One first writes the total molecular wavefunction as

$$\Psi = \Psi^e_- \chi_- + \Psi^e_+ \chi_+ \tag{5.14}$$

or

$$\Psi = \Psi^e_1 \chi_1 + \Psi^e_2 \chi_2 \tag{5.15}$$

and inserts it into the equation $\hat{H}\Psi = E\Psi$. We will first consider a so-called adiabatic

representation, in which Eq. (5.14) is employed.

Multiplying both sides by Ψ^e_- or Ψ^e_+ and integrating over the electronic coordinates, one obtains the following two coupled equations for the nuclear vibrational wavefunctions

$$(\hat{T}^n + E^e_- + W_{--} - E)\chi_- = -(W_{-+} + F_{-+}\frac{d}{dR})\chi_+ \tag{5.16}$$

$$(\hat{T}^n + E^e_+ + W_{++} - E)\chi_+ = -(W_{+-} + F_{+-}\frac{d}{dR})\chi_- \tag{5.17}$$

where

$$F_{-+} = -\frac{1}{\mu}\int \Psi^e_- \frac{d\Psi^e_+}{dR} d\tau_e \tag{5.18}$$

$$F_{+-} = -\frac{1}{\mu}\int \Psi^e_+ \frac{d\Psi^e_-}{dR} d\tau_e \tag{5.19}$$

$$W_{--} = -\frac{1}{2\mu}\int \Psi^e_- \frac{d^2\Psi^e_-}{dR^2} d\tau_e \tag{5.20}$$

$$W_{++} = -\frac{1}{2\mu}\int \Psi^e_+ \frac{d^2\Psi^e_+}{dR^2} d\tau_e \tag{5.21}$$

$$W_{-+} = -\frac{1}{2\mu}\int \Psi^e_- \frac{d^2\Psi^e_+}{dR^2} d\tau_e \tag{5.22}$$

$$W_{+-} = -\frac{1}{2\mu}\int \Psi^e_+ \frac{d^2\Psi^e_-}{dR^2} d\tau_e. \tag{5.23}$$

W and F are called the motion coupling terms, as they describe the contributions from the derivatives of the adiabatic electronic wavefunctions with respect to R. Omission of the off-diagonal F and W from Eqs. (5.16) and (5.17) leads to the uncoupled adiabatic equations we discussed in chapter 2.

If Eq. (5.15) is employed, one expects to obtain two diabatic coupled equations

$$(\hat{T}^n + E^e_1 - E)\chi_1 = -H^e_{12}\chi_2 \tag{5.24}$$

$$(\hat{T}^n + E^e_2 - E)\chi_2 = -H^e_{12}\chi_1 \tag{5.25}$$

which results from the supposition that the motion coupling terms of diabatic wave-functions should be zero;

$$W_{ij} = F_{ij} = 0, \;\; i,j = 1,2. \tag{5.26}$$

Then it follows that the motion coupling terms in adiabatic representation can be expressed in terms of derivatives of θ with respect to R;

$$\begin{aligned} F_{-+} &= -\frac{1}{\mu}\int(\Psi_1^e\cos\theta - \Psi_2^e\sin\theta)\frac{d}{dR}(\Psi_1^e\sin\theta + \Psi_2^e\cos\theta)d\tau_e \\ &= -\frac{1}{\mu}\frac{d\theta}{dR}\int({\Psi_1}^2\cos^2\theta + {\Psi_2}^2\sin^2\theta - 2\Psi_1\Psi_2\sin^2\theta)d\tau_e \\ &= -\frac{1}{\mu}(\cos^2\theta + \sin^2\theta)\frac{d\theta}{dR} \\ &= -\frac{1}{\mu}\frac{d\theta}{dR} \end{aligned} \tag{5.27}$$

and similarly

$$F_{+-} = \frac{1}{\mu}\frac{d\theta}{dR} \tag{5.28}$$

$$\begin{aligned} W_{--} &= W_{++} \\ &= \frac{1}{2\mu}\left(\frac{d\theta}{dR}\right)^2 \end{aligned} \tag{5.29}$$

$$\begin{aligned} W_{-+} &= -W_{+-} \\ &= -\frac{1}{2\mu}\frac{d^2\theta}{dR^2}. \end{aligned} \tag{5.30}$$

Substituting Eq. (5.13) into Eq. (5.8) leads to

$$\tan 2\theta = \sqrt{\frac{(E_+^e - E_-^e)^2}{(E_2^e - E_1^e)^2} - 1} \quad \text{if } E_2^e > E_1^e \tag{5.31}$$

$$= -\sqrt{\frac{(E_+^e - E_-^e)^2}{(E_2^e - E_1^e)^2} - 1} \quad \text{if } E_2^e < E_1^e \tag{5.32}$$

and

$$\cos 2\theta = \sqrt{\frac{(E_2^e - E_1^e)^2}{(E_+^e - E_-^e)^2}} \quad \text{if } E_2^e > E_1^e \tag{5.33}$$

$$= -\sqrt{\frac{(E_2^e - E_1^e)^2}{(E_+^e - E_-^e)^2}} \quad \text{if } E_2^e < E_1^e \tag{5.34}$$

$$\sin 2\theta = \sqrt{1 - \frac{(E_2^e - E_1^e)^2}{(E_+^e - E_-^e)^2}}. \tag{5.35}$$

These trigonometric functions show roughly how θ behaves as R is varied. Starting from being zero at $R = 0$, θ should not exhibit any noticeable change far away from the crossing point. As R approaches the crossing θ will suddenly increase, having a value of $\pi/4$ at the crossing point, and swiftly converge to $\pi/2$ which is the asymptotic limit at $R = \infty$. The first order derivative of θ is then a sharply peaked function of R whose maximum lies at R_x, the second order derivative being a function with double peaks with opposite signs that are located at both sides of R_x.

The exact determination of the R-dependence of θ requires knowledge of both the adiabatic and the diabatic pairs of the potential curves, or one pair (adiabatic or diabatic) of the potential curves and the electronic coupling H_{12}^e as functions of R. Although neither the electronic coupling nor the diabatic potential curves are uniquely defined, it is favoured to work with the diabatic coupled equations due to their much simpler structure in comparison to the adiabatic equations. More discussions regarding the concept of diabatic wavefunction can be found elsewhere ([Torop 1987] and references therein).

Despite the lack of precise mathematical formulation of diatomic molecular wavefunctions, one can still make a number of useful qualitative remarks. If a given diatomic molecular system under the effect of curve crossing is described well by the adiabatic approximation scheme, the actual eigenstates should be adequately represented by the

adiabatic wavefunctions, and the motion coupling terms in the coupled adiabatic nuclear equations will be small. We may then expect the electronic coupling H_{12}^e, the off-diagonal matrix element of the electronic Hamiltonian between two diabatic electronic wavefunctions, to be appreciable. As adiabatic wavefunctions will change their character smoothly going through the adiabatic crossing, motion coupling terms as well as adiabatic potential curves should also vary smoothly.

On the other hand, if a given system behaves diabatically, the adiabatic approximation method becomes a poor choice for describing the actual molecular wavefunction. Motion coupling terms and adiabatic potential curves will then change sharply near the crossing, and H_{12}^e can be expected to be smaller than it is in an adiabatically behaving system. It is not possible to uniquely define or calculate independently the diabatic electronic wavefunction. However one can state that, since H_{12}^e will be small in a diabatic system, nuclear vibration is well represented by solving the uncoupled diabatic equations, that is, Eqs. (5.24) and (5.25) with their right sides set to zero. In other words, only diabatic potential curves govern the nuclear vibration to a satisfactory accuracy. If H_{12}^e is zero then the adiabatic and the diabatic states are the same, and θ can be taken to be zero. This occurs in one-electron diatomic molecules.

Therefore, the shape of adiabatic potential curves near the crossing can provide an estimate of how a given diatomic molecule behaves. The crossing point R_x should coincide well to the value of R at which two adiabatic potential curves show the closest approach and half the difference between the curves gives the maximum value of H_{12}^e. Berry [Berry 1957] presented an insightful discussion about these issues, taking NaI and KI molecules as examples. As can be seen from Fig. 5.1, two potential curves of KI approach each other more closely and move apart more sharply when compared to those

of NaI. KI shows much stronger diabatic character than NaI, which is in accordance with our present discussion. It must be also noted that, regardless of the behaviour of the electronic wavefunctions, the total molecular state always tends to become more diabatic with increasing energy, since the velocity of nuclear motion also becomes larger.

In ab initio calculations, one will experience great difficulty in obtaining converged results if a system behaves diabatically. This is because an ab initio calculation is based on the adiabatic approximation method and, due to the adiabatic potential curves approaching each other closely, there is greater possibility of energy values near the crossing point becoming nearly degenerate.

For a system which is not close to either the diabatic or the adiabatic case, one has to solve coupled equations for nuclear vibration to obtain adequate vibrational wavefunctions and their eigenvalues. As was previously mentioned, solutions can be obtained from either adiabatic or diabatic coupled equations. In order to avoid confusion we will call the solutions obtained from solving the coupled nuclear equations 'wavefunctions in adiabatic (or diabatic) representation', and use the terms 'adiabatic wavefunction' and 'diabatic wavefunction' to refer to the solutions of approximate uncoupled equations, which can be obtained to a good accuracy by the WKB method.

Various equations that appear in our discussion so far have all been written in atomic units for notational convenience. From now on the standard units will be used instead.

5.3 Predissociation by Curve Crossing

Following the discussions in the previous section, we will discuss how to assess the behaviour of a diabatic molecule whose adiabatic potential curves undergo an avoided crossing. In doing so, one will see that it is not just the shape of potential curves in the

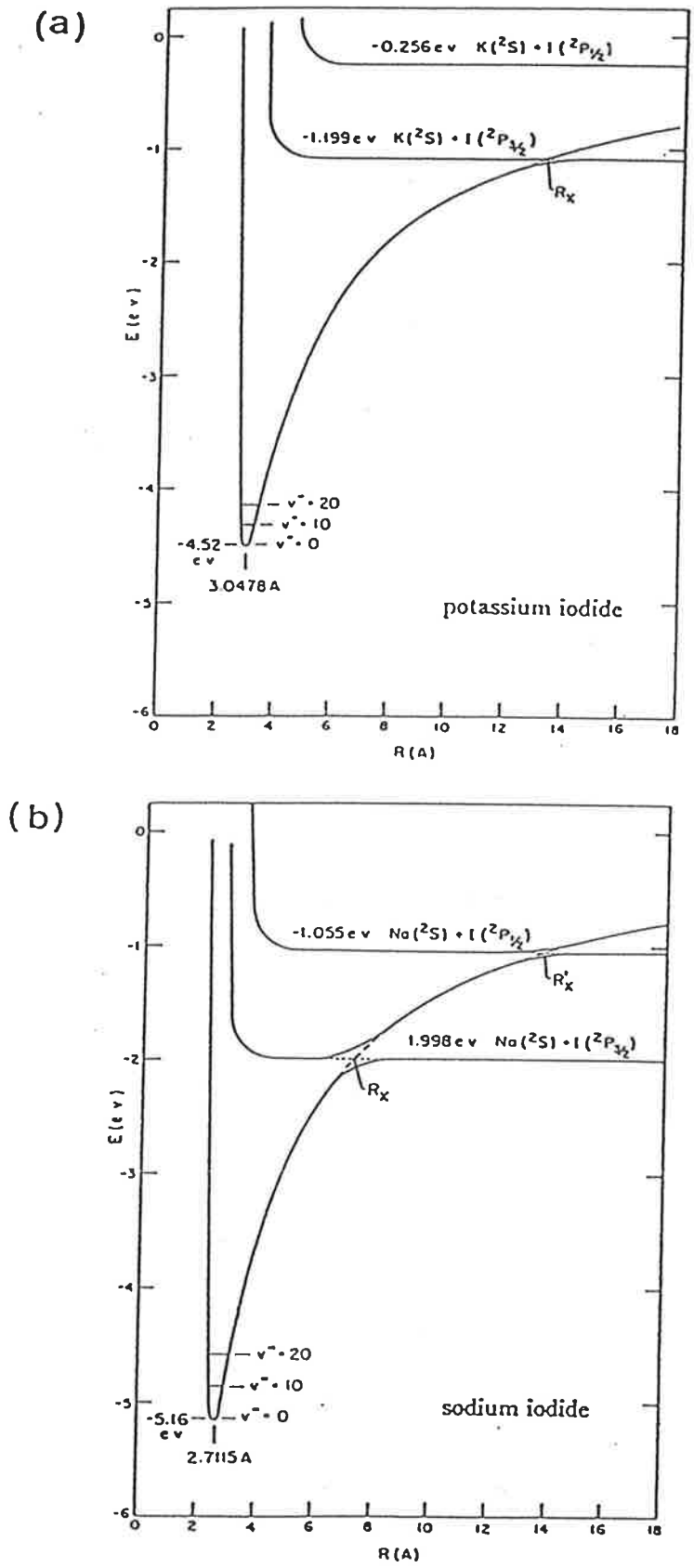

Figure 5.1: Potential curves for (a) KI and (b) NaI, taken from [Berry 1957].

crossing region that determines whether a given state of the system is either adiabatic or diabatic.

5.3.1 Transition induced by nonadiabatic coupling

With the assumption that the potential curve varies smoothly with respect to R, far away from the crossing point one may write adiabatic vibrational wavefunctions using the WKB approximation method [Child 1991];

$$\chi_{\pm}(R) = \frac{P_{\pm}^{+}}{\sqrt{k_{\pm}(R)}} \exp\left[i\int_{R_x}^{R} k_{\pm}(R')dR'\right] + \frac{P_{\pm}^{-}}{\sqrt{k_{\pm}(R)}} \exp\left[-i\int_{R_x}^{R} k_{\pm}(R')dR'\right], \quad R \ll R_x, \tag{5.36}$$

and

$$\chi_{\pm}(R) = \frac{Q_{\pm}^{+}}{\sqrt{k_{\pm}(R)}} \exp\left[i\int_{R_x}^{R} k_{\pm}(R')dR'\right] + \frac{Q_{\pm}^{-}}{\sqrt{k_{\pm}(R)}} \exp\left[-i\int_{R_x}^{R} k_{\pm}(R')dR'\right], \quad R \gg R_x. \tag{5.37}$$

If the energies of these two wavefunctions are close, the effect of nonadiabatic coupling on these wavefunctions can be interpreted as causing a radiationless transition between the two vibrational states χ_+ and χ_-. It is also assumed that the values of the vibrational energies lie higher than the value of the diabatic potential curves at the crossing point.

The following relationships between the wavefunction coefficients can be found by using a method based on a theory of the Stokes phenomenon (see appendix A of

[Child 1991] and references therein),

$$\begin{pmatrix} Q_+^+ \\ Q_-^+ \end{pmatrix} = \begin{pmatrix} \exp(i\chi)\sqrt{1-\exp(-2\pi\nu)} & -\exp(-\pi\nu) \\ \exp(-\pi\nu) & \exp(-i\chi)\sqrt{1-\exp(-2\pi\nu)} \end{pmatrix} \begin{pmatrix} P_+^+ \\ P_-^+ \end{pmatrix}$$

$$\begin{pmatrix} P_+^- \\ P_-^- \end{pmatrix} = \begin{pmatrix} \exp(i\chi)\sqrt{1-\exp(-2\pi\nu)} & \exp(-\pi\nu) \\ -\exp(-\pi\nu) & \exp(-i\chi)\sqrt{1-\exp(-2\pi\nu)} \end{pmatrix} \begin{pmatrix} Q_+^- \\ Q_-^- \end{pmatrix}$$

with

$$\nu = \frac{i}{2\pi}\int_{R_-}^{R_+}[k_-(R)-k_+(R)]dR \tag{5.38}$$

$$\chi = \arg\Gamma(i\nu) - \nu\ln\nu + \nu + 4/\pi. \tag{5.39}$$

R_+ and R_- are complex values for which E_+^e and E_-^e become equal.

Let us suppose, for example, a nuclear vibrational state is initially described by χ_+ for $R \ll R_X$(i.e., $P_+^- = 0$). Then the probability that, when R(real R) is increased beyond R_X, transition to a state described by χ_- occurs is given by $|Q_-^+/P_+^+|^2 = \exp(-2\pi\mathrm{Re}(\nu))$. Similarly, the probability that no transition occurs is $|Q_+^+/P_+^+|^2$. It is also interesting to note that there is no relation between coefficients with diffirent superscripts (i.e., coefficients of incoming and outgoing waves).

5.3.2 Landau-Zener parameter

Child further indicated that if the so-called Landau-Zener conditions are assumed in a region near R_x;

1. the diabatic potential curves are linear in R; $E_i^e = E_x - F_i(R-R_x)$, $i = 1,2$

2. the electronic coupling H_{12}^e and $k_+ + k_-$ are constant,

Eq. (5.38) becomes

$$\nu = \frac{(H_{12}^e)^2}{\hbar v \Delta F} \tag{5.40}$$

where $v = \hbar(k_+ + k_-)/2\mu$ and $\Delta F = |F_1 - F_2|$. The expression on the right side of Eq. (5.40) is called the Landau-Zener parameter.

The Landau-Zener parameter was originally introduced in the following different way. Starting from the above assumption about the diabatic potential curves and electronic coupling, Landau (§90 of [Landau 1977]) and Zener [Zener 1932] sought to find the transition probability between two adiabatic electronic wavefunctions. The electronic wavefunction is written as

$$\Psi^e = a_+(t)\Psi_+^e + a_-(t)\Psi_-^e \tag{5.41}$$

with coefficients $a_+(t)$ and $a_-(t)$ being taken to vary in time. Ψ^e is then inserted into time dependent Schrödinger's equation

$$i\frac{\partial \Psi^e}{\partial t} = (\hat{H}^e + \hat{T}^n)\Psi^e \tag{5.42}$$

where the time dependence of $\hat{H} = \hat{H}^e + \hat{T}^n$ arises from the internuclear distance R varying in t.

If initial value conditions for a_1, a_2 are

$$a_+(-\infty) = 1, \;\; a_-(-\infty) = 0,$$

it is found that

$$|a_-(\infty)|^2 = \exp\left(-\frac{2\pi {H_{12}^e}^2}{\hbar v \Delta F}\right) \tag{5.43}$$

is the probability that a transition from state + to state − occurs in a single passage through the diabatic crossing point. Thus a term $P_{LZ} \equiv \exp(-2\pi\nu)$ is often interpreted as an adiabatic transition probability. Large value of ν indicates that a given system is adiabatic, and small ν means the system behaves diabatically.

Therefore, one can see that it is not just H^e_{12} that determines the behaviour of a given molecular system. For any magnitude of H^e_{12}, if v is large enough, ν is small and the system is diabatic. As v in ν has the dimension of velocity, large v implies semiclassically that the vibrations of the two nuclei are fast. Hence if a molecule is in a high energy vibrational state it may behave diabatically even if H^e_{12} is large. Another term ΔF in ν, being a difference in slope of two potentials near R_x, also contributes to some degree to the magnitude of P_{LZ}. The larger the difference between the slopes, the more likely it becomes for a system to be diabatic.

5.3.3 Predissociation

For NaI, we have seen that the two lowest adiabatic 0^+ electronic states undergo an avoided crossing. The ground state is ionic when $R \ll R_x$ then becomes atomic for $R \gg Rx$, and vice versa for the first excited state. In the adiabatic limit where the effect of $\hat{T}^n$ on the electronic wavefunction is completely ignored, 0^+ bound states whose total energies are greater than the atomic dissociation limit (and smaller than the ionic dissociation limit) can only belong to the upper adiabatic potential curve and will be stable. However in the real situation the effect of $\hat{T}^n$ on Ψ^e near R_x is not negligible so that a transition can occur from a bound state (whose wavefunction is denoted by Ψ_+) to a state (Ψ_-) which is atomic for $R \gg R_x$ and thus belongs to the lower adiabatic potential curve, thereby causing a dissociation into two neutral atoms. Such

a radiationless transition is called a predissociation. In addition to the probability with which the predissociation occurs, it is also of importance to understand how an emission or absorption spectrum involving electronic transitions is affected by it.

Since in the energy region between the atomic and ionic dissociation limit the + states are discrete while the − states are continuous, a mixture of a + and a − rovibrational state can be expected to cause a broadening of the discrete energy level, the line width of which is related to the lifetime of the corresponding energy eigenstate. As we will see in more detail in the next section, it was shown by Child (p. 63 of [Child 1991]) that the level spacing and line widths of predissociating rovibrational states can be calculated from the energies of Ψ_+s and of Ψ_1s.

5.4 Analysis of NaI UV Spectrum

5.4.1 Early experiments and discussions

A wide variety of experiments and discussions on alkali halides that were reported prior to 1980 are well reviewed and documented by Davidovits and McFadden [Davidovits 1979]. The photoabsorption spectrum of NaI, unlike those of other alkali halides which are continuous, was found to show a dense line structure in the near-UV region (c.f., Fig. 5.2 for example). Although this feature was understood to imply the presence of bound excited states, further investigation was difficult due to the complex and dense nature of the spectrum and insufficient resolving power of the spectroscopic apparatus. However, with the use of laser technology UV spectra of higher resolution could be obtained and it became possible to conduct more intensive studies on the excited states of NaI. What is given below is a summary of two such studies, one having been carried out by van Veen

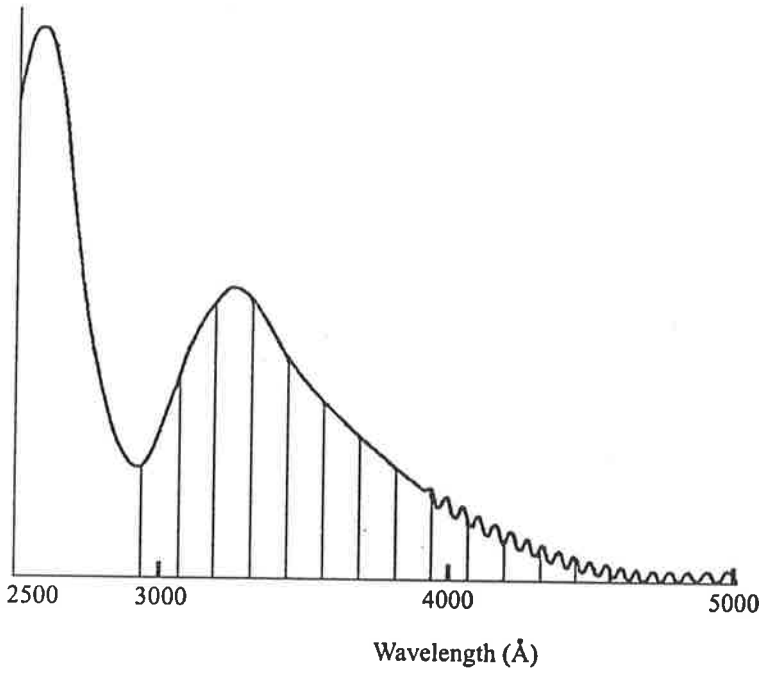

Figure 5.2: Schematic spectrum of NaI vapor, taken from [Berg 1969]. Lined region indicates the transition wavelengths for which rotational structure was observed in their spectrum.

et al. [van Veen 1981] and the other by Schaefer et al. [Schaefer 1982, Schaefer 1984], both of which discuss key issues crucial in the understanding of the excited states of NaI. Thus it is of great importance to examine and assess their investigations carefully.

5.4.2 Van Veen et al.

Van Veen et al. [van Veen 1981] conducted a photofragmentation spectroscopy experiment in which the ratio of parallel ($\Delta\Omega = 0$) and perpendicular ($\Delta\Omega = 1$) transitions is calculated from measurements of the angular distributions of dissociated Na photofragments. The individual parallel and perpendicular absorption cross sections were then obtained by multiplying these ratios by the total absorption cross section, and segments

of the potential curves for $\Omega' = 1$ and 0^+ excited states were obtained. Their experiments were carried out in the transition wavelength range from 337 nm (3.68 eV) to 300nm (4.13 eV) and the analytic form of the segment of the excited state potential curves was chosen to be

$$E_2^e(R) = A\exp[-b(R - R_0)] \tag{5.44}$$

where R_0 is the equilibrium internuclear distance of the $X^1\Sigma^+$ state. A and $-Ab$ are the energy value and slope of an excited state potential curve at $R = R_0$ respectively, their values being 3.88 (3.63) eV and 33.2 (36.4) eV/nm for the $\Omega = 0^+$ (1) state. Fig. 5.3 shows these potential curves together with their absorption cross section.

Since the velocity distribution of the photofragments was also obtained from the experiment of van Veen et al., the kinetic energies E of the dissociated Na fragments could be calculated. The dissociation energy D_0 of NaI is then found by the relation

$$E = h\nu - D_0 + E_{v''J''}$$

where ν is the frequency of a laser pulse incident on a NaI beam and predetermined $E_{v''J''}$ [Rusk 1962] is the energy of the ground state whose vibrational and total angular momentum quantum numbers are v'' and J''. h is the Planck's constant, and E,ν were measured from the experiment. The initial state that yields the maximum absorption cross section belongs to the lowest vibrational state, that is, v''=1. Lastly, from the Boltzman distribution of rotational states, J'' of the initial state with maximum probability for a given sample temperature is found. As a result, D_0 was calculated to be 3.18 eV with uncertainty 0.01 eV [van Veen 1979].

Van Veen et al.'s study is valuable in that it provides the magnitudes of absorption

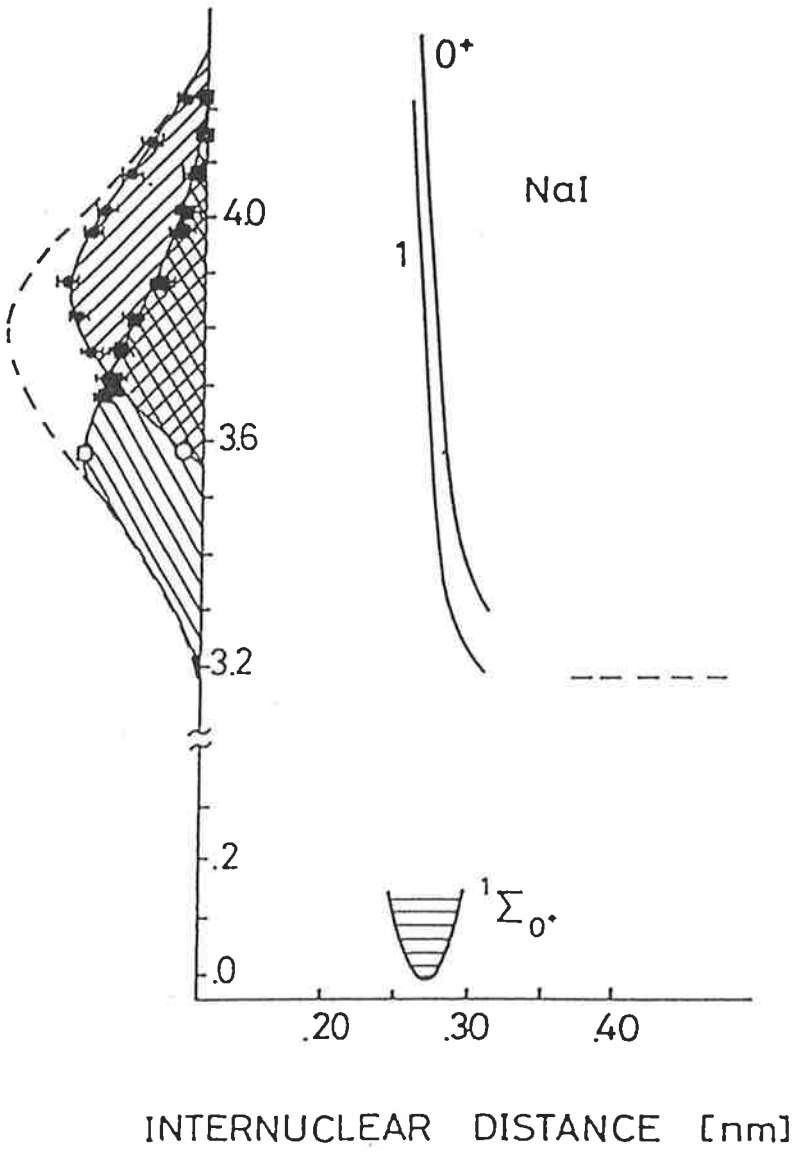

Figure 5.3: Potential curves of NaI from van Veen et al. [van Veen 1981]. Plots drawn on the vertical axis are the absorption cross sections they have measured, where a solid curve marked by a square and the other marked by a circle represent cross sections of the absorptions to the $\Omega = 1$ and 0^+ states respectively. The broken curve encompassing both solid curves is the total absorption cross section.

cross section for various energies. However, it is not very clear how they used their results to derive the corresponding excited state potential curves which are found to be inconsistent with later studies. More discussions will follow in the next chapter.

5.4.3 Schaefer et al.

A quantitative study of the rovibrational level structure of the excited states of NaI was carried out by Schaefer et al. [Schaefer 1982, Schaefer 1984] who performed UV laser induced fluorescence (LIF) experiments using a frequency doubled (SHG) pulsed dye laser in the range of 29960-33175 cm^{-1} (337.8-331.4 nm; 3.71-4.11 eV) to record the intensity of fluorescence lines, each of which was emitted by a transition from a photo-excited state to the electronic ground state of NaI, as a function of the frequency of the incident laser beam. The resultant spectrum (which we will call the LIF spectrum) is much simpler than the absorption spectrum because only excited states whose lifetimes are long enough can fluoresce before they predissociate. Child showed (p. 63 of [Child 1991]) that the energies E and the line widths Γ of narrow excited states can be expressed as

$$E = \frac{E_1 + xE_+}{1+x} \tag{5.45}$$

$$\Gamma = \frac{2\pi x(1+\gamma x)(E_1 - E_+)^2}{\hbar\bar{\omega}_1(1+x)^3} \tag{5.46}$$

where

$$\gamma = \hbar\bar{\omega}_1/\hbar\bar{\omega}_+, \quad x = u\gamma.$$

E_1 and E_+ in the above equations are the energies of states with the same rotational quantum number. $\hbar\bar{\omega}_1$ and $\hbar\bar{\omega}_+$ are respectively the local spacings of the corresponding diabatic and adiabatic vibrational energy levels. Thus, according to the above formula,

the energy of an excited rovibrational state is the weighted average of E_1 and E_+, the energies of the lower diabatic and upper adiabatic bound states. The potential curve for the upper adiabatic states is $E_+^e(R)$, while that of the lower diabatic states is given by

$$\begin{aligned} E_1^e(R) &= E_-^e(R) \text{ if } R < R_x \\ &= E_+^e(R) \text{ if } R > R_x \end{aligned}$$

which is called a 'modified' diabatic potential curve. Finally

$$u = \exp(-2\pi\nu) - 1$$

where ν is given by Eq. (5.38) which turns into Eq. (5.40) for the Landau-Zener model.

From Eq. (5.46), an excited state with zero width occurs if E_1 and E_+ of the same total angular momentum quantum number J are equal so that $E = E_+ = E_1$. The greater the difference between E_1 and E_+ is the larger Γ becomes and the corresponding excited state will have shorter lifetime. Accordingly, the fluorescence excitation spectra exhibits sharp lines if the excited states are long lived. An advantage of using Eq. (5.45) lies in that the rovibrational energy levels of the excited states can be obtained without the need to solve coupled nuclear Schrödinger's equations. Determination of the $A0^+$ state adiabatic potential curve by Schaefer et al. is based on this approach. Their analysis is the first attempt to quantitatively investigate the rovibrational structure of the $A0^+$ states of NaI and provided a firm ground on which the majority of later investigations could be based. Unfortunately, their articles did not present clear explanation of their analysis procedure and had to be reviewed intensively. What is given below is a

summary of the review.

5.4.4 Review of the analysis of Schaefer et al.

After measuring the frequencies of the incident laser beam for which fluorescence was detected, the differences between the observed lines in all possible combinations are tabulated and compared to the $X^1\Sigma^+$ rovibrational energy spacings calculated from the known constants [Schaefer 1982, Rusk 1962]. This was done with the use of the combination relation (p. 177 of [Herzberg 1950])

$$R(J-1) - P(J+1) = E''_{v'',J+1} - E''_{v'',J-1} \equiv \Delta_2 F''(J)$$

where E'' is an energy of the initial $X^1\Sigma^+$ rovibrational state and v'' its vibrational quantum number.

When an element in the tabulation of line spacings is found to be equal to a certain $\Delta_2 F''(J)$, those two lines of which the difference is taken originate from an excited rovibrational state with J and were obtained by excitations from the $X^1\Sigma^+$ states with $J-1$ (R branch) and with $J+1$ (P branch) and a certain vibrational quantum number v''. This 'pick-and-match' procedure is repeated until all the observed lines are satisfactorily accounted for. Once the lines are matched with the appropriate P or R labels and $J \pm 1$ values, one constructs a ladder of excited state energy levels each of which is assigned a total angular momentum quantum number J' by adding to them the energy of the $X^1\Sigma^+$ states from which the excitation took place. Since all the observed lines could be accounted for in this way, it was concluded that no Q branch is present and thus the excited states are of 0^+ symmetry, which will be called the $A0^+$ states from now on.

One should not be confused between the $A0^+$ states and the 'adiabatic' $A0^+$ states, the former being the levels measured from the experiment and the latter the levels belonging to the adiabatic $A0^+$ potential curve.

When the energies of the $A0^+$ states obtained as above were plotted versus $J(J+1)$ it was observed that the plot consists of groups of energy values that lie close to each other, forming approximately linear lines. These are represented in Fig. 5.4 by solid lines, which are referred to as 'band fragments'. Unfortunately the exact values of the calculated energies were not provided.

Using the vibrating rotator model (p. 109 of [Herzberg 1950]) in which the nuclear wavefunction of a diatomic molecule is written as Eq. (2.31), a bound state energy of a diatomic molecule can be obtained approximately if, instead of solving Eq. (2.32), perturbation theory is applied with the centrifugal potential term regarded as a perturbing operator and a normalized vibrational eigenfunction χ_v of the rotationless nuclear equation as the zeroth order wavefunction. To the first order the total energy becomes

$$E = T_v + B_v \tilde{J}, \quad \tilde{J} \equiv J(J+1) \tag{5.47}$$

where T_v is an eigenvalue of the nuclear Schrödinger's equation for a rotationless vibration, and

$$B_v = \frac{\hbar^2}{2\mu} \int \chi_v^2 \frac{1}{R^2} dR \tag{5.48}$$

is a rotational constant. Thus for each v, E is approximately represented as a linear function of $\tilde{J} \equiv J(J+1)$.

If E_1 of the diabatic $X^1\Sigma^+$ states and E_+ of the adiabatic $A0^+$ states are expressed

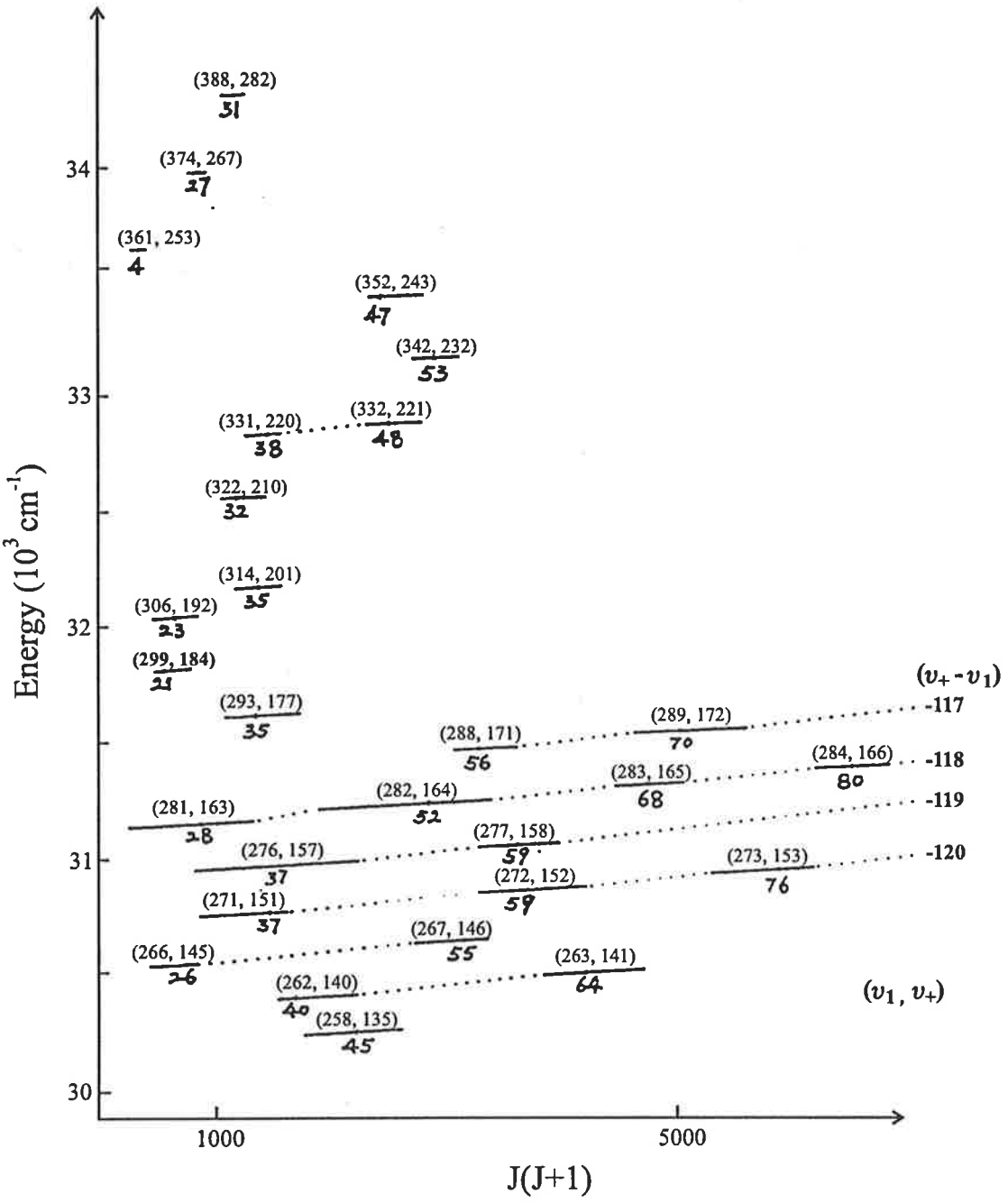

Figure 5.4: Energy levels obtained from the LIF spectroscopy [Schaefer 1984]. Handwritten numbers indicate the J values for which the sharpest lines with minimum line widths (central lines) are observed [Qin 1996].

as Eq. (5.47), the lines with minimum width satisfy the relation

$$T_{v_+} + B_{v_+}\tilde{J} = T_{v_1} + B_{v_1}\tilde{J},$$

that is,

$$\tilde{J} = \frac{T_{v_1} - T_{v_+}}{B_{v_+} - B_{v_1}} \tag{5.49}$$

or

$$J^2 + J - \frac{T_{v_1} - T_{v_+}}{B_{v_+} - B_{v_1}} = 0. \tag{5.50}$$

Graphically, the values of $\tilde{J}$ which satisfy Eq. (5.50) are points at which two lines E_1 and E_+ intersect. Since J can only be an integer (as NaI has an even number of electrons so that its spin is an integer), the sharpest lines in the spectra occur for integer J values that are closest to the positive root of Eq. (5.50). If J is increased or decreased from one of these intersections for a fixed pair of v_+ and v_1, the width of corresponding excited state energy levels increase so that the fluorscence lines from them broaden with decreasing intensity. Thus the structure of the fluorescence spectra can be understood; they consist of yet undetermined $v'' - (v_1, v_+)$ bands each of which has the sharpest line, called the 'central' line, whose J is determined from Eq. (5.50), and the rest of the lines broadening out.

One should also note that in order for the lines E_1 and E_+ to intersect either

$$T_{v_1} > T_{v_+}, \;\; B_{v_+} > B_{v_1} \tag{5.51}$$

or

$$T_{v_1} < T_{v_+}, \;\; B_{v_+} < B_{v_1} \tag{5.52}$$

must be fulfilled as $\tilde{J}$ has to be positive.

The energy E of the $A0^+$ states calculated from the observed fluorescence spectra can also be expressed using Eq. (5.47);

$$E_{(v_1,v_+),J} = T_{(v_1,v_+)} + B_{(v_1,v'_+)}\tilde{J} \tag{5.53}$$

where

$$T_{(v_1,v'_+)} = \frac{T_{v_1} + xT_{v_+}}{1+x}$$

and

$$B_{(v_1,v'_+)} = \frac{B_{v_1} + xB_{v_+}}{1+x}.$$

Using the J values as calculated above, Schaefer et al. fitted each of the band fragments with Eq. (5.53) to obtain their T and B values, which they called the 'effective' vibrational term values and rotational constants. Each effective rovibrational energy is, as is implied in Eq. (5.53), labelled by a pair of the diabatic and adiabatic vibrational quantum numbers (v_1, v_+) and the already determined rotational quantum number J. Fig. 5.4 also shows the final assignment of (v_1, v_+) which is not yet known at this stage.

Prior to the absolute assignment of v_1 and v_+ values, one band fragment was chosen as the reference fragment labelled by the yet undetermined vibrational quantum numbers (v'_1, v'_+) and the assignment of the vibrational quantum numbers for the other observed band fragments were made in reference to (v'_1, v'_+). The procedure described below had to be deduced from the contents of [Schaefer 1982, Schaefer 1984] as the datails were not explained clearly in their articles.

It seems that Schaefer et al. first assumed the rotational constants B_{v_+} and B_{v_1} do

not vary strongly enough to affect the assignment of the vibrational quantum numbers and were kept constant. Then the $\tilde{J}$ of the central lines in each band fragments depend only on $T_{v_1} - T_{v_+}$. With this assumption, one considers the change in $\tilde{J}$ that occurs when one moves from one band fragment to another. If both v_+ and v_1 are increased by one in reference to the band fragment labelled by (v_1', v_+'), $\tilde{J}$ of the central line in this new band fragment $(v_1' + 1, v_+' + 1)$ is given by

$$\begin{aligned} \tilde{J}[1,1] &\equiv \tilde{J}[v_1' + 1, v_+' + 1] \\ &= \frac{T_{v_1'+1} - T_{v_+'+1}}{B_+ - B_1} \\ &= \frac{(T_{v_1'} + \omega_{v_1'+1}) - (T_{v_+'} + \omega_{v_+'+1})}{B_+ - B_1} \end{aligned}$$

with the rotational constants B_+ and B_1 kept fixed, so that

$$\begin{aligned} \Delta\tilde{J} &\equiv \tilde{J}[1,1] - \tilde{J}[0,0] \\ &= \frac{\omega_{v_1'+1} - \omega_{v_+'+1}}{B_+ - B_1} \end{aligned} \tag{5.54}$$

and therefore

$$\tilde{J}[1,1] = \tilde{J}[0,0] + \frac{\omega_{v_1'+1} - \omega_{v_+'+1}}{B_+ - B_1},$$

where

$$\begin{aligned} \omega_{v_1'+1} &= T_{v_1'+1} - T_{v_1'}, \\ \omega_{v_+'+1} &= T_{v_+'+1} - T_{v_+'} \end{aligned}$$

are the diabatic and the adiabatic local vibrational spacings.

The energy of the central line of a band fragemnt $(v_1'+1, v_+'+1)$ can then be written as

$$\begin{aligned} E[1,1] &= T_{v_1'+1} + B^d \tilde{J}[1,1] \\ &= T_{v_1'} + \omega_{v_1'+1} + B_1 \tilde{J}[1,1] \\ &= T_{v_1'} + \omega_{v_1'+1} + B_1 \left(\tilde{J}[0,0] + \frac{\omega_{v_1'+1} - \omega_{v_+'+1}}{B_+ - B_1} \right) \end{aligned} \tag{5.55}$$

or equivalently

$$\begin{aligned} E[1,1] &= T_{v_+'+1} + B_+ \tilde{J}[1,1] \\ &= T_{v_+'} + \omega_{v_+'+1} + B_+ \tilde{J}[1,1] \\ &= T_{v_+'} + \omega_{v_+'+1} + B_+ \left(\tilde{J}[0,0] + \frac{\omega_{v_1'+1} - \omega_{v_+'+1}}{B_+ - B_1} \right) \end{aligned} \tag{5.56}$$

because the diabatic and the adiabatic energies are the same at a central line. Consequently, the difference between the energies of the above two central lines is

$$\begin{aligned} E[1,1] - E[0,0] &= \omega_{v_1'+1} + B_1 \frac{\omega_{v_1'+1} - \omega_{v_+'+1}}{B_+ - B_1} \\ &= \omega_{v_+'+1} + B_+ \frac{\omega_{v_1'+1} - \omega_{v_+'+1}}{B_+ - B_1} \end{aligned}$$

from which one arrives at the relation

$$\begin{aligned} \Delta E &\equiv E[1,1] - E[0,0] \\ &= \omega_{v_1'+1} + B_1 \Delta \tilde{J} \\ &= \omega_{v_+'+1} + B_+ \Delta \tilde{J}. \end{aligned}$$

Since ω and B values are all positive, ΔE and $\Delta \tilde{J}$ have the same sign.

This relation was seen to hold for the series of band fragments linked by the dotted lines in Fig. 5.4, where seven such series consisting of two to four component band fragments are illustrated. In other words, if one band within a series is labelled by (v_1', v_+'), the next fragment of higher energy linked by the dotted line is given the assignment $(v_1' + 1, v_+' + 1)$, thereby keeping $v_+ - v_1$ constant within a series. This progression of increasing (v_1, v_+) continues until J becomes too high for the corresponding band fragment to be observed experimentally due to the very low population of the lower state from which the excitation should take place. Then a new series starts with different value of $v_+ - v_1$.

Having found the manner in which (v_1, v_+) values progress within a series, the next step is to determine the change in (v_1, v_+) as one moves from one series to another. Schaefer et al. noticed that the monotonic increase in J of the central lines within a series implies that, according to Eq. (5.54), either

$$\omega_{v_1} > \omega_{v_+}, \quad B_1 < B_+ \tag{5.57}$$

or

$$\omega_{v_1} < \omega_{v_+}, \quad B_1 > B_+ \tag{5.58}$$

must hold for any pair of diabatic and adiabatic states that gives rise to an observed state in a band fragment. For convenience it will be assumed that the relation (5.58) is chosen, which was found to be the correct one later in the articles of Schaefer et al.

The copious number of band fragments that were detected in the observed energy region was taken to imply that the local spacings of diabatic and adiabatic states are

very close to the effective local vibrational spacing. Schaefer et al. chose this value to be 32 cm^{-1} that they stated to be the minimal spacing of the successive levels, which must mean the minimum difference between the effective vibrational term values T extrapolated from the observed band fragments with the use of Eq. (5.53). Thus the Δv_+ and Δv_1, changes in the adiabatic and diabatic quantum numbers between the last fragment of one series and the first fragment of another series, must have been obtained by finding the integer closest to the value $\Delta T/32$, although this was not mentioned in their articles.

It follows from the relation (5.58) that Δv_+ is greater than Δv_1, and Δv_+ is then the integer closest to and smaller than $\Delta T/32$, while Δv_1 is the integer closest to and larger than $\Delta T/32$. Hence $v_+ - v_1$ of a new series is increased by one. One should remember that this reasoning is not applied to the band fragments belonging to the same series, for which $\Delta v'_d$ and $\Delta v'_a$ are equal.

However, the choice of 32 cm^{-1} as the minimum T difference is questionable. From Tab. 5.1 where the measured transition frequencies of the eight central lines and the extrapolated vibrational term values T of the corresponding band fragments are reported, one can see that the difference between the values of T for the band fragments assigned as $(v'_1 + 8, v'_+ + 7)$ and $(v'_1 + 7, v'_+ + 6)$ is 30.8cm^{-1} and hence is smaller than the so-called minimum of 32 cm^{-1}. Had the value of 30.8 cm^{-1} been used instead of 32 cm^{-1} to determine the increase in the vibrational quantum numbers for a fragment in the second row of the Tab. 5.1, it would have been labelled $(v'_1 + 15, v'_+ + 13)$ rather than $(v'_1 + 14, v'_+ + 12)$, which would in turn have changed the assignments of all the other band fragments of higher energy.

In addition, the assignment of the fragment in the sixth row is unclear for a different

v_1	v_+	$T_{v_1}(=T_{v_+})(\mathrm{cm}^{-1})$
$v_1'+15$	$v_+'+13$	31413.4
$v_1'+14$	$v_+'+12$	31387.9
$v_1'+9$	$v_+'+8$	31229.9
$v_1'+8$	$v_+'+7$	31193.4
$v_1'+7$	$v_+'+6$	31162.6
$v_1'+6$	$v_+'+5$	31129.9
$v_1'+1$	$v_+'+1$	30969.5
v_1'	v_+'	30935.5

Table 5.1: Relative vibrational quantum number assignments and calculated term energies from the observed central lines, taken from [Schaefer 1982].

reason. The difference between $(v_1'+1, v_+'+1)$ and $(v_1'+6, v_+'+5)$ is 160.4 cm^{-1} so that $\Delta T/32$ is 5.01 and $\Delta T/30.8$ is 5.20, while the increase in v_1 being 5 not 6. An assignment scheme which is consistent for both of the above examples would be to choose an integer closest to the value of ΔT divided by a chosen vibrational spacing, but then there is no plausible reason why the change in v_+ should not be 5 and the change in v_1 6. It is not clear why the minimum spacing had to be used to determine the change in (v_1, v_+) either. Thus it seems that there is quite appreciable uncertainty in the assignment of vibrational quantum numbers to the band fragments.

At any rate, the relative assignment of (v_1, v_+) can now be made for all the observed band fragments in reference to the fragment with the lowest effective vibrational term value, as is shown in Tab. 5.1 for eight fragments. Then the central lines of the observed band fragments, of which one knows the absolute J values for certainty and the relative assignments $(\bar{v}_1, \bar{v}_+)$ of (v_1, v_+), are fitted to the two Dunham-type expansions of rovibrational energy levels

$$E_{v_{1/+}J} = \sum_{i,j=0} Y_{ij}^{1/+} (\bar{v}_{1/+} + \frac{1}{2})^i [J(J+1)]^j \tag{5.59}$$

to obtain sets of expansion parameters $Y_{ij}^{1/+}$ (one set for the diabatic and the other for the adiabatic levels). This fitting gave the first estimate of the parameters $Y^{1/+}$ and also the consistency check on the relative assignments of (v_1, v_+) which they regarded as acceptable.

If a given system is strongly adiabatic, x in Eq. (5.45) is large and the observed energies E will be close to E_{v_+J}, and conversely in a strong diabatic case E will be close to E_{v_1J}. When an attempt was made to reproduce all the observed lines by either diabatic or adiabatic expansion parameters, it was found that the adiabatic parameters generated the lines reasonably and were then used to obtain the adiabatic energy levels. Next, optimization of the diabatic expansion parameters were carried out with the use of Eq. (5.45) while the adiabatic expansion parameters were kept fixed. The overall procedure also involved the determination of diabatic coupling strength, detailed discussion of which will not be presented here as it was adequately explained by Schaefer et al.

Having generated the diabatic and the adiabatic energy levels as above, a fitting procedure was performed again, the end result being two sets of expansion parameters in Eq. (5.59) for the adiabatic and diabatic energy levels and the absolute assignments of vibrational quantum numbers v_1 and v_+.

In order to obtain the diabatic $X^1\Sigma^+$ and the adiabatic $A0^+$ state potential curves by the RKR method [Mason 1962], one needs to have the energies of all the rovibrational states starting from $v_1, v_+ = 0$ to the upper bound of one's interest. In the fitting of the diabatic energy levels to find Y_{lk}^1, the ground state energy levels obtained from some fluorescence emission spectra of their own and microwave spectroscopy[Rusk 1962] were also included, and the remaining unobserved levels were extrapolated from final Y_{lk}^1s. The final Y_{lk}^+s for the adiabatic $A0^+$ states were optimized with the condition

that the atomic dissociation limit of NaI, for which an estimate by van Veen et al. [van Veen 1981] was employed, is the minimum of the adiabatic $A0^+$ potential curve. Levels that lie below the observed energy region were then simply extrapolated from those Y_{lk}^+s.

Although the pioneering investigation by Schaefer et al. made it possible to gain a much deeper understanding of the rovibrational energy structure of NaI, their proposed potential curve of the $A0^+$ state was found to be far from being adequate in several ways. Because the ground state rovibrational levels were fairly accurately identified and accuracy in the measurement of transition frequency is very high, determination of J and v'' for observed lines can be trusted without any uncertainty. However, we discussed that the assignments of (v_1, v_+) are ambiguous. Thus the Dunham parametrisation of the adiabatic and diabatic levels can not be taken as being definite or unique, and should only be regarded as a means of conveniently representing the observed energy levels.

The problem in Schaefer et al.'s study is that the Dunham parameters optimized to express the adiabatic and diabatic levels in their investigated energy region are then used to extrapolate to all the other unobserved levels of lower energies. Even if the v_1 and v_+ assignments were correct, the parameters are only optimized to represent the observed levels and thus the error in the calculation of the energies will increase as the corresponding extrapolated levels are located farther from the investigated energy region. Consequently, the potential curves which are obtained from these extrapolated levels via an RKR-like method become less credible, especially for the adiabatic $A0^+$ potential curve for which no experimental information is available at the lower energy region. As will be discussed in more detail in the next chapter, it is indeed found that Schaefer et al.'s curves are not consistent with the measured absorption intensities

reported in other studies. It has also been found [Wang 1990] that Schaefer et al.'s adiabatic $A0^+$ potential curve do not even agree with their own estimate of the diabatic coupling strength.

It should also be pointed out that Schaefer et al. generated the 'pure' diabatic $X^1\Sigma^+$ potential curve, whereas according to Child's semiclassical model the diabatic nuclear wavefunctions are solutions of the modified diabatic potential curve as defined above.

Lindner et al. [Lindner 1994], in their follow-up study of Schaefer et al.'s work, also acknowledged the inadequateness of extrapolating the lower energy levels unobserved in the LIF spectra from the Dunham parameters. They then proceeded by performing both LIF and Λ-type two-photon (ΛTP) spectroscopy to observe $A0^+$ state rovibrational levels that lie below Schaefer et al.'s investigated energy region. More details are given in Section 6.3 of this thesis.

Further discussions regarding more recent studies on NaI, including refinements on Schaefer et al.'s analysis as well as alternative ways to derive potential curves, are presented in the next chapter.

Chapter 6

Determination of the $A0^+$ state potential curves of NaI

6.1 Analytic Expressions for the Potential Curves

Wang et al. [Wang 1990] found that the potential curves of Schaefer et al., which are obtained by the procedure described in the previous section, correspond to a coupling strength that is three times larger than their own numerical estimate. This inconsistency can be verified by comparing the difference between the energies of the diabatic $X^1\Sigma^+$ and the adiabatic $A0^+$ potentials at the diabatic crossing point $R_x = 6.93$ Å to their H_{12}^e estimate of 0.054 eV, which should be equal.

Therefore, in spite of the uncertainties in the estimates of the crossing point and the coupling strength [Wang 1990], Schaefer et al.'s potential can not be deemed reasonable. As Schaefer et al.'s potentials are generated by applying an RKR-like procedure to their vibrational energies and rotational constants which are extrapolated from the Dunham expansion parameters optimized to reproduce the observed spectral lines, one is led to

conclude that the extrapolation gave incorrect prediction to the positions of low energy $A0^+$ vibrational levels even if one accepts that the observed levels are satisfactorily accounted for by the Dunham parameters.

Unlike Schaefer et al.'s approach, Wang et al. sought to express the potential curves as analytic functions of R whose coefficients are optimized to reproduce the observed energy levels only. Qin [Qin 1996] then followed on from Wang et al.'s investigation with tighter constraints to give potential curves which reproduce the observed energy levels more accurately.

A review of various analytic expressions for a description of the diabatic ground state potential curves of alkali halide diatomic molecules is presented by Jordan [Jordan 1979]. In order to analytically express the diabatic $X^1\Sigma^+$ potential of NaI, Qin and Wang et al. used the formulas

$$E_1^e(R) = \left[A_1 + \left(\frac{B_1}{R}\right)^8\right] \exp(-R/\rho_1) - \frac{C_1}{R^6} + D_i - \frac{e^2}{4\pi\epsilon_0}\left(\frac{D_1}{R} + \frac{\alpha^+ + \alpha^-}{2R^4}\right) \qquad (6.1)$$

and

$$E_1^e(R) = \left[A_1 + \left(\frac{B_1}{R}\right)^8\right] \exp(-R/\rho_1) - \frac{C_1}{R^6} + D_i - \frac{e^2}{4\pi\epsilon_0}\left(\frac{D_1}{R} + \frac{\alpha_+ + \alpha_-}{2R^4} + \frac{2\alpha_+\alpha_-}{R^7}\right) \qquad (6.2)$$

respectively, with the value of each parameter given in Tab. 6.1. Their potentials are shown in Fig. 6.1 together with those derived by Schaefer et al. It is to be noted that Wang et al. used a 'pure' diabatic potential(as opposed to a 'modified' diabatic potential defined in 5.4.3). This aspect will further be commented on in 6.3.2.

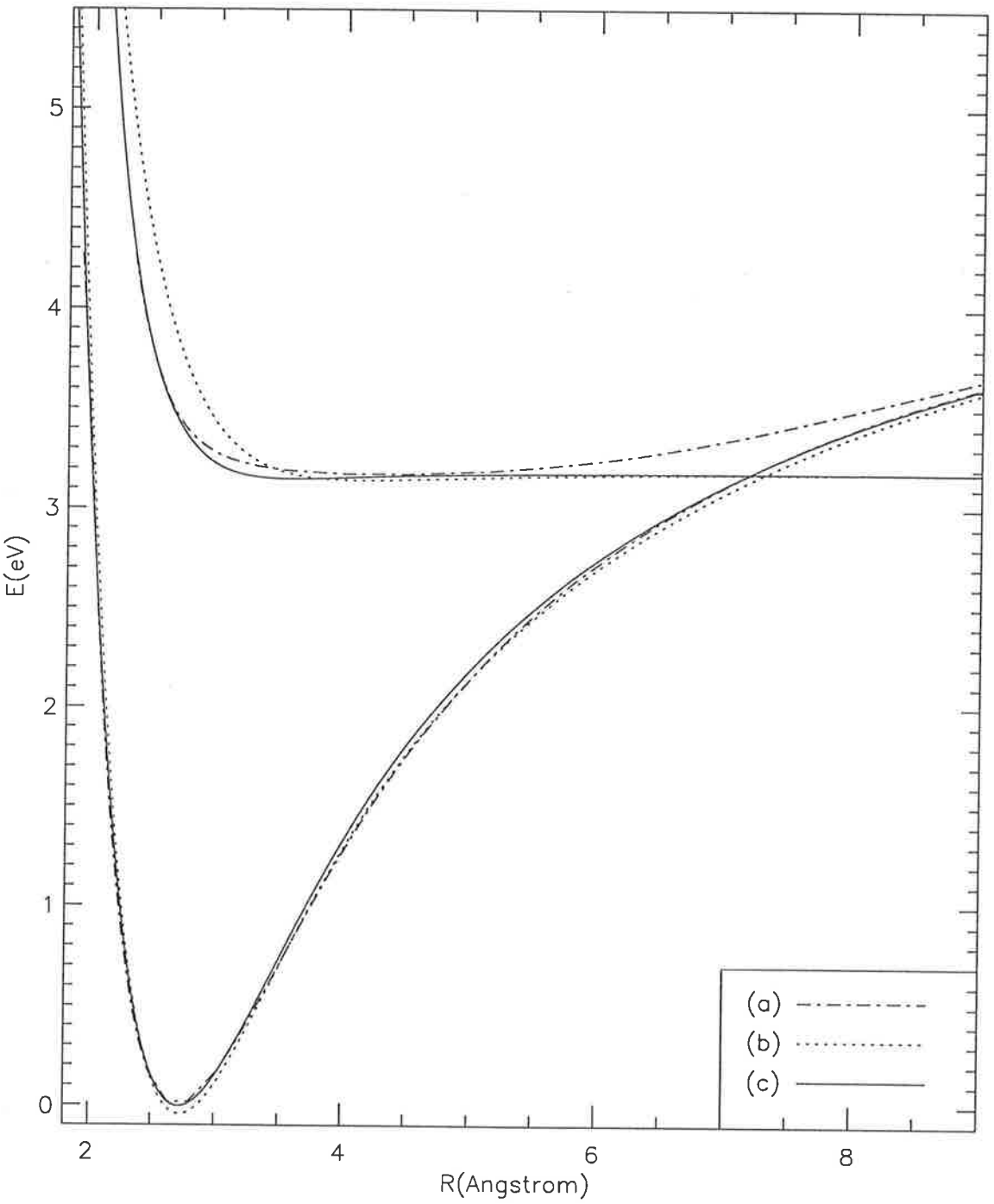

Figure 6.1: Plots of $X^1\Sigma^+$ (lower curves) and $A0^+$ (upper curves) potentials derived from Schaefer et al.'s observed energy levels; (a) Schaefer et al., (b) Wang et al. and (c) Qin.

Parameters	Wang et al.	Qin
A_1	2758.0	1744.7
B_1	1.742	2.107
ρ_1	0.3603	0.3910
C_1	12.72	19.54
D_i	5.312	5.258
D_1	1.072	1.0215
α_+	1.375	n/a
α_-	5.446	n/a
$\alpha^+ + \alpha^-$	n/a	11.09
A_2	3150.0	3100.0
R_0	0.61	n/a
B_2	2.710	3.33
ρ_2	0.4277	0.3168
C_2	1000.0	150
D_e	3.18	3.18
h_x	0.055	0.055
β_{12}	0.6858	n/a
R_x	7.293	7.14

Table 6.1: Parameters for the NaI potential curves (in eV-Å units) of Wang et al. and of Qin.

Wang et al.'s expression for the diabatic $A0^+$ potential curve $E_2^e(R)$ is

$$E_2^e(R) = \left[A_2 + \left(\frac{B_2}{R+R_0}\right)^{12}\right] \exp\left(-\frac{R+R_0}{\rho_2}\right) - \frac{C_2}{(R+R_0)^6} + D_e \qquad (6.3)$$

where D_e is the atomic dissociation limit of NaI. Qin's expression is the same as Eq. (6.3) except that R_0 is excluded;

$$E_2^e(R) = \left[A_2 + \left(\frac{B_2}{R}\right)^{12}\right] \exp\left(-\frac{R}{\rho_2}\right) - \frac{C_2}{R^6} + D_e. \qquad (6.4)$$

The adiabatic $A0^+$ potential curve E_+^e is then obtained from $E_1^e(R)$ and $E_2^e(R)$ via

Eq. (5.12). In Wang et al.'s calculation the diabatic coupling was defined as

$$H_{12}^{e}(R) = h_{\mathrm{x}} \exp[\beta_{12}(R - R_{\mathrm{x}})^2],$$

while in Qin's derivation it was assumed to be constant in R. In both investigations, h_{x} and D_e were constrained to be 0.055 eV and 3.18 eV respectively. All other parameters were obtained from optimization. These potentials are also shown in Fig. 6.1.

The main graphical differences between Wang et al.'s and Schaefer et al.'s potential curve of the $A0^+$ state are the locations of inner limb and the energy values near the diabatic crossing point. Wang et al. [Wang 1990] also indicated that the adiabatic $A0^+$ potential curve of Schaefer et al. leads to too large rotational constants of the corresponding vibrational states and it may be necessary to slightly revise the assignment of the vibrational or rotational quantum numbers to the observed LIF spectrum.

Qin argued that it is not possible to change the rotational quantum number assignments to the observed lines in the spectrum and only the vibrational quantum numbers can be changed, which is right as the determination of J by the $\Delta_2 F''(J)$ method is very reliable. Qin then made several modifications to the Wang et al.'s procedure and reoptimized the potential curves, his resultant $A0^+$ potential being closer to the Schaefer's potential than Wang et al.'s potential is. One can see from Fig 6.1 that the repulsive limb of Qin's reoptimized potential is almost identical to that of Schaefer et al. except at very low energy regions.

Qin's modification also resulted in the change of vibrational quantum numbers by +9 for the upper adiabatic states and +3 for the lower diabatic states. His optimization includes the use of the modified diabatic $X^1\Sigma^+$ potential curve. However, as was dis-

cussed in the previous chapter, the optimized Dunham parameters are not to be used to predict the energy levels oustside their investigated energy region and these potential curves, especially those of the $A0^+$ state, can not be trusted. The fact that all of the above three derivations, even though being different from each other, are capable of reproducing the excited state energy levels calculated from Schaefer et al.'s spectra indicates that an analysis based only on the energy levels is not enough for a determination of the $A0^+$ potential. Therefore a different approach must be found in order to derive the $A0^+$ potential curve.

One reminder is necessary before we move on, in that we will regard the $A0^+$ potential reoptimized by Qin as a proper representation of the energy levels observed by Schaefer et al. This is because the original potential of Schaefer et al. is even inconsistent with their own experimental estimate of the electronic coupling strength as is explained above, and also Qin's reoptimized potential is reported to reproduce Schaefer et al.'s observed energy levels more accurately than the potential of Wang et al. By the 'Schaefer-Qin' potential we thus mean the diabatic $A0^+$ potential of Qin expressed by Eq. (6.4), from which the adiabatic $A0^+$ potential is derived with the use of the transformation formula (5.12) and the constant electronic coupling strength of 0.055 eV. Since the repulsive limbs of the $A0^+$ potential by Schaefer et al. and Schaefer-Qin potential are almost identical to each other, this replacement does not affect the discussions regarding the absorption intensity presented below.

6.2 Franck-Condon Factor

Another problem with Schaefer et al.'s potential which we will now discuss is that, in contrast to their claim, the Franck-Condon factors (the FCs in short) for the $v'' = 0$

state from their potential curve do not agree with that of the potential from van Veen et al.'s photofragmentation spectroscopy. We will also show in this section that Schaefer et al.'s $A0^+$ potential is not consistent with the experimentally measured photoabsorption intensity.

In addition, we will discuss how the intensity measurements of absorption spectra can be used to gain infomations on the repulsive limb of an excited state potential. Unfortunately, we do not have accurate measurements of absorption intensities and therefore our analysis will not be precise.

6.2.1 Franck-Condon factor and the intensity of an absorption spectrum

The FC is mathematically expressed as the square of the overlap integral of a lower and an upper state vibrational wavefunction $\chi''_{v''}$ and $\chi'_{v'}$;

$$FC(v'', E_t) = (\int \chi''_{v''}\chi'_{v'}dR)^2 \tag{6.5}$$

where $E_t = E' - E''$, the difference between the energies of upper and lower vibrational states. FC as a function of the lower state vibrational quantum number and the transition energy describes approximately the general intensity distribution of the transitions between the states belonging to the different potential curves. Since the ground state low vibrational levels are accurately known, the FC's and the associated intensity of transition spectra can be used to gain information on the excited states. Unfortunately in Schaefer et al.'s LIF articles, relative intensities were not reported and therefore no information regarding the values of FC could be drawn. On the other hand, the poten-

tial curve fragment of van Veen et al. is only of the repulsive limb and thus can not be used to generate the rovibrational energy levels.

In Qin's investigation [Qin 1996] to resolve the above dilemma, absorption spectra of NaI were produced using a DCM dye laser in a transition energy region from 30000 to 31200 cm^{-1} and compared to a model spectrum whose line shape I_ν of a transition frequency ν was expressed as

$$I_\nu = \frac{I_0}{\omega_v} V(\nu - \nu_0), \tag{6.6}$$

where V is an empirical approximation to the Voigt profile [Whiting 1968]. The width ω_v of V is given by

$$\omega_v = \frac{w_l}{2} + \sqrt{\frac{\omega_l^2}{2} + \omega_g^2}$$

where ω_g and ω_l are the Doppler width and the predissociation line width respectively. Assuming that the oscillator strengths are the same for all vibrational levels, Qin expressed I_0 as

$$I_0 = A_0 Bz(v'') FC(v'', E_t) S_J \exp(-B_{v''} J''(J''+1)hc/kT), \tag{6.7}$$

where A_0 is a scaling constant, S_J the Hönl-London factor, $Bz(v'')$ the Boltzmann population distribution of the initial vibrational state with v'' its quantum number, k Boltzmann's constant, c the velocity of light, h Planck's constant, and T the temperature of the NaI vapor. The remaining details of the modelling will be given in Subsection 6.2.4.

In order to generate the excited state energy levels, Qin reoptimized the Dunham parameters of Schaefer et al. to represent the observed sharpest lines only. The energy levels calculated from the reoptimized parameters, via Child's semiclassical theory, are

then regarded as the experimental energy levels.

Before discussing the study by Qin, we will look at van Veen et al.'s analysis more closely. Although it was not clearly explained in their article, van Veen et al.'s excited state potential curve seems to have been derived by comparing the observed absorption cross section to the sum of FCs for the six lowest $X^1\Sigma^+$ vibrational states, each of which were weighted according to the Boltzmann population distribution at the experimental temperature of NaI vapour.

Provided that the electronic transition dipole moment is constant in R and the rotational effect is not significant, the magnitude of the resultant weighted sum of the FC's should vary similarly in the transition energy E_t to that of the observed absorption intensity (or cross section) times a constant factor. Their derivation is also based on an approximation scheme in which an excited state vibrational wavefunction is replaced by a delta function located at the turning point on the repulsive limb for a given energy. Although it seems a very crude approximation to replace a vibrational wavefunction with a delta function, this method works surprisingly well (see p. 399 of [Herzberg 1950] and references therein). As is discussed below, the delta function approximation plays a key role in deducing the shape of the repulsive limb of the excited electronic state potential curve.

6.2.2 Delta function approximation method

If an excited state vibrational wavefunction $\chi'_{v'}$ in Eq. (6.5) is approximately represented as a delta function whose maximum is located at the classical turning point for the

corresponding energy E', Eq. (6.5) reduces to

$$FC(v'', E_t) = (\chi''_{v''}(R[E']))^2, \quad E' = E_t + E'', \tag{6.8}$$

that is, $FC(v'', E_t)$ is equal to the square of the ground state vibrational wavefunction $\chi''_{v''}$ at $R[E']$ where $R[E']$ is the location of the classical turning point for E'. Therefore, without considering the fine structure of rotational levels, the intensity of absorption from the v'' state is approximately described by the square of $\chi''_{v''}$.

Since FC in Eqs. (6.5) and (6.8) can also be expressed as a function of E';

$$FC(v'', E') = (\chi''_{v''}(R[E']))^2, \tag{6.9}$$

we can find the locations of the turning points and hence elaborate the shape of the excited electronic state potential curve from Eq. (6.9) if FC and $\chi''_{v''}$ are known. Below we describe how the repulsive limb of the NaI $A0^+$ state potential curve is deduced from limited informations about the absorption intensity and about FCs for $v'' = 0$ and $v'' = 1$ states.

6.2.3 Location of the maximum absorption

With the assumption that the transition from the $v'' = 0$ state is dominant where the maximum absorption is observed, one can estimate the value of an excited potential curve at the ground state equilibrium distance at which the $v'' = 0$ state vibrational wavefunction will have its maximum amplitude. For a given temperature of NaI vapour in van Veen et al.'s experiment the above assumption is sensible as the $v'' = 0$ state is most highly populated [Qin 1996] and the FC of the $v'' = 0$ state is much larger than

that of the $v'' = 1$ state near the ground state equilibrium distance. Therefore, under the delta function approximation scheme, the absolute energy value of the upper state for which the maximum absorption is detected corresponds to the value of the excited state potential curve at the ground state equilibrium distance. According to Fig. 5.3, the maximum absorption from $X^1\Sigma^+$ to $A0^+$ was detected around 3.9 eV, and the value of van Veen's $A0^+$ state potential curve at the ground state equilibrium (which is taken to be 2.7 Å) is 3.88 eV (or about 31290 cm^{-1}). Hence, although the FCs for van Veen et al.'s potential can not be generated as only a fragment of its repulsive limb can be drawn from van Veen et al.'s expression (Eq. (5.44)), it is clear that FCs for the potentials of van Veen et al. and of Schaefer et al. are not consistent with each other. FCs from van Veen et al.'s potential for transitions involving the $v'' = 0$ state will have a maximum at $E' \approx 3.88$ eV whereas the maximum of FCs from Schaefer et al.'s potential (and of Schaefer-Qin potential) will be located at far smaller value of E' as can be seen from Fig. 6.1.

In addition, transitions to the $\Omega = 1$ state are seen to yield a maximum in the cross section at 3.63 eV (or about 29270 cm^{-1}). If one only considers transitions from the $v'' = 0$ state, whose vibrational energy is about 130 cm^{-1}, the value of the transition energy for which the total maximum absorption cross section occurred may be estimated to lie between 29140 $(= 29270 - 130)$ cm^{-1} and 31160 $(= 31290 - 130)$ cm^{-1}. A measurement of total absorption intensity by Berg and Skewes [Berg 1969] agrees with van Veen et al.'s observation in that a maximum intensity was detected near the transition wavelength of 3240 Å, being 30860 cm^{-1} in wavenumber and is roughly in accordance with the estimated location of the maximum total absorption cross section detected from the photofragmentation spectroscopy of van Veen et al. and absorption measurements by

Davidovits and Brodhead [Davidovits 1967].

Since no accurate data on absorption intensity are available, it is not possible to carry out more quantitative analysis regarding the FCs. Likewise, a comparison between the intensity plot of Berg and Skewes and the cross section of van Veen et al. does not by itself lead to any definite conclusion on how the inner limb of the $A0^+$ state potential curve should be. One conclusion that can be made, however, which is consistent with the above observations is that the value of the $A0^+$ potential curve at the ground state equilibrium distance is close to the sum of the transition energy yielding the maximum absorption intensity and the energy of the $v'' = 0$ state. Berg and Skewes observed a maximum absorption at 30860 cm^{-1} which corresponds to 30990 cm^{-1} in absolute energy scale (as $E''(v'' = 0) = 130$ cm^{-1}), or 3.84 eV. The maximum absorption to the $A0^+$ state was seen to occur at 3.88 eV by van Veen et al., while their total absorption cross section peaks near 3.80 eV according to Fig. 5.3 which differs from the result of Berg and Skewes by about 0.04 eV. Thus we can safely estimate that the value of the $A0^+$ potential at the ground state equilibrium distance should lie between 3.83 eV and 3.93 eV, taking the uncertainty of ± 0.05 eV from the location of maximum absorption to $A0^+$ observed by van Veen et al.

Neither the Schaefer-Qin potential, Wang et al.'s potential nor Schaefer et al.'s potential meet this condition at all, their repulsive limbs being located at too small R with a steep slope. In addition to the fact that the FC from Schaefer et al.'s potential for $v'' = 0$ state disagrees with the FC from van Veen et al.'s potential as was discussed above, these potentials can not in any way be consistent with either the absorption cross section observed by van Veen et al. or the intensity of absorption spectra recorded by Berg and Skewes and by Davidovits and Brodhead.

6.2.4 Crossover of the Franck-Condon factors

Now we will briefly discuss Qin's work, focusing mainly on his analysis based on the FCs. Considerations regarding the rotational constants will be given in the next section.

As all the terms in Eq. (6.7) except the FC are straightforwardly obtained, an absorption spectrum could be modelled to find the ratio of FCs for different v'' values that best simulate the experimental spectrum if the electronic transition dipole moment is assumed constant in R. The Doppler width ω_g in Eq. (6.6) was taken to be 0.12 cm^{-1}, although the actual width is about 0.05 cm^{-1}, in order to approximately describe the convolution of the Doppler width and the instrument function whose band width was between 0.07 and 0.1 cm^{-1}. The predissociation line width ω_l of an absorption line was approximately expressed as

$$\omega_l = 3 \cdot 10^{-8}(\Delta J(2J_c + \Delta J + 1))^2 \text{ cm}^{-1}$$

where J_c is the rotational quantum number of the central line of a band fragment to which a given absorption line belongs and $\Delta J \equiv J - J_c$. It should be emphasized that the modelling of the absorption spectra according to Eqs. (6.6) and (6.7) is not precise and can not be expected to reproduce the observed spectra with good accuracy.

Qin only considered absorptions from $v'' = 0$ and $v'' = 1$ states to conclude that, by comparing the his model spectra to his observed absorption spectra, $FC(v'' = 1, E_t)$ is larger than $FC(v'' = 0, E_t)$ for transition energies E_t lower than 30500 cm^{-1} and vice versa otherwise. In other words, if $FC(v'' = 1, E_t)$ and $FC(v'' = 0, E_t)$ are plotted versus E_t, they will cross each other at $E_t \approx 30500$ cm^{-1}. Contributions to the spectrum from the initial states with v'' higher than 1 was assumed insignificant, which is reasonable

according to the magnitudes of $Bz(v'')$ for the temperature of the NaI vapour.

The $A0^+$ diabatic potential curve proposed by Qin is analytically expressed as

$$E_2^e(R) = \frac{12}{R^3} \exp\left\{-\left[0.01 + \left(\frac{R}{7.5}\right)^6\right](R - 2.7) + \left(\frac{2.42}{R}\right)^{15}\right\} + 3.18 \qquad (6.10)$$

whose plot is shown in Fig. 6.2 along with the other proposals. The potential of Cong et al. will be discussed in Subsection 6.2.5, and that of Lindner et al. whose work we briefly mentioned in Subsection 5.4.4 will be further discussed in the next section. Qin obtained Eq. (6.10) by requiring that the new potential curve should meet the conclusions he drew on FCs while being able to reproduce the observed band fragments of Schaefer et al.'s LIF study.

One can observe from Fig. 6.3 that his conclusion about FCs is well represented, and no resemblance can be found at all between Qin's and Schaefer-Qin's FCs. For the purpose of calculating the FCs the excited state vibrational wavefunctions are approximated as those belonging to the diabatic $A0^+$ potential. This is a fair approximation since the magnitude of FC is mainly determined by the shape of the wavefunction near the classical turning point on the repulsive limb of the $A0^+$ potential as long as the other turning point (in case of the adiabatic bound potential) is located at a sufficiently large value of R.

Furthermore, it is apparent that the potential of van Veen et al. does not meet Qin's observation of $FC(v'' = 1)$ becoming greater than $FC(v'' = 0)$ for E_t lower than 30500 cm^{-1}. As can be seen from Fig. 6.2, van Veen et al.'s curve is too steep for the $v'' = 1$ transitions to have greater contribution to the absorption spectrum for transition energies below 30500 cm^{-1}. The implication brought by such a steepness of the repulsive

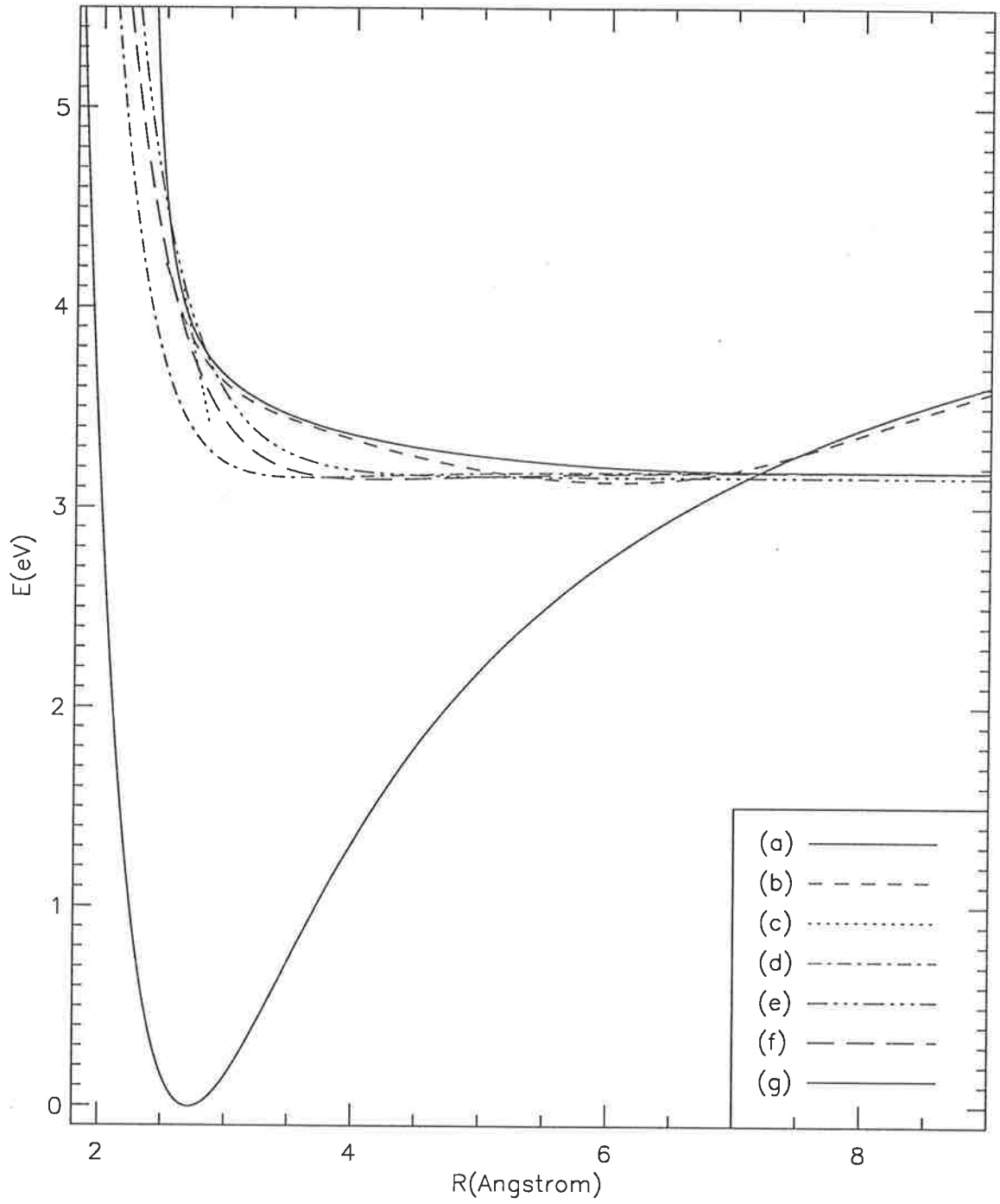

Figure 6.2: $A0^+$ potentials proposed from various experimental studies; (a) Qin (upper solid line), (b) Lindner et al., (c) van Veen et al., (d) Schaefer-Qin, (e) Cong et al., (f) Wang et al. and (g) diabatic $X^1\Sigma^+$ potential by Qin (lower solid line).

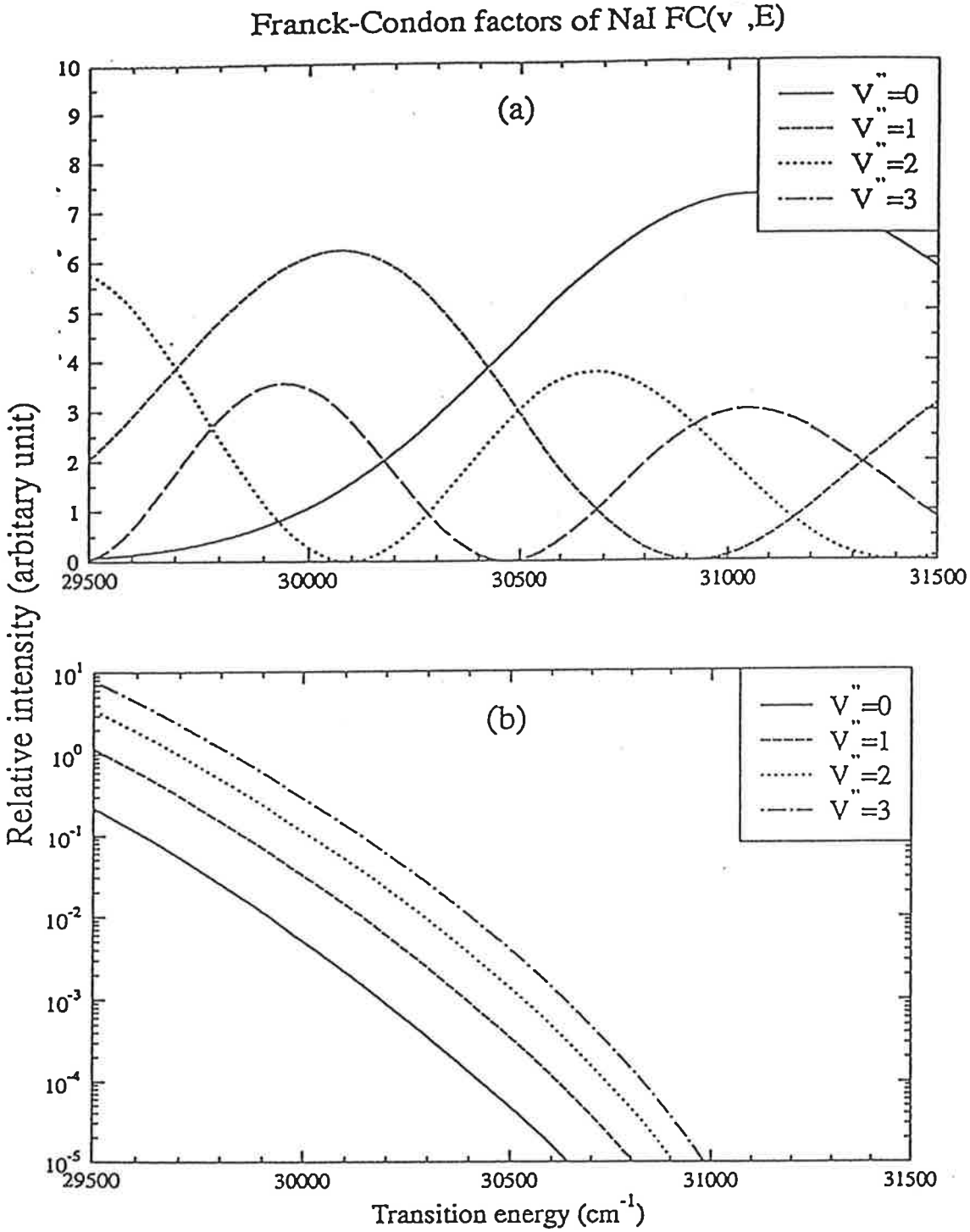

Figure 6.3: Franck-Condon factors of (a) Qin's potential and (b) Schaefer-Qin potential for transitions from $v'' = 0 - 3$, taken from [Qin 1996].

limb of the $A0^+$ potential curve is that the transition from $v'' = 0$ almost dominates the absorption spectrum. Therefore van Veen et al.'s potential can not be accepted as reasonable, and only the value of the potential at the ground state ($v'' = 0$) equilibrium distance should be trusted within the range of uncertainty discussed above.

Qin's observation about the behaviour of FCs can further be used to deduce the shape of the repulsive limb. In doing so, the inappropriateness of van Veen et al.'s potential will also be clearly demonstrated.

We first note that

$$FC(v'' = 0, E_t = 30500 \text{ cm}^{-1}) = FC(v'' = 0, E' = 30630 \text{ cm}^{-1})$$

and

$$FC(v'' = 1, E_t = 30500 \text{ cm}^{-1}) = FC(v'' = 1, E' = 30900 \text{ cm}^{-1}),$$

as the vibrational energy of $v'' = 0$ and $v'' = 1$ states are about 130 cm^{-1} and 400 cm^{-1} respectively. Thus the FCs being equal for $E_t = 30500$ cm^{-1} implies

$$FC(v'' = 0, E' = 30630 \text{ cm}^{-1}) = FC(v'' = 1, E' = 30900 \text{ cm}^{-1}).$$

Although this equality should only hold approximately, we will treat it as being exact and assess its uncertainty later.

With the use of Eq. (6.9), one may then write

$$(\chi_0''(R[E' = 30630 \text{ cm}^{-1}]))^2 = (\chi_1''(R[E' = 30900 \text{ cm}^{-1}]))^2$$

or in eV scale

$$(\chi_0''(R[E' = 3.80 \text{ eV}]))^2 = (\chi_1''(R[E' = 3.83 \text{ eV}]))^2$$

and correspondingly

$$FC(v'' = 0, E' = 3.80 \text{ eV}) = FC(v'' = 1, E' = 3.83 \text{ eV}). \tag{6.11}$$

Meanwhile, from Fig. 6.4 showing the squares of normalized ground state vibrational wavefunctions with $v'' = 0$ and 1, one can see that their squared amplitudes cross at 2.67 Åand 2.78 Å, that is,

$$[\chi_0''(R = 2.67 \text{ Å})]^2 = [\chi_1''(R = 2.67 \text{ Å})]^2$$

and

$$[\chi_0''(R = 2.78 \text{ Å})]^2 = [\chi_1''(R = 2.78 \text{ Å})]^2.$$

Therefore, according to the delta function approximation, it follows that

$$FC(v'' = 0, E'(R \approx 2.67 \text{ Å})) = FC(v'' = 1, E'(R \approx 2.67 \text{ Å}))$$

and

$$FC(v'' = 0, E'(R \approx 2.78 \text{ Å})) = FC(v'' = 1, E'(R \approx 2.78 \text{ Å}))$$

where $E'(R)$ denotes the value of turning point energy E' at R. Our job is then to find the estimate of either $E'(R \approx 2.67 \text{ Å})$ or $E'(R \approx 2.78 \text{ Å})$.

Furthermore, we estimated in Section 6.2.3 that the maximum of $FC(v'' = 0)$ is located between $E' = 3.83$ and 3.93 eV, thus $FC(v'' = 0, E')$ is an increasing function of

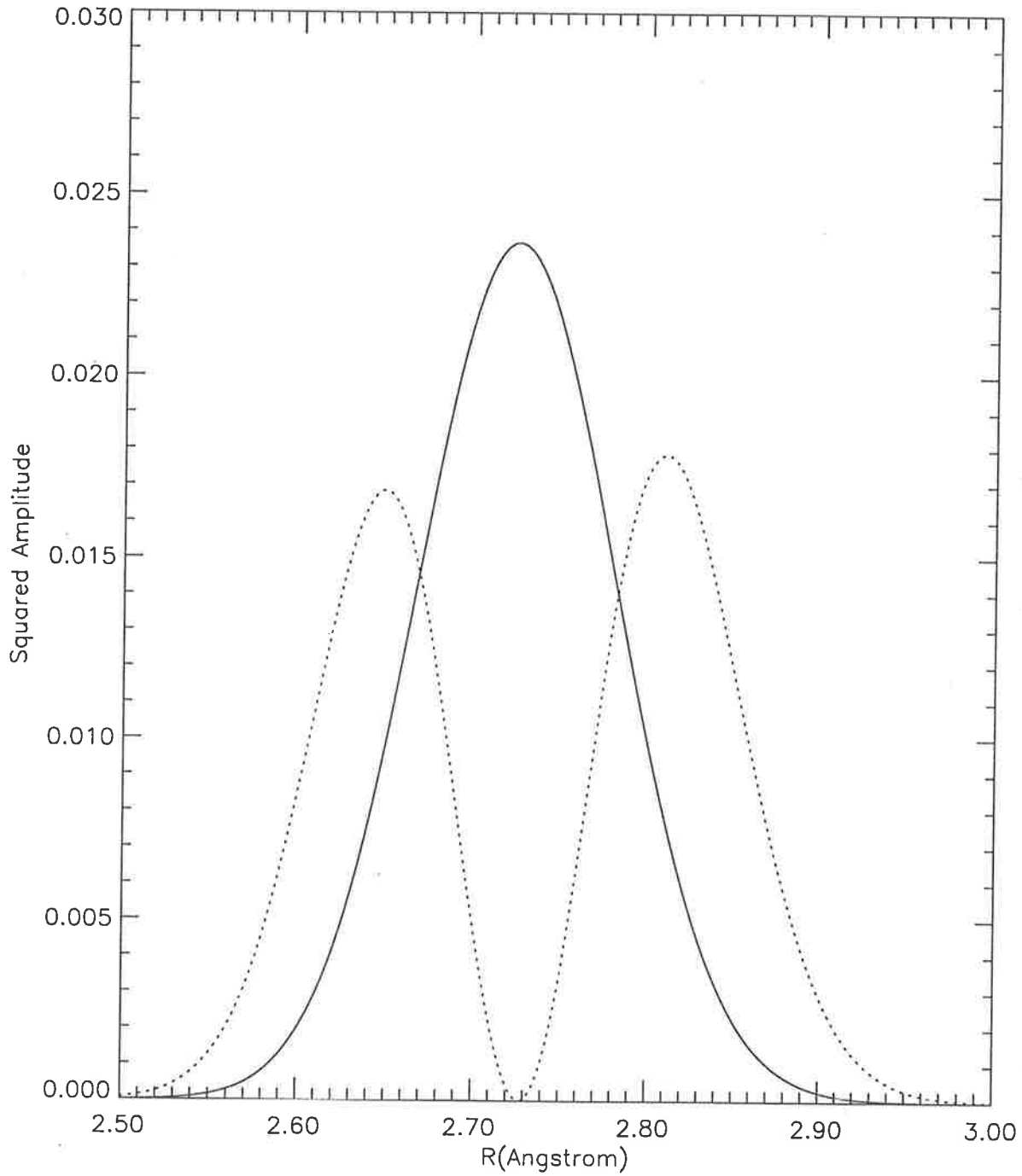

Figure 6.4: Squares of the vibrational wavefunctions for $v'' = 0$ (solid line) and $v'' = 1$ (dotted line) states.

E' if $E' < 3.83$ eV. In order for $FC(v'' = 1)$ to cross with $FC(v'' = 0)$, $FC(v'' = 1)$ then has to be a decreasing function of E' in the same region. Therefore, from Eq. (6.11), the common value of E' for which $FC(v'' = 0)$ and $FC(v'' = 1)$ are equal must lie between 3.80 and 3.83 eV. This then leads to either

$$3.80 \text{ eV} < E'(R \approx 2.60 \text{ Å}) < 3.83 \text{ eV}$$

or

$$3.80 \text{ eV} < E'(R \approx 2.78 \text{ Å}) < 3.83 \text{ eV}.$$

However, we know that the values of the $A0^+$ potential in a region covering both of these points should decrease with increasing R, thus the first inequality is not sensible. Hence we arrive at the estimate that the $A0^+$ potential around 2.78 Å should have values between 3.80 and 3.83 eV.

Qin also stated that a change of the ratio

$$R_{FC}(E_t) \equiv FC(v'' = 0, E_t))/FC(v'' = 1, E_t)$$

by not more than 20 percent did not spoil the approximate fit of his model spectrum to his observed spectrum, thus the upper and lower bounds on E' based on the crossover of FCs should be adjusted accordingly as follows.

Fig. 6.5 shows the comparison between Qin's model spectra and the observed absorption spectra for transition energy regions where E_t is less than 30500 cm^{-1}. For each region his best estimate of R_{FC} is given, and Fig. 6.6 demonstrates as an example how his model spectrum changes with different choice of R_{FC} in the region from

E_t = 30356 cm^{-1} to 30382 cm^{-1}. Although the best value of R_{FC} in this region was estimated to be 0.7, one can not definitely say that $R_{FC} = 0.3$ or $R_{FC} = 1.0$ gives a poorer fit to the experimental spectrum than $R_{FC} = 0.7$ does. However, in the region of E_t values shown in Fig. 6.6, it was found that the agreement between the model and the observed spectrum becomes poorer if one uses the value of R_{FC} larger than 1.0 or smaller than 0.3 [McCoy 1999]. Thus it appears that, the uncertainty in R_{FC} should be about 45 per cent instead of 20. Therefore if E_t is greater than 30350 cm^{-1} the value of R_{FC} may be expected to become comparable to 1 due to the 45 per cent uncertainty.

Thus it may be broadly estimated that the crossover of $FC(v'' = 0)$ and $FC(v'' = 1)$ occurs if the value of E_t is between 30350 cm^{-1} and 30650 cm^{-1}, from which it follows that the value of E' near $R = 2.78$ Å should lie between 30480 cm^{-1} and 31050 cm^{-1}. Then the estimates on the repulsive limb of $A0^+$ potential can be summarized as;

- 3.83 eV $< E^e_{2/+}(R \approx 2.71$ Å$) < 3.93$ eV, and
- 3.78 eV $< E^e_{2/+}(R \approx 2.78$ Å$) < 3.85$ eV.

The above estimates on the energy values can then be used to determine the validity of suggested potential curves. Fig. 6.7 shows a number of proposed $A0^+$ potentials for R values from 2.65 Å to 2.85 Å, and each rectangle represents one of the above conditions on the repulsive limb of the $A0^+$ potential, which is drawn by allowing ± 0.01 Åuncertainties on the values of R. The potentials of Cong et al. and of Lindner et al. are discussed later in this section and in the next section respectively.

As was indicated, the potentials of Schaefer-Qin, Wang et al. and Schaefer et al. do not meet any of these conditions (note that the potentials of Schaefer-Qin and of Schaefer et al. do not even appear in Fig. 6.7), while van Veen et al.'s potential satisfies the first

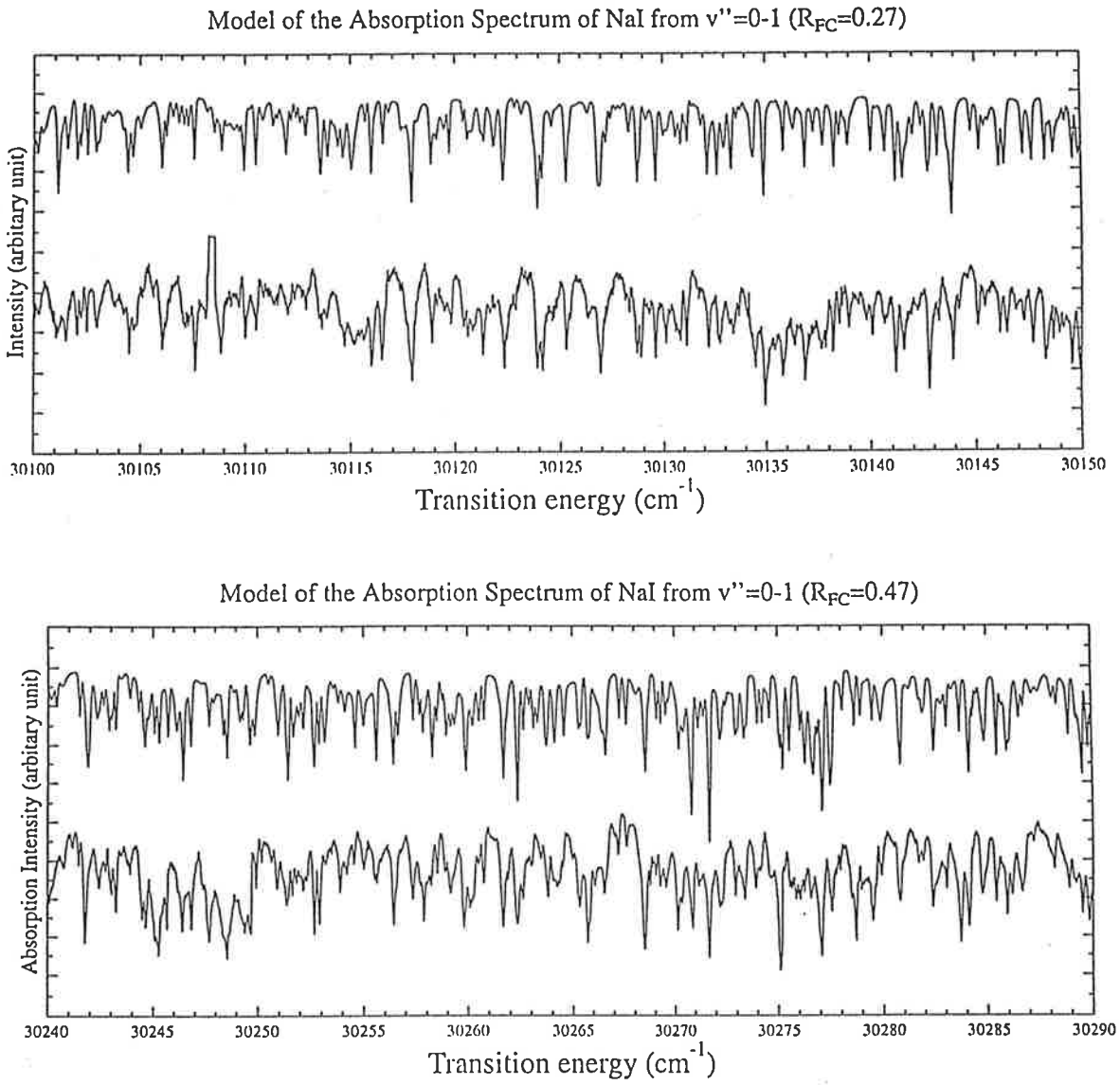

Figure 6.5: Comparison of the model and the observed absorption spectra, taken from [Qin 1996]. Best estimate of R_{FC} is given for each region.

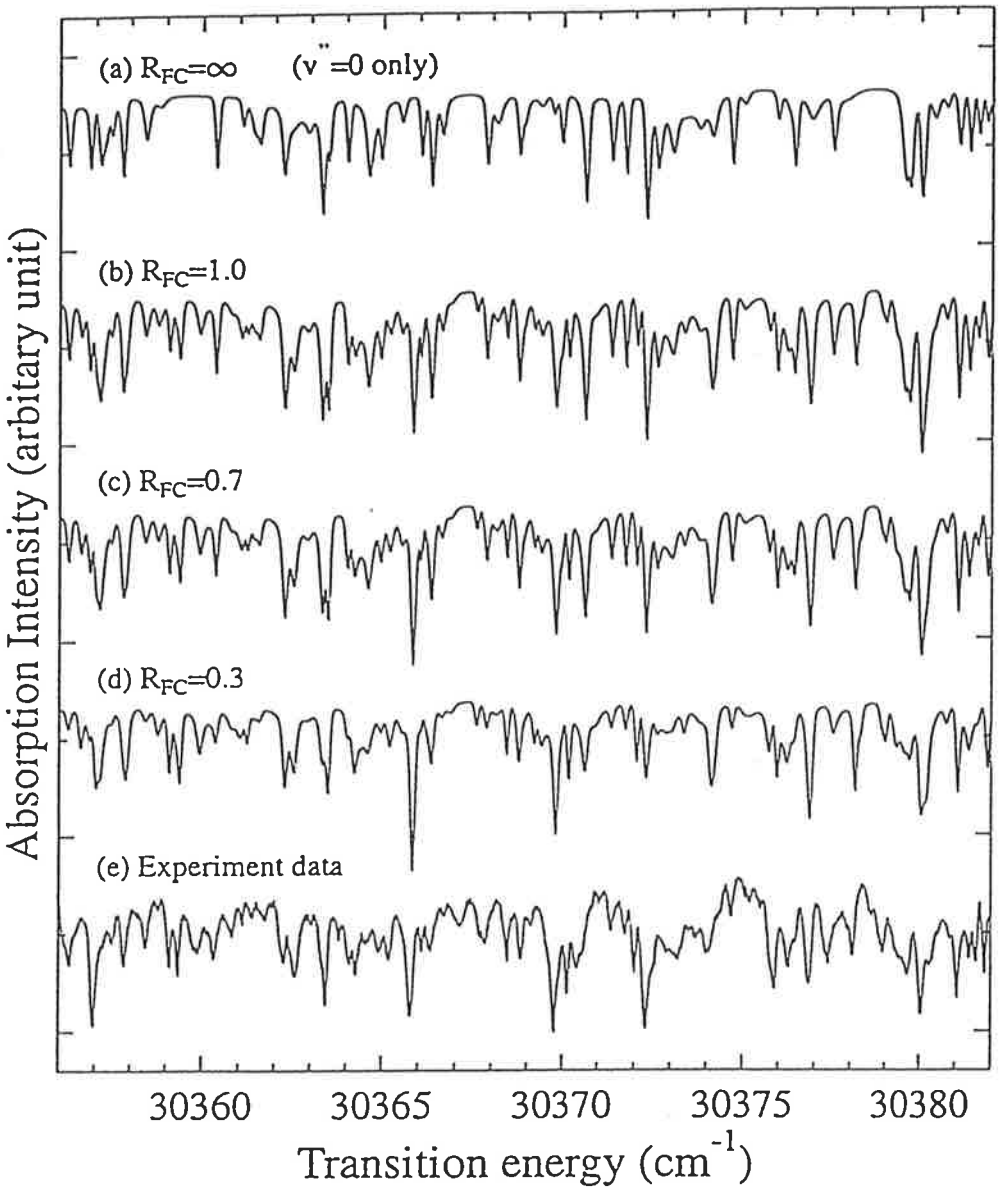

Figure 6.6: Comparison of the model and the observed absorption spectra for various values of R_{FC}, taken from [Qin 1996].

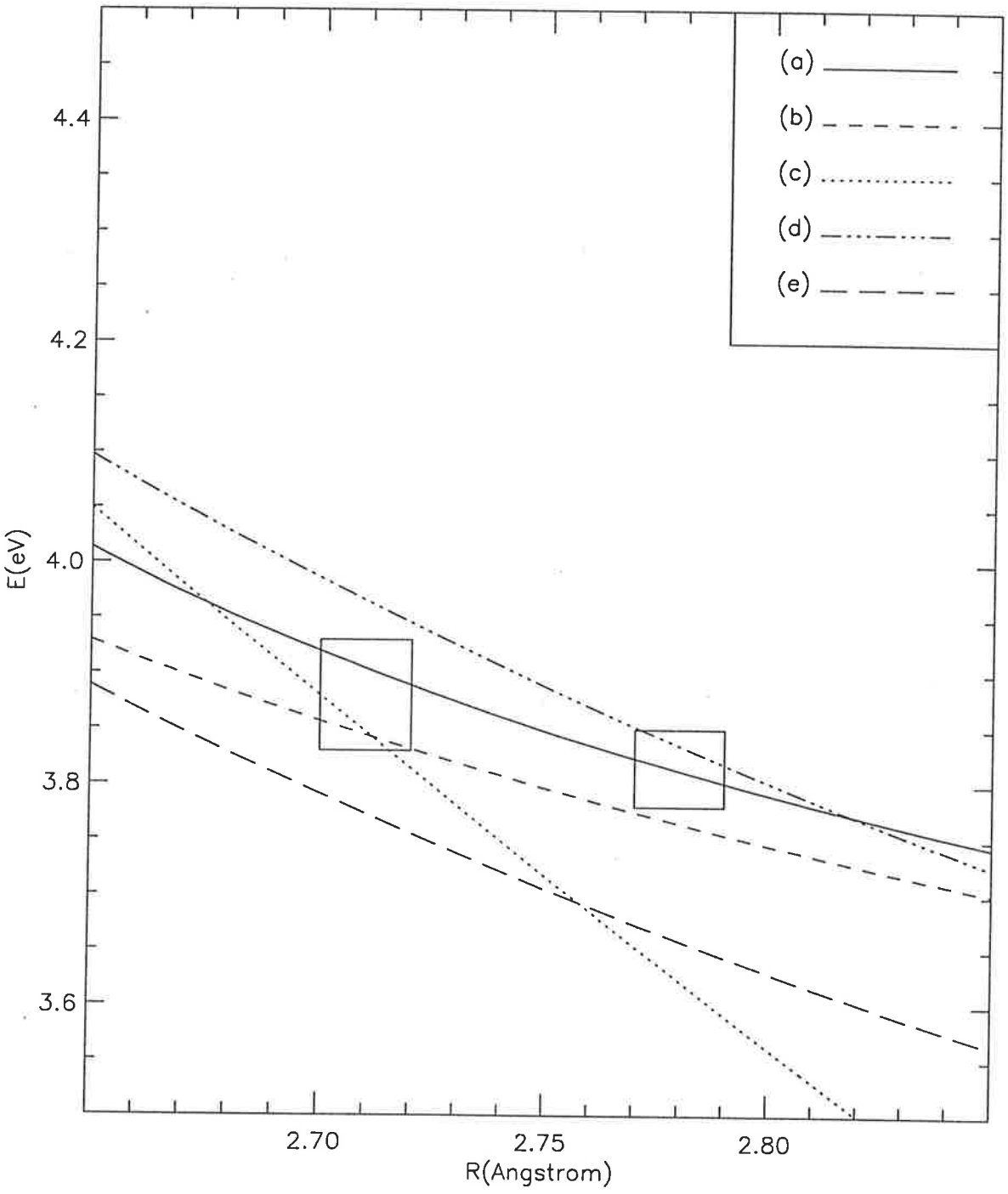

Figure 6.7: Several proposed $A0^+$ potentials in the region of R between 2.65 Å and 2.85 Å; (a) Qin, (b) Lindner et al., (c) van Veen et al. (d) Cong et al. and (e) Wang et al.

one but is too steep to meet the second condition. All four of those potentials can thereby be ruled out safely. Qin's diabatic potential meets all of the above conditions, and Lindner et al.'s adiabatic potential satisfies the first and almost meets the second condition. As the second condition was deduced from Qin's analysis only, the estimates of R_{FC} and its uncertainties can neither be established definitely nor confirmed from other researches. Thus Linder et al.'s potential can not be considered unacceptable.

6.2.5 Potential curve from FTS and remarks

A potential shown in Figs. 6.2 and 6.7 is from a study by Cong et al. [Cong 1996] who carried out a femtosecond transition-state spectroscopy (FTS) study in which the time evolution of excited state wave packet is recorded and analyzed. Their derivation of the adiabatic $A0^+$ potential curve consisted of two steps; the shape of the repulsive limb was determined first and the attractive limb second. We will only look at their repulsive limb, which is given in analytic form as

$$E_2^e(R) = V_0 \exp[-\alpha(R - R_0)] + D_e \tag{6.12}$$

which is almost the same as Eq. (5.44) employed by van Veen et al., the difference being that Cong et al.'s potential converges to the atomic dissociation limit at large R. Cong et al. then fixed all the parameters in Eq. (6.12) leaving only α to be optimized, which governs the slope of the repulsive limb near the ground state equilibrium distance, and found that $\alpha = 2.5 \pm 0.5$. V_0, R_0 and D_e are fixed to be 6557 cm^{-1}, 2.71 Å and 25406 cm^{-1} respectively.

One can see from Fig. 6.7 that Cong et al.'s potential does not agree with the first

criterion deduced from the position of maximum absorption, and it is easy to understand why; the value of V_0 in Eq. (6.12) is set too high. They indicated that $V_0 = 6557$ cm^{-1} was taken from the studies of van Veen et al. and Schaefer et al. However, this leads the value of $E_2^e(R)$ at $R = 2.71$ Å to be 31963 cm^{-1} or about 3.96 eV which is higher than the value of van Veen et al.'s potential for the same R. Furthermore, it is not clear how the information regarding V_0 could be obtained from the studies of Schaefer et al. As a matter of fact we reasoned above that Schaefer et al. did not take transition intensity into consideration and their potential gives a wrong estimate on the position of maximum absorption. Hence Cong et al.'s choice of V_0 appears to be inappropriate.

Meanwhile, the second condition obtained from Qin's consideration of FCs are in accordance with Cong et al.'s estimate of α, which was one of the main parts of their analysis. This aspect is encouraging in that it supports Qin's observation regarding R_{FC}.

The other feature of Cong et al.'s study, which involves the optimization of the attractive limb of the adiabatic $A0^+$ potential, was not considered here since the accuracy and error bounds related to their analysis is unclear. Their investigation based on the FTS technique, while being innovative and potentially promising, involved several rather drastic approximations. Furthermore, the manner in which they represented the potentials is not precise enough to attempt the generation of rovibrational energy levels.

Thus one is left with three potentials that were claimed to be of spectroscopic accuracy; the potentials of Schaefer et al., of Qin, and of Lindner et al. Since the potential of Schaefer et al. is already ruled out, we will concentrate on discussing the proposals of Qin and of Linder et al. in the next section.

We emphasize that the conditions on the potential obtained in this section are not

precise, and due to their broad region of uncertainty not all potential curves which meet the above conditions may be physically reasonable.

Furthermore, the rotational structure of the energy levels were ignored when deriving the above conditions. If this is taken into account, the energy E' of an excited state corresponding to given turning point needs to be adjusted accordingly, as we will discuss at the end of the section 6.4. We also remark that main purposes of deriving these criteria was to demonstrate clearly that the $A0^+$ potential curves of Schaefer et al. and of van Veen et al. are unreasonable and also to show how information on the excited state potential curve can be obtained from observing the intensity of absorption spectra.

6.3 Rotational Constants of the Adiabatic $A0^+$ Potentials

Another condition which the $A0^+$ potential curve must satisfy is that it has to reproduce satisfactorily the excited state rovibrational energy levels obtained from analysis of the observed spectra. To meet this aim, one must first be able to record a transition spectrum with a resolution high enough to detect positions of line peaks and identify which ground robvibrational state contributes to each transition line. Lindner et al. and Qin performed quantitative investigations on the line structures of NaI spectra using the energy levels calculated by Schaefer et al. and derived their $A0^+$ potential curves. In the previous section, we discussed the validity of their potentials based on transition intensities and FCs. Here we will look at the aspects related to the structure of rovibrational levels. First, we will briefly outline their procedures, starting with that of Lindner et al.

6.3.1 Study of Lindner et al.

As was discussed in the previous chapter, Schaefer et al. laid out a major foundation for a quantitative study of $A0^+$ rovibrational states by recording and analysing LIF spectra in the range of 29960-33175 cm^{-1}. Lindner et al. [Lindner 1994] carried this experiment further down to $E_t = 26500$ cm^{-1} (or 28840 cm^{-1} in absolute energy scale) and then used the Schaefer et al.'s procedure and assignments to determine relative vibrational and absolute rotational quantum numbers of the observed lines.

These measurements were followed by Λ-type two-photon double resonance (ΛTP) spectroscopy to observe the levels with yet lower energies. By recording ΛTP spectra with the $C0^+$ state [Bluhm 1990] acting as an intermediate, they could observe that the levels whose energies range from 27000 to 28100 cm^{-1} appear as a series of doublets in their ΛTP spectra.

Lindner et al. then proceeded to derive the adiabatic $A0^+$ potential curve from their observed levels using an RKR-like method. They considered a number of hypothetical choices on the behaviour of rotational constants and vibrational spacings at low energy regions to show that there exists more than one potential curve that can reproduce the observed levels while having different shapes. It was then regarded that the extrapolation from the Dunham parameters optimized to represent ΛTP data provides the most reasonable potential. It is this potential that we examined in the previous section, whose analytic form is

$$E_+^e(R) = T_e + \sum_i c_i \frac{2(R - R')}{R + R'} \tag{6.13}$$

and the value of each parameter is shown in Tab. 6.2. The study of Lindner et al. is valuable in that they observed and analyzed more energy levels than Scheafer et al. did

Parameter	Value
T_e	25207.1007
c_1	$-0.1502494016\times10^{3}$
c_2	0.1737301262×10^{5}
c_3	0.4514765326×10^{5}
c_4	0.7768902881×10^{5}
c_5	$-0.5129463380\times10^{6}$
c_6	$-0.1475633993\times10^{7}$
c_7	0.6539361306×10^{7}
c_8	0.1268036939×10^{8}
c_9	$-0.6252025595\times10^{8}$
c_{10}	$-0.6786157600\times10^{8}$
c_{11}	0.3867614303×10^{9}
c_{12}	0.2242980236×10^{9}
c_{13}	$-0.1559135102\times10^{10}$
c_{14}	$-0.4174881154\times10^{9}$
c_{15}	$0.4171305644\times10^{10}$
c_{16}	0.2613650242×10^{9}
c_{17}	$-0.7421981781\times10^{10}$
c_{18}	0.5538641480×10^{9}
c_{19}	$0.8594152650\times10^{10}$
c_{20}	$-0.1380944576\times10^{10}$
c_{21}	$-0.6113925529\times10^{10}$
c_{22}	$0.1208743839\times10^{10}$
c_{23}	$0.2349215841\times10^{10}$
c_{24}	$-0.3966808612\times10^{9}$
c_{25}	$-0.3468203298\times10^{9}$
c_{26}	$-0.1185605217\times10^{5}$
c_{27}	0.8518228015×10^{4}
c_{28}	$-0.1522248561\times10^{5}$
c_{29}	0.2631024230×10^{5}
R'	6.0515886

Table 6.2: Parameters for the $A0^+$ potential of Lindner et al. expressed by Eq. (6.13) in cm^{-1}-Å units.

to revise the adiabatic $A0^+$ potential curve initially proposed by Schaefer et al. It is particularly crucial to find as many levels as one can if one wants to employ an RKR-like method to derive a potential curve. One aspect noteworthy in their study is that, as can bee seen from Fig. 6.2, the minimum of their adiabatic $A0^+$ potential lies lower than their estimated atomic dissociation limit of NaI.

Next, Lindner et al. assumed that the energies of observed levels can be represented in good approximation as adiabatic rovibrational states only, considering that a state behaves more adiabatically as its energy becomes lower. Two sets of states (one obtained from LIF and the other from ΛTP spectroscopy) which are assumed to be identical to the adiabatic states, were then separately fitted to Dunham-type power series expansions (c.f., Eq. (5.59)). Finally, the levels in two sets are combined and optimized together to a single Dunham-type series in order to obtain a unified assignment of relative vibrational quantum numbers.

6.3.2 Study of Qin

Qin's diabatic $A0^+$ potential was derived in a different way. Since the absorption spectra he observed contain many more lines than the LIF spectra of Schaefer et al. and are further complicated by Doppler broadening due to the high temperature required to vapourize an NaI crystal, quantitative identification of individual lines was nearly impossible. Thus he instead generated a model spectrum consisting of absorptions from $v'' = 0$ and 1 states only and varied it until the best agreement with the experimental spectra was obtained. The behaviour of R_{FC} thus found and its implication on the shape of the repulsive limb of $A0^+$ were discussed in the previous section. The remaining procedure of Qin's derivation was then to find a potential which is consistent with

the observations regarding the behaviour of R_{FC} while being able to generate Schaefer et al.'s observed band fragments. The analytic formula for his diabatic $A0^+$ potential is given by Eq. (6.10), from which the adiabatic potential is constructed via Eq. (5.12) with E_1^e expressed as Eq. (6.1). The electronic coupling H_{12}^e was assumed constant in R with a value of 0.055 eV.

Here it should be noted that Qin worked with the $A0^+$ state adiabatic vibrational levels and rotational constants rather than the actual band fragments, which is perfectly reasonable, given that the diabatic $X^1\Sigma^+$ potential E_1 is accurately known. This appears to be a fair assumption, since the ground state rovibrational structure for energies below the atomic dissociation limit is quantitatively well determined and the outer limb of E_1 must be very close to the ionic attractive potential. However, as the modified diabatic potential has to be used in the construction of the band fragments, some complication may arise due to the fact that different choice of coupling function affects the shape of the modified diabatic potential and hence its vibrational energy levels and rotational constants. For example, although Qin reported that with the use of a modifed diabatic potential the vibrational energies were shifted by about 30 cm^{-1} which is comparable to a vibrational spacing in the Schaefer et al.'s experimental energy region, for a more physically reasonable coupling function that dies off as $|R - R_x|$ increases the shift is found to be not as significant and is also to some degree dependent on the shape of coupling function. Furthermore, neither the exact R dependence of the coupling function nor the value of R_x is known, whose estimates accepted and/or reported in various articles range from 6.93 Å [Lindner 1994] to as large as 7.3 Å [Wang 1990]. While it is difficult to argue any further because of the lack of knowledge about the coupling function, it appears that the consequence of not using a modified potential

is no more serious than the uncertainties which may arise from other sources (e.g., ambiguity in the shape and magnitude of the electronic coupling, approximating band fragments as adiabatic levels, deviation in the optimization of rovibrational levels and corresponding potential curves, and so forth).

Meanwhile, if one uses directly the experimentally determined diabatic rovibrational levels rather than those generated by solving the Schrödinger's equation with a given potential, the above dilemma can be avoided. Since Schaefer's analysis on the energies of band fragments is reliable, this is the safest way to circumvent the problem. Furthermore, Qin provided the refined version of Dunham-type expansion parameters which are able to reproduce the band fragment more accurately. Therefore, regarding the diabatic levels optimized by Qin as the accurate ones to be used in the formation of band fragments, one can then concentrate on analyzing the rovibrational structure of adiabatic states.

6.3.3 Comparison of the studies of Lindner et al. and of Qin

Figs. 6.8 and 6.9 show comparisons of the vibrational energy spacings ΔG_v and rotational constants B_v (whose subscripts '+' denoting adiabatic levels are omitted for notational convenience) of Schaefer et al., Qin., and Lindner et al. Plots for the results of Schaefer et al. and of Qin were obtained from the solutions of the nuclear vibrational equation without rotation

$$\left[-\frac{1}{2\mu}\frac{d^2}{dR^2} + E_+^e(R)\right]\chi_v(R) = E_v^n\chi_v(R) \tag{6.14}$$

where the each adiabatic $A0^+$ potential $E_+^e(R)$, except that of Lindner et al. which was provided in adiabatic form, was generated from the diabatic potentials $E_2^e(R)$ of Eqs. (6.4), (6.10) with the use of the constant electronic coupling function $H_{12}^e = 0.055$

eV, the diabatic $X^1\Sigma^+$ potential expressed as Eq. (6.1) and the transformation formula Eq. (5.12).

Solutions to Eq. (6.14) were computed with a Fortran program utilizing the renormalized Numerov method [Johnson 1977], written by Wang [Wang 1990] and modified by Qin [Qin 1996]. Then ΔG_vs were calculated by taking the energy differences between the adjacent vibrational states $(E^n_{v+1} - E^n_{v-1})$, and B_vs using the Eq. (5.48).

These values are plotted in Figs. 6.8 and 6.9 versus vibrational energies rather than vibrational quantum numbers. Since the absolute assignment of vibrational quantum numbers are used only to reproduce the adiabatic levels at the experimental energy regions, they can not be regarded as the correct assignments. Thus it is more meaningful to discuss plots versus energy.

Both of the above plots display that results of Qin and Lindner et al. agree well in the Schaefer et al.'s experimental energy region, while discrepancies arise where Lindner et al. observed more levels by performing ΛTP spectroscopy. Vibrational spacings of Lindner et al. increase while Qin's results decrease. Disagreement between rotational constants is less apparent; when vibrational energy is greater than 27740 cm^{-1} the rotational constants of Qin are slightly bigger than those of Lindner et al., and vice versa for energies smaller than 27740 cm^{-1}. It is the increase of ΔG_v in the ΛTP region that is mainly responsible for a disagreement between two potentials. This is also one of the reasons why the minimum of Lindner et al.'s potential is located below the atomic dissociation limit of NaI, the other reason being that the vibrational quantum numbers of Lindner et al. are larger than those of Qin by 10 to 11 when the levels of the same energy are compared to each other. While Qin constrained his potential to lie above the estimated atomic dissociation limit of 3.18 eV during his optimization,

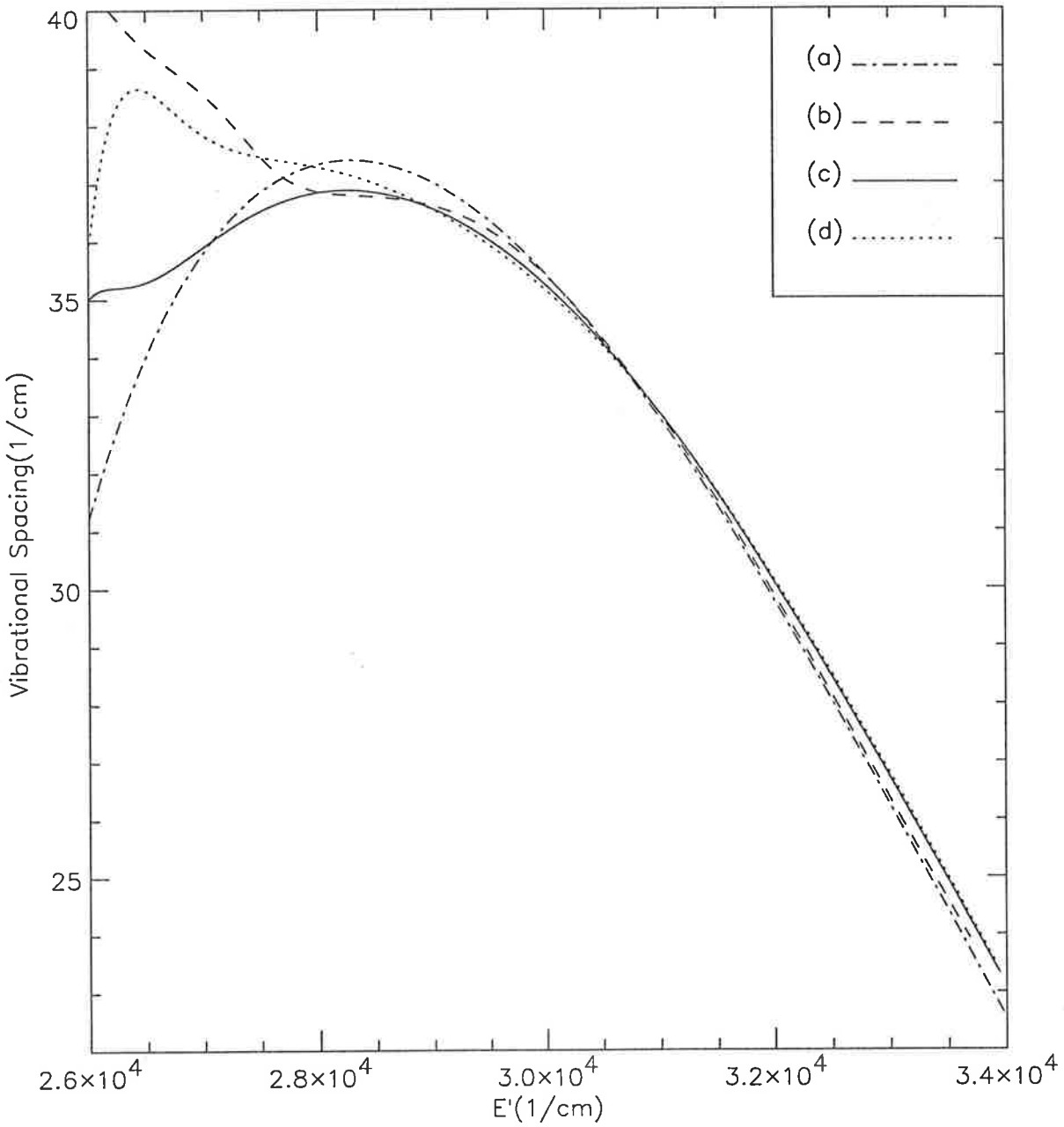

Figure 6.8: Plots of the energy spacings of the adiabatic $A0^+$ vibrational states; (a) Schaefer-Qin, (b) Lindner et al., (c) Qin and (d) Qin's potential modified in this study as discussed in 6.3.4.

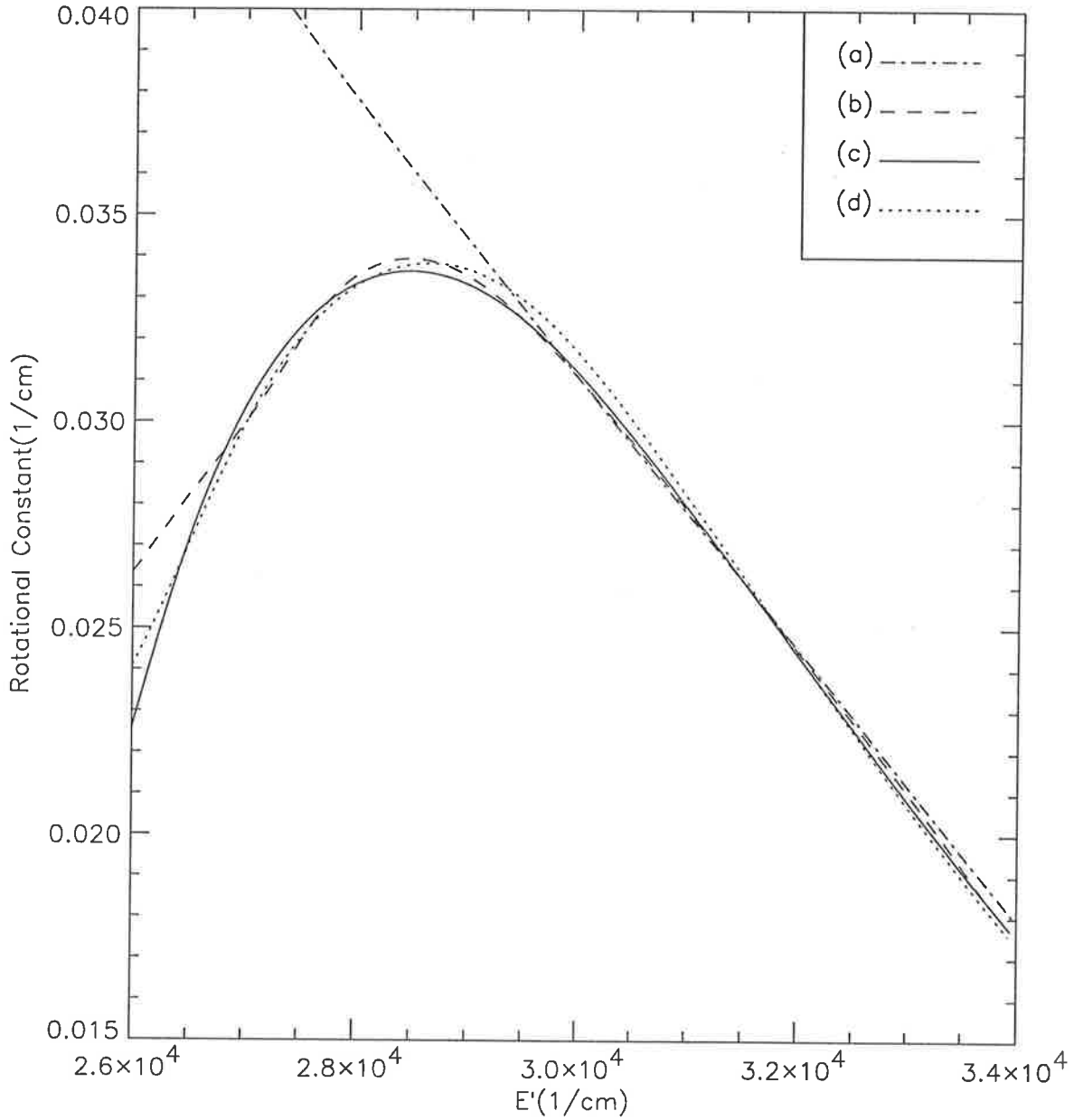

Figure 6.9: Plots of the rotational constants of the adiabatic $A0^+$ vibrational states of (a) Schaefer-Qin, (b) Lindner et al., (c) Qin and (d) Qin's potential modified in this study as discussed in 6.3.4.

Linder et al.'s potential was derived without such constraint and merely obtained by an RKR-like procedure with the lower unobserved levels extrapolated from their Dunham-type expansion parameters. Consequently Lindner et al.'s optimization is bound to generate more vibrational levels than those of Qin, and coupled with the fact that ΔG_v of Lindner et al. increases in the ΛTP region, caused the minimum of their potential to lie considerably lower than the atomic dissociation limit. Although it is an interesting issue to consider whether the $A0^+$ state potential (being adiabatic or diabatic) should really have such a low minimum, further study in this direction is beyond the scope of this thesis.

Examination of the adiabatic $A0^+$ state rovibrational structure thus indicates that Qin's potential needs to be adjusted in order to generate the energy levels lying at Lindner et al.'s ΛTP experimental energy region properly. On the other hand, it was suggested in the previous section that the values of Lindner et al.'s potential near the maximum absorption region are a little bit lower than the estimates obtained from an analysis based on absorption intensity and FC of $v'' = 0$ and 1 states. The fact that the attractive limb of Lindner et al.'s potential is slightly lower than that of Qin's potential seems to be consistent with this observation. However, the disagreement can not be simply resolved by vertically shifting the potential since that will also cause all of the associated rovibrational levels to be shifted and thereby to be misplaced.

6.3.4 Modification of Qin's potential

Next, it was considered whether the potential proposed by Qin can be modified to reproduce the energy levels observed from ΛTP spectroscopy as well without having to change the value of the dissociation energy and the potential minimum or violate the

conditions set by FC considerations. It was then found that if one uses

$$E_2^e(R) = \frac{12}{R^3} \exp\left\{ - \left[0.0165 + \left(\frac{r}{5.864} \right)^9 \right] (R - 2.7) + \left(\frac{2.46}{R} \right)^{20} \right\} + 3.18 \qquad (6.15)$$

instead of Eq. (6.10), better agreement can be made with the Lindner et al.'s ΛTP observation. Plots of the vibrational spacings and rotational constants are shown in Figs. 6.8 and 6.9. It was seen that, in order to generate a similar ΔG_v pattern as was observed by ΛTP spectroscopy, the bottom of Qin's potential needs to be made steeper like the potential of Lindner et al. as is shown in Fig. 6.10. However, the above modification of Qin's potential caused the levels outside the ΛTP region to be misplaced slightly. Thus it is not yet clear if more satisfactory agreement can be made by a modification of Qin's potential without changing the values of the potential minimum and the dissociation energy. Furthermore, Qin's choice of the atomic dissociation energy (=3.18 eV), which is from van Veen et al.'s estimate, differs from 3.15 eV estimated by Bluhm et al. [Bluhm 1993] who claimed better accuracy than any other experimental estimates. It is yet to be determined whose estimate is more reliable.

It should also be noted that the choice of 3.18 eV as the atomic dissociation limit (D_e) by Qin is not totally correct as it is actually D_0 to which one needs to add the zero point correction of 129 cm^{-1} (or about 0.016 eV) to find D_e. However, since the difference between the estimates of van Veen et al. and of Lindner et al. is far greater than this error, we did not attempt to adjust Qin's choice.

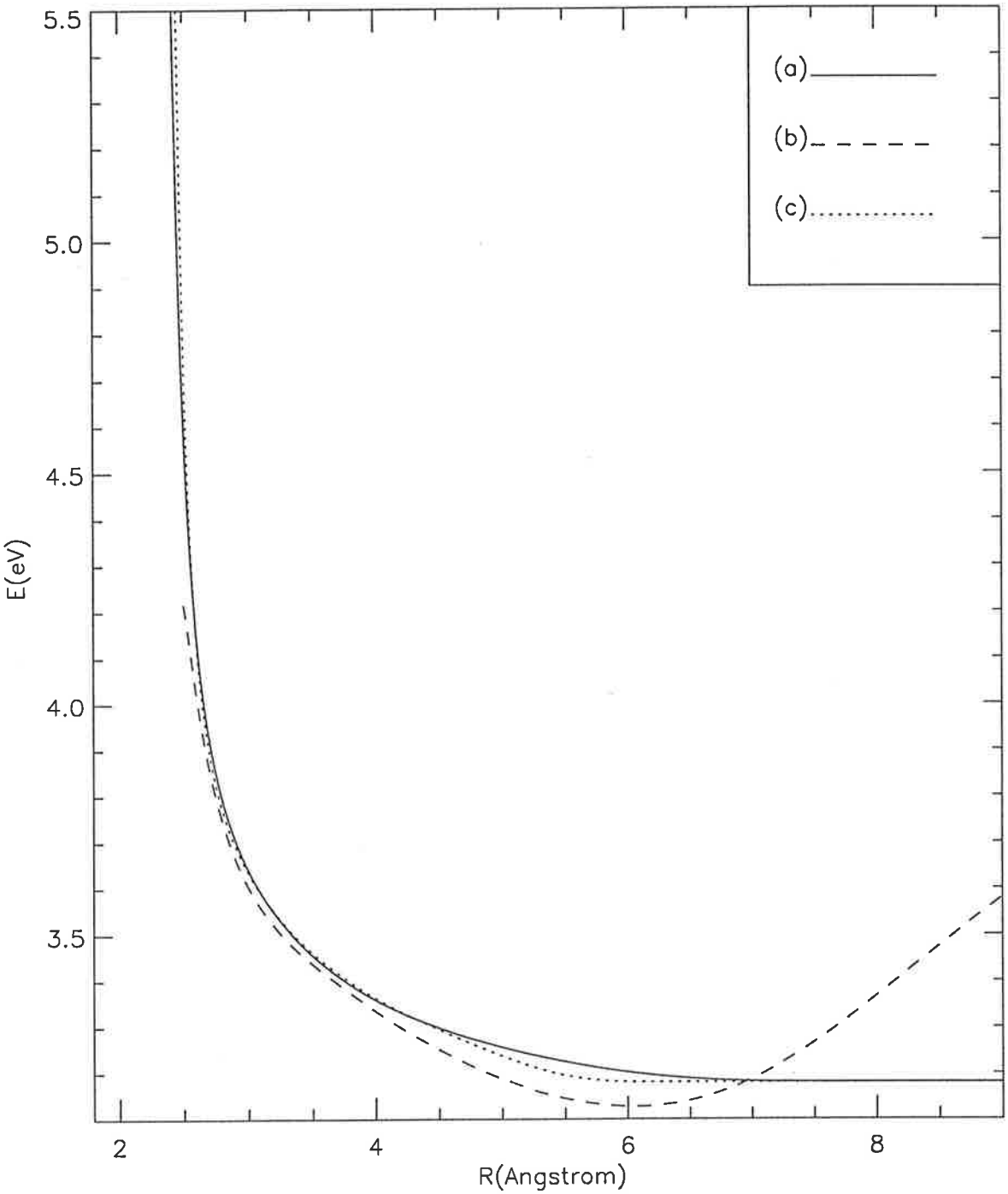

Figure 6.10: Plots of $A0^+$ potentials by (a) Qin and (b) Lindner et al., and (c) Modified version of Qin's potential.

6.4 Comparison of the Experimental Potential Curves to Ab Initio Potential Curves

As the final step in our research, the experimentally determined potentials of Qin and of Lindner et al. are compared to our ab initio potentials, which are shown in Fig. 6.11. Each theoretical result was vertically shifted so that its atomic dissociation limit coincides with that of the experimental potentials.

With the observation discussed in Chapter 4 regarding the similarity between the potentials of the first excited 0^+ and of the uncorrected $^1\Pi$ in mind, the repulsive limbs of our ab initio $^1\Pi$ and the experimental $A0^+$ potentials were placed under a close comparison and shown in Fig. 6.12 for R values ranging from 2.2 Å to 3.5 Å. Here it is encouraging to observe that the $^1\Pi$ potential is closer to the $A0^+$ potential than the excited $^1\Sigma^+$ potential, which has a much shallower repulsive limb compared to those of the experimental $A0^+$ potentials.

However, our theoretical calculations are not accurate enough for a quantitative study of NaI phototransition process, although they were obtained from fairly large size CASSCF and SA-CASSCF-MRSDCI calculations. Our theoretical value of the atomic dissociation energy is appreciably lower than the known experimental estimates, and the shape of the attractive limb is not in a good agreement with the experimental potential.

While the attractive limb of the ionic potential is not supposed to be affected much by the inclusion of spin-orbit interaction, the value of the $A0^+$ potential at smaller R may change considerably as was shown by Koseki et al. [Koseki 1995]. Thus our ab initio calculations can not be directly compared to experimental results, not until the spin-orbit effect is also considered. Even so, more comprehensive calculation may be

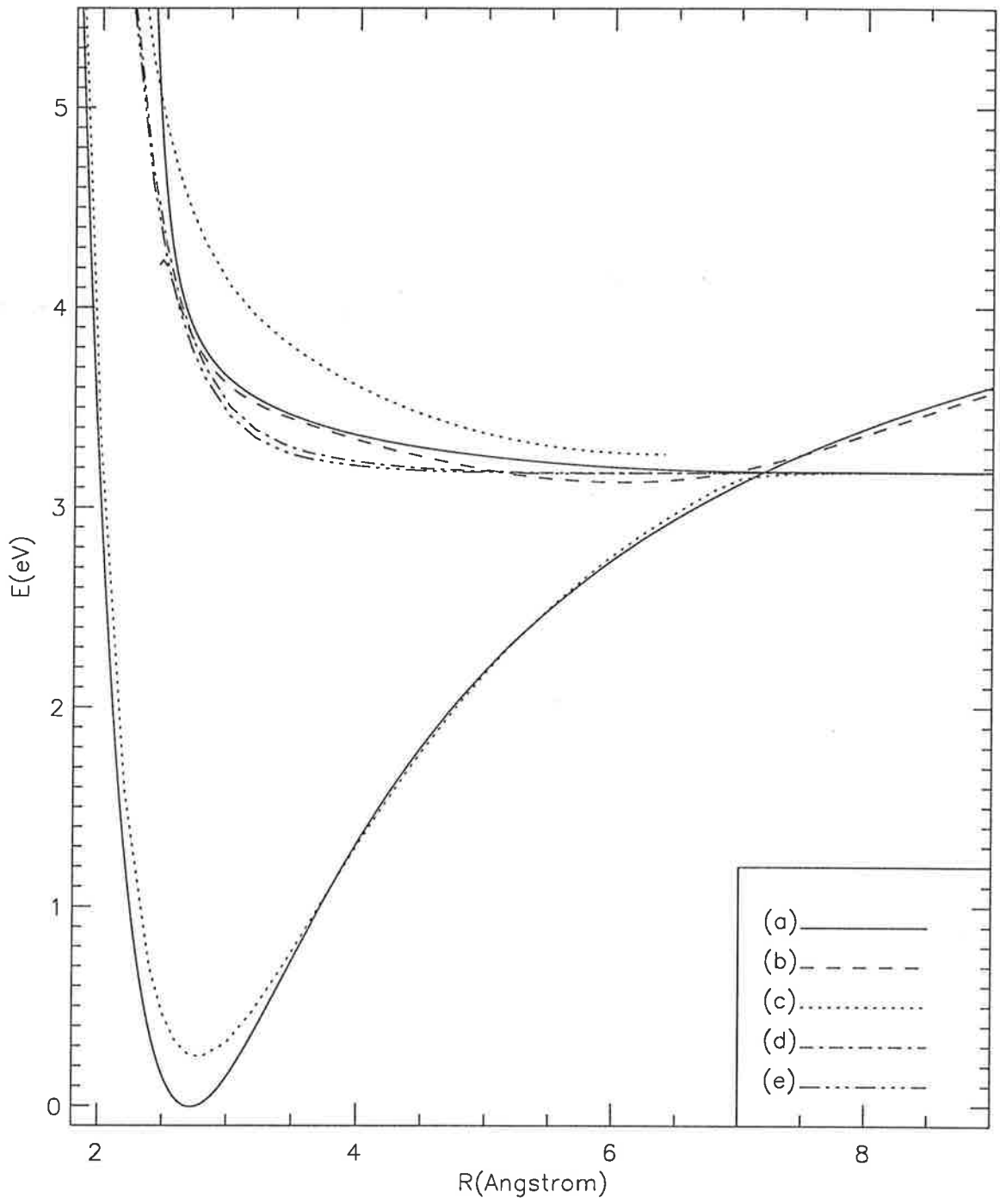

Figure 6.11: Plots of various potential curves; (a) diabatic $X^1\Sigma^+$ and $A0^+$ potentials of Qin, (b) adiabatic $A0^+$ potential of Lindner et al., and ab initio potentials of (c) the ground and the first excited $^1\Sigma^+$, (d) the lowest $^1\Pi$ and (e) the lowest $^3\Pi$.

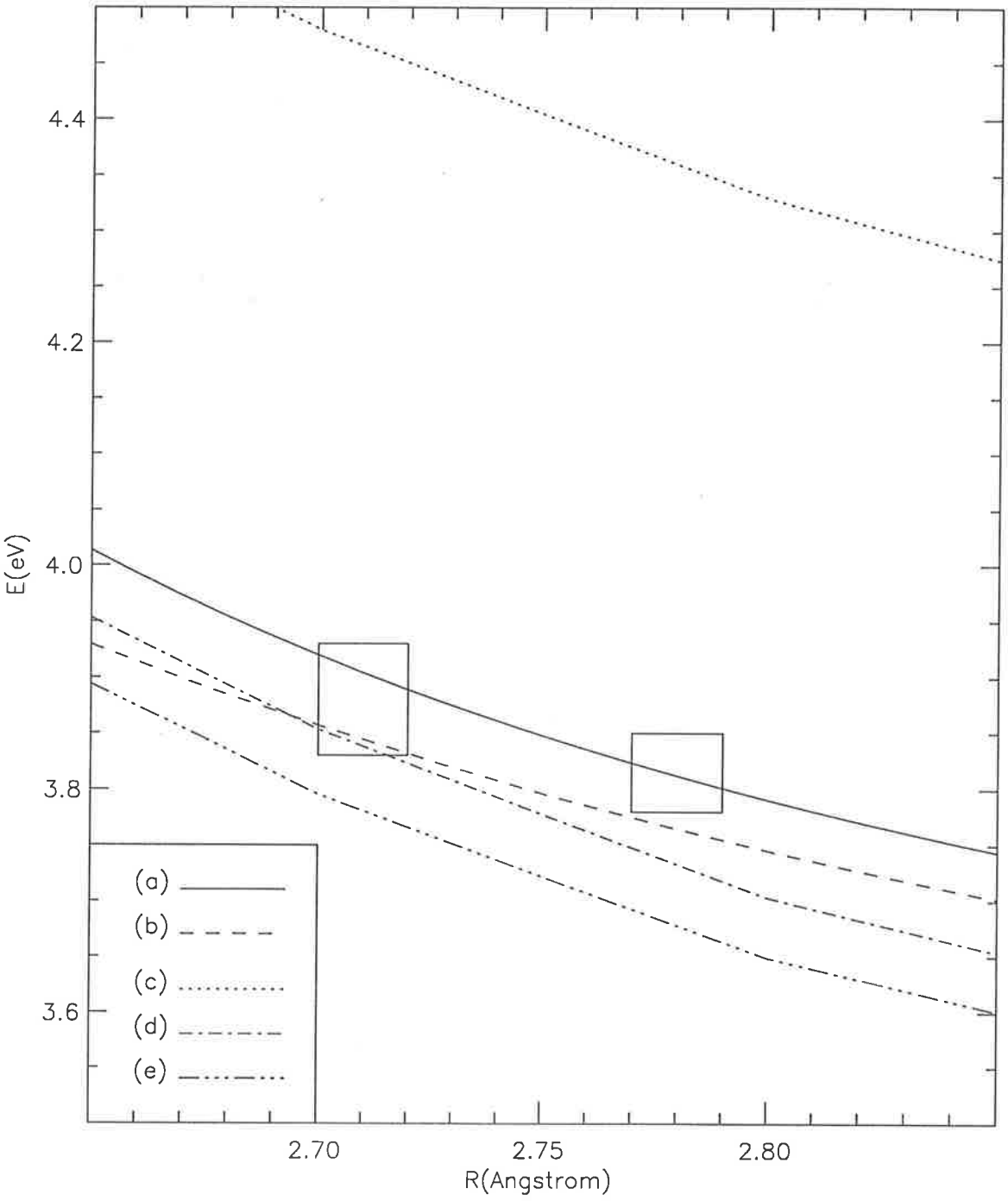

Figure 6.12: Closer comparison of the experimental and ab initio potentials; $A0^+$ potentials by (a) Qin and (b) Lindner et al., ab initio potentials of (c) the first excited $^1\Sigma^+$, (d) the lowest $^1\Pi$ and (e) the lowest $^3\Pi$.

necessary to obtain better estimates of the ioinic and atomic dissociation limits, which we were not able to carry out in this research with given time and resources.

Summarizing, Lindner et al.'s and Qin's potentials appear to be most reasonable among various others proposed so far, although a rather low minimum that appears in Lindner et al.'s potential requires further consideration. It will be also desirable to find more precise values of the diabatic curve crossing point and the atomic dissociation limit. Experimentally this means finding ways of reaching the energy region that lies below the lower limit of Lindner et al.'s ΛTP spectroscopy, and theroretically combining the large size MCSCF-CI with the spin-orbit coupling effect calculation with which one may then attempt a modelling of the phototransition spectra.

Finally, we note that the rotational structure of the energy levels was not taken into account when our criterion based on the bahaviour of FC amplitudes was derived. For a temperature of about 650 °C at which absorption spectra of Qin and of Berg and Skewes were recorded, rotational states of $J \approx 50$ are most highly populated. Since the rotational constants of $v'' = 0$ and $v'' = 1$ states are roughly 0.116 cm^{-1} while that of $A0^+$ vibrational states around 30000 cm^{-1} are about 0.025 cm^{-1} (c.f., Fig. 6.9), the values of the excited state energy E', which were initially obtained by adding the ground state vibrational energy to the values of transition energy E_t, need to be roughly lowered by $(0.116 - 0.025)50(50 + 1)$ or about 230 cm^{-1} (0.028 eV) if one takes the rotational structure into account. However, as our criteria based on FCs possess quite broad uncertainties and not only the behaviour of FCs but also the rovibrational level representation was considered in our examination of $A0^+$ potentials, this adjustment was not deemed to be meaningful in our consideraton. Whether the rotational effect is included or not, the $A0^+$ potential curves of Schaefer et al. and of van Veen et al. are

physically incorrect and those of Qin and of Lindner et al. remain reasonable.

Chapter 7

Conclusions

Our investigation to further the understanding of phototransition dynamics between the $X^1\Sigma^+$ and the $A0^+$ states of NaI consisted of two parts; theoretical ab initio calculation of the Σ^+ and other excited states which dissociate to the lowest atomic states of Na and I, and examination of several experimental studies and of the corresponding $A0^+$ potential curves.

Ab initio results reported in this thesis were obtained with a use of the quantum chemistry calculation package MOLPRO. CASSCF calculations for the lowest states of $^1\Sigma^+$ (which are also the ground state of NaI), $^3\Sigma^+$, $^1\Pi$, and $^3\Pi$ symmetries as well as the first excited $^1\Sigma^+$ state were carried out at various R values. Calculations for the $^1\Sigma^+$ states were complicated by an avoided crossing of two adiabatic states which prevented convergence when $R > 6.5$ Å, thus state-averaged CASSCF-MRSDCI calculations with a smaller number of active MO's in the CASSCF stage were additionally performed for these states and led to converged results.

As the multiplet splitting between I($^2P_{3/2}$) and I($^2P_{1/2}$) is not negligible, calculation of the spin-orbit coupling effects is necessary to obtain proper ab initio results. However,

this option was not yet available for MOLPRO while another ab initio package GAMESS, which is known to be capable of spin-orbit coupling calculation, could not handle the symmetry of MOs which in turn made it impossible to perform such calculations.

Examination of various experimental studies concerning $X^1\Sigma^+ \leftrightarrow A0^+$ phototransition dynamics was carried out and two potentials, proposed by Qin and by Lindner et al., were reasoned to be most reliable. Criteria which we applied to determine the validity of proposed potentials were based on whether they are consistent with the absorption intensity variations and rovibrational structure of the adiabatic $A0^+$ eigenstates that were experimentally observed. The structure of ΔG_v obtained from the ΛTP spectroscopy of Lindner et al. seems to be the main source of disagreement between the potentials of Qin and of Lindner et al., and should be a subject of further study.

From the ab initio calculations reported by Koseki et al., it appears that the spin-orbit calculation will generate an ab initio potential closer to the experimentally determined $A0^+$ potentials. Thus, it is imperative to perform spin-orbit coupling calculations using wavefunctions whose calibre are at least on par with or better than those reported in this thesis. Meanwhile, since it was observed that the breakdown of symmetry appears to be less drastic when smaller active space is employed in a CASSCF calculation using GAMESS, it may be worthwhile as a future work to see if the results of better quality than Koseki et al. can be obtained by reducing the number of active MOs which may then enable spin-orbit calculations.

From an experimental point of view, the best and direct approach to advance would be to measure high resoulution phototransition spectra at an energy region covering the low vibrational levels (if not the lowest level) belonging to the $A0^+$ electronic state, since one will then be able to answer many yet unresolved questions like the precise value of the

atomic dissociation energy and the location of diabatic curve crossing. Unfortunately, as the repulsive limb of the $A0^+$ potential is supposedly quite shallow, the intensity of such a transition may be too weak to detect. However, if both the intensity and the discrete line structure of phototransitions are carefully measured, it may be possible to refine the criteria presented in Chapter 5 of this thesis and thereby to help obtain a more accurate $A0^+$ potential curve.

List of Figures

List of Tables

Bibliography

[Bauschlicher 1982] Bauschlicher, Jr., C. W., Lengsfield III, B. H., and Liu, B. "The Dissociation Energy of MgO", *J. Chem. Phys.*, **77**, 4084(1982)

[Beebe 1979] Beebe, N. H. F. "Modification of Virtual Orbitals", *Int. J. Quantum. Chem.*, **15**, 589(1979)

[Bender 1966] Bender, C. F. and Davidson, E. R. "A Natural Orbital Based Energy Calculation for Helium Hydride and Lithium Hydride", *J. Phys. Chem.*, **70**, 2675(1966)

[Berg 1969] Berg, R. A. and Skewes, G. W. "Discrete Structure in the Spectrum of Sodium Iodide Vapor", *J. Chem. Phys.*, **51**, 5430(1969)

[Berry 1957] Berry, R. S. "Interaction of Vibrational and Electronic Motion in Alkali Halide Molecules", *J. Chem. Phys.*, **27**, 1288(1957)

[Berry 1979] Berry, R. S. "Optical Spectra of the Alkali Halide Molecules", in "Alkali Halide Vapors", ed. by Davidovitz, P. and McFadden, D. L. Academic Press, New York(1979)

[Bluhm 1990] Bluhm, H., Lindner, J., and Tiemann, E. "High-Resolution Spectroscopy of NaI around the Atomic Asymptotes Na($3p\ ^2P_{1/2,3/2}$) + I($^2P_{3/2}$)", *J. Chem. Physics.*, **93**, 4556(1990)

[Bluhm 1993] Bluhm, H., Lindner, J., and Tiemann, E. "Double Resonance Spectroscopy of NaI and KI : the van der Walls states $\Omega = 1$ and $\Omega = 2$ of the First Atomic Asymptote" *Chem. Phys.*, **181**, 173(1994)

[Born 1951] Born, M. "Kopplung der Elektronen- und Kernbewegung in Molekeln und Kristallen", *Gött. Nachr. math. phys. Kl.*, 1(1951)

[Born 1954] Born, M. and Huang, K. "Dynamical theory of crystal lattices", appendix VIII, Oxford University Press, London(1954)

[Born 1927] Born, M. and Oppenheimer, J. R. "Zur Quantentheorie der Molekeln", *Annalen der Physik*, **84**, 457(1927)

[Child 1991] Child, M. S. "Semiclassical mechanics with molecular applications" Clarendon Press, Oxford(1991)

[Condon 1981] Condon, E. U. and Shortley, G. H. "The Theory of Atomic Spectra", Cambridge University Press(1951)

[Cong 1996] Cong, P., Roberts, G., Herek, J. L., Mohktari, A. and Zewail A. H. "Femtosecond Real-Time Probing of Reactions. 18. Experimental and Theoretical Mapping of Trajectories in the NaI Dissociation Reaction", *J. Phys. Chem.*, **100**, 7832(1996)

[Davidovits 1967] Davidovits, P. and Brodhead, D. C. "Ultraviolet Absorption Cross Sections for the Alkali Halide Vapors", *J. Chem. Phys.*, **46**, 2968(1967)

[Davidovits 1979] Ed. by Davidovits, P. and McFadden, D. L. "Alkali Halide Vapors : Structure, Spectra, and Reaction Dynamics", Academic Press, New York(1979)

[Dunning 1977] Dunning, Jr., T. H. and Hay, P. J. "Gaussian Basis Sets for Molecular Calculations", in "Methods of Electronic Structure Theory", Ed. by Schaefer III, H. F., Plenum Press, New York(1977)

[Fuentealba 1982] Fuentealba, P., Preuss, H., Stoll, H. and von Szentpaly, L. "A Proper Account of Core-polarizations with Pseudopotentials : Single Valence-electron Alkali Compounds" *Chem. Phys. Lett.*, **89**, 418(1988)

[Hammermesh 1962] Hammermesh, M. "Group Theory and Its Application to Physical Problcms", Addison-Wesley, Reading(1962)

[Herzberg 1950] Herzberg, G. "Molecular Spectra and Molecular Structure I. Spectra of Diatomic Molecules", 2nd Ed., van Nostrad Reinhold Company, Ner York(1950)

[Hochstrasser 1966] Hochstrasser, R. M. "Molecular Aspects of Symmetry", W. A. Benjamin Inc., New York(1966)

[Huzinaga 1984] Ed. by Huzinaga, S., Andzelm, J., Klobukowski, M., Radzio-Andzelm, E., Sakai, Y. and Tatewaki, H. "Gaussian Basis Sets for Molecular Calculations", Elsevier, Amsterdam(1984)

[Igell-Mann 1988] Igel-Mann, G., Stoll, H. and Preuss, H. "Pseudopotentials for Main Group Elements(IIIa through VIIa)" *Mol. Phys.*, **65**, 1321(1988)

[Johnson 1977] Johnson, B. R. "New Numerical Methods Applied to Solving the One-Dimensional Eigenvalue Problem", *J. Chem. Phys.*, **67**, 4086(1977)

[Jordan 1979] Jordan, K. D. "Structure of Alkali Halides : Theoretical Methods", in "Alkali Halide Vapors", ed. by Davidovitz, P. and McFadden, D. L. Academic Press, New York(1979)

[Jørgensen 1981] Jørgensen, P. and Simons, J. "Second Quantization-based Methods in Quantum Chemistry", chapter 2, p. 20, Academic Press, New York(1981)

[Kahn 1976] Kahn, L. R., Baybutt, P. and Truhlar, D. G. "Ab Initio Effective Core Potentials : Reductions of All-electron Molecular Structure Calculations to Calculations Involving Only Valence Electrons", *J. Chem. Phys.*, **65**, 3826(1976)

[Kaplan 1975] Kaplan, J. G. "Symmetry of Many Electron Systems" Academic Press, New York(1975)

[Karwowski 1992] Karwowski, J. "The Configuration Interaction Approach to Electron Correlation", in "Methods in Computational Molecular Dy-

namics", ed. by Wilson, S. and Diercksen, G. H. F., Plenum Press, New York(1992)

[Knowles 1985] Knowles, P. J. and Werner, H.-J. "An Efficient Second-order MC-SCF Method for Long Configuration Expansions", *Chem. Phys. Lett.*, **115**, 259(1985)

[Koseki 1995] Koseki, S., Gordon, M. S., Schmidt, M. W. and Matsunaga, N. "Main Group Effeictive Nuclear Charges for Spin-orbit Calculations", *J. Phys. Chem.*, **99**, 12764(1995)

[Kovács 1969] Kovács, I. "Rotational Structure in the Spectra of Diatomic Molecules", translated by Nemes, L., Amer Elsevier(1969)

[Landau 1977] Landau, L. D. and Lifshitz, E. M. "Quantum Mechanics(non-relativistic theory)" 3rd Ed., Pergamon Press, Oxford(1977)

[Lefebvre-Brion 1986] Lefebvre-Brion, H. and Field, R. W. "Perturbations in the Spectra of Diatomic Molecules", Sec. 2.4., Academic Press, New York(1986)

[Lengsfield III 1980] Lengsfield III, B. H. "General Second Order MCSCF Theory : A Density Matrix Formalism", *J. Chem. Phys.*, **73**, 382(1980)

[Lindner 1994] Lindner, J., Bluhm, H., Fleisch, A. and Tiemann, E. "Low Vibrational Levels of the Ionic-covalent State $A0^+$ of NaI and Its Potential Function", *Can. J. Phys.*, **72**, 1137(1994)

[Löwdin 1955] Löwdin, P. O. "Quantum Theory of Many-Particle Systems. I. Physical Interpretations by Means of Density Matrices, Natural Spin-Orbitals, and Convergence Problems", *Phys. Rev.*, **97**, 1474(1955)

[MacDonald 1933] MacDonald, J. K. L. "Successive Approximations by the Rayleigh-Ritz Variation Method", *Phys. Rev.*, **43**, 830(1933)

[Mason 1962] Mason, E. A. and Monchick, L. in "Intermolecular Forces", ed. by Hirschfelder, J. O., Interscience(1967)

[MOLPRO] MOLPRO is a package of ab initio programs written by H.-J. Werner and P. J. Knowles, with contributions from J. Almöf, R. D. Amos, A. Berning, M. J. O. Deegan, F. Eckert, S. T. Elbert, C. Hampel, R. Lindh, W. Meyer, A. Nicklass, K. Peterson, R. Pitzer, A. J. Stone, P. R. Taylor, M. E. Mura, P. Pulay, M. Schuetz, H. Stoll, T. Thorsteinsson, and D. L. Cooper.

Calculations were made with version 96.4 of MOLPRO on the SGI Power Challenge computer at the Australian National University Supercomputer Facility, Canberra, ACT0200, Australia.

[McCoy 1999] private communication, McCoy, D. G., Department of physics and mathematical physics, University of Adelaide, Australia.

[Paldus 1992] Paldus, J. "Unitary Group Approach to the Many-electron Correlation", in "Methods in Computational Molecular Dynamics", ed. by Wilson, S. and Diercksen, G. H. F., Plenum Press, New York(1992)

[Pauncz 1979] Pauncz, R. "Spin Eigenfunctions", Plenum Press, New York(1979)

[Qin 1996] Qin, W. H. "Application of CuBr Laser to the UV Spectroscopy of NaI", Doctoral thesis, University of Adedlaide(1996)

[Richards 1981] Richards, W. G., Trivedi, H. P., and Cooper, D. L. "Spin-Orbit Coupling in Molecules", Clarendon Press, Oxford(1981)

[Roos 1987] Roos, B. O. "The Complete Active Space Self-Consistent Field Method and Its Applications in Electronic Structure Calculations", *Adv. Chem. Phys.*, **69**, 399(1987)

[Ruedenberg 1982] Ruedenberg, K., Schmidt, M. W., Gilbert, M. M. and Elbert, S. T. "Are Atoms Intrinsic to Molecular Electronic Wavefunctions? I. The FORS Model", *Chem. Phys.*, **71**, 41(1982)

[Ruedenberg 1982a] Ruedenberg, K., Schmidt, M. W., Gilbert, M. M. and Elbert, S. T. "Are Atoms Intrinsic to Molecular Electronic Wavefunctions? II. Analysis of FORS orbitals", *Chem. Phys.*, **71**, 51(1982)

[Ruedenberg 1982b] Ruedenberg, K., Schmidt, M. W., Gilbert, M. M. and Elbert, S. T. "Are Atoms Intrinsic to Molecular Electronic Wavefunctions? III. Analysis of FORS Configurations", *Chem. Phys.*, **71**, 65(1982)

[Rusk 1962] Rusk, J. R. and Gordy, W. "Millimeter Wave Molecular Beam Spectroscopy : Alkali Bromides and Iodides", *Phys. Rev.*, **127**, 817(1962)

[Sakai 1992] Sakai, Y., Miyoshi, E. and Anno, T. "A Congifuration Interaction Study of the Ground and First Excited $^1\Sigma^+$ States of the NaI Molecule", *Can. J. Chem*, **70**, 309(1992)

[Schaefer 1982] Schaefer, S. H., Bender, D. and Tiemann, E. "UV laser spectroscopy on NaI", *Chem. Phys. Lett.*, **92**, 273(1982)

[Schaefer 1984] Schaefer, S. H., Bender, D. and Tiemann, E. "The Predissociation of NaI" *Chem. Phys.*, 89, 64(1984)

[Schmidt 1993] Schmidt, M. W., Baldridge, K. K., Boatz, J. A., Elbert, S. T., Gordon, M. S., Jensen, J. H., Koseki, S., Matsunaga, N., Nguyen, K. A., Su, S., Windus, T. L., Dupuis, M. and Montgomery, Jr., J. A. "General Atomic and Molecular Electronic Structure System", *J. Comput. Chem.*, **14**, 1347(1993)

[Shepard 1987] Shepard, R. "The Multiconfiguration Self-Consistent Field Method", *Adv. Chem. Phys.*, **69**, 63(1987)

[Stevens 1984] Stevens, W. J., Basch, H. and Krauss, M. "Compact Effective Potentials and Efficient Shared-exponent Basis Sets for the First- and Second-row Atoms", *J. Chem. Phys.*, **81**, 6026(1984)

[Stevens 1992] Stevens, W. J. and Krauss, M. "Relativistic Compact Effective Potentials and Efficient, Shared-exponent Basis Sets for the Third-, Fourth-, and Fifth-row Atoms", *Can. J. Chem.*, **70**, 612(1992)

[Szabo 1989] Szabo, A. and Ostlund, N. S. "Modern quantum chemistry : Introduction to advanced electronic structure theory" Revised 1st Ed., McGraw-Hill, New York(1989)

[Torop 1987] Torop, L., McCoy, D. G., Blake, A. J., Wang, J. and Scholz, T. "Effects of the Close Approach of Potential Curves in Photoabsorption

by Diatomic Molecules-I. Theory and Computational Procedures"' *J. Quant. Spectrosc. Radiat. Transfer*, **38**, 9(1987)

[van Veen 1979] van Veen, N. J. A., de Vries, M. S. and de Vries, A. E. "Accurate Determinations of the Dissociation Energies of Alkali Halides", *Chem. Phys. Lett.*, **64**, 213(1979)

[van Veen 1981] van Veen, N. J. A., de Vries, M. S., Sokol, J. D., Baller, T. and de Vries A. E. "Wavelength Dependence of Photofragmentation Processes of the First Excited States of Na and K Halides", *Chem. Phys.*, **56**, 81(1981)

[Wang 1990] Wang, J., Blake, A. J., McCoy, D. G. and Torop, L. "Analytical Potential Curves for the $X^1\Sigma^+$ and 0^+ States of NaI", *Chem. Phys. Lett.*, **175**, 225(1990)

[Werner 1980] Werner, H. -J. and Meyer, W. "A Quadratically Convergent Multiconfiguration-Self-Consistent Field Method with Simultaneous Optimization of Orbitals and CI Coefficients", *J. Chem. Phys.*, **73**, 2342(1980)

[Werner 1985] Werner, H. -J. and Knowles, P. J. "A Second Order Multiconfiguration SCF Procedure with Optimum Convergence", *J. Chem. Phys.*, **82**, 5053(1985)

[Werner 1987] Werner, H. -J. "Matrix-formulated Direct Multiconfiguration Self-Consistent Multiconfiguration Reference Configuration-Interaction Methods", *Adv. Chem. Phys.*, **69**, 1(1987)

[Whiting 1968] Whiting, E. E. "An Empirical Approximation to the Voigt Profile", *J. Quant. Spectrosc. Radiat. Transfer*, **8**, 1379(1968)

[Wigner 1959] Wigner, E. P. "Group Theory and Its Applications to the Quantum Mechanics of Atomic Spectra", Academic Press, New York(1959)

[Wilson 1987] Wilson, S. "Basis Sets", *Adv. Chem. Phys.*, **67**, 439(1987)

[Zener 1932] Zener, C. "Non-adiabatic Crossing of Energy Levels" *Proc. Roy. Soc.*, **A137**, 696(1932)